MECHANICAL AND THERMAL AGING BEHAVIORS OF LEAD FREE SOLDER JOINT WITH ADDITION OF POROUS COPPER INTERLAYER

NASHRAH HANI BINTI JAMADON

FACULTY OF ENGINEERING
UNIVERSITY OF MALAYA
KUALA LUMPUR

2017

MECHANICAL AND THERMAL AGING BEHAVIORS OF LEAD FREE SOLDER JOINT WITH ADDITION OF POROUS COPPER INTERLAYER

NASHRAH HANI BINTI JAMADON

THESIS SUBMITTED IN FULFILMENT OF THE REQUIREMENTS FOR THE DEGREE OF DOCTOR OF PHILOSOPHY

FACULTY OF ENGINEERING
UNIVERSITY OF MALAYA
KUALA LUMPUR

2017

UNIVERSITY OF MALAYA

ORIGINAL LITERARY WORK DECLARATION

Name of Candidate: Nashrah Hani Binti Jamadon

Matric No: KHA120016

Name of Degree: Doctor of Philosophy

Title of Project Paper/Research Report/Dissertation/Thesis :

Mechanical And Thermal Aging Behaviors Of Lead Free Solder Joint With Addition Of Porous Copper Interlayer

Field of Study: Manufacturing Processes

I do solemnly and sincerely declare that:

(1) I am the sole author/writer of this Work;
(2) This Work is original;
(3) Any use of any work in which copyright exists was done by way of fair dealing and for permitted purposes and any excerpt or extract from, or reference to or reproduction of any copyright work has been disclosed expressly and sufficiently and the title of the Work and its authorship have been acknowledged in this Work;
(4) I do not have any actual knowledge nor do I ought reasonably to know that the making of this work constitutes an infringement of any copyright work;
(5) I hereby assign all and every rights in the copyright to this Work to the University of Malaya ("UM"), who henceforth shall be owner of the copyright in this Work and that any reproduction or use in any form or by any means whatsoever is prohibited without the written consent of UM having been first had and obtained;
(6) I am fully aware that if in the course of making this Work I have infringed any copyright whether intentionally or otherwise, I may be subject to legal action or any other action as may be determined by UM.

Candidate's Signature Date:

Subscribed and solemnly declared before,

Witness's Signature Date:

Name:

Designation:

ABSTRACT

The use of lead-based (Pb-based) solder alloy has been reduced mainly in electronics packaging due to Pb toxicity to the environment and human health. Sn-3.0Ag-0.5Cu (SAC305) Pb-free solder alloy is considered compatible combination of lead-free solder to replace conventional Pb-based solder alloy. However, it is still not as reliable as eutectic Pb-based solder alloy due to the formation of brittle intermetallic compounds (IMC), which cause a serious degradation of the joints strength. Therefore, to improve the performance characteristics of this Pb-free SAC305 solder joint, the physical soldering process was modified by incorporating a porous Cu interlayer in the soldering configuration. The SAC305 solder alloy and porous Cu interlayer was placed in a sandwich-like layer between the ends of the Cu rods to be joined. Porous Cu with 15 ppi (pore per inch, P15) and 25 ppi (P25) with approximately ϕ0.3 mm and ϕ0.1 mm pore sizes were used, respectively. A solder joint without a porous Cu interlayer was also prepared as the control sample. The soldering process was carried out at three temperatures of 267ºC, 287ºC and 307ºC, each with holding times set at 60 s, 180 s and 300 s. Tensile testing was performed to evaluate the joining strength of the solder alloy at a loading rate of 0.5 mm/min. According to the results, the tensile strength of both the control and solder containing porous Cu tended to increase with increasing soldering temperature or time. It was also found that solder containing porous Cu exhibited a strength exceeding that of the control sample by up to 10-20 MPa at each soldering temperature for each respective soldering time. The pores in the porous Cu have facilitated channels for the molten solder to penetrate into the internal porous structure before the final gripping occurred. The microstructural observation demonstrated that the growth of IMC layers at the joining interface had an apparent effect on joint reliability. Despite the relatively thin IMC layer at the SAC305/Cu substrate interface for all samples at 60 s, with higher soldering time of 180 s and 300 s, the thickness for both control and

with porous Cu samples increased 1 μm for every 20°C increase of soldering temperature. In addition, a thermal aging test was performed to investigate the isothermal effect on the tensile strength and its microstructure. The isothermal aging test was done in an oven, heated to 150°C for durations of 100, 200 and 500 hours. The results indicate the significant reduction in joint strength with increasing aging time due to grain coarsening that developed from the atomic reactions in the solder alloy and porous Cu during isothermal aging**.** It was also observed that cracks occurred predominantly at the porous Cu/SAC305 interfaces. The present study provides a fundamental understanding of the mechanical and thermal aging characteristics of Pb-free SAC305 solder joints resulting from the addition of a porous Cu interlayer.

ABSTRAK

Penggunaan aloi pematerian dengan menggunakan plumbum (Pb) telah amat berkurangan terutama dalam pakej elektronik, berikutan kehadiran unsur Pb yang toksik kepada alam sekitar dan kesihatan manusia. Kaedah pematerian aloi bebas Pb, iaitu Sn-3.0Ag-0.5Cu (SAC305) telah dikenalpasti sebagai antara kaedah pematerian tanpa unsur Pb bagi menggantikan proses pematerian aloi Pb yang konvensional. Namun kaedah ini masih belum menyaingi seperti aloi pateri yang berasaskan Pb. Dengan itu bagi meningkatkan prestasi aloi pateri SAC305 bebas plumbum, proses pematerian fizikal telah diubahsuai iaitu dengan menambah lapisan tembaga yang berliang (Cu poros) pada konfigurasi pematerian. Lapisan tengah Cu poros ini diletakkan di tengah-tengah antara SAC305 aloi dan keda-duanya dicantumkan dengan bahagian hujung batang Cu. Dua jenis Cu poros yang digunakan ialah 15 ppi (liang seinchi, P15) dan 25 ppi (P25) dengan saiz liang masing-masing beranggaran ϕ0.3 mm dan ϕ0.1 mm. Pematerian aloi tanpa lapisan Cu poros telah disediakan sebagai sampel kawalan. Proses pematerian telah dilakukan pada tiga suhu yang berbeza iaitu 267°C, 287°C dan 307°C, dengan tiap satu dalam tempoh masa 60 s, 180 s dan 300 s. Ujian daya tegangan telah dilakukan bagi mengukur kekuatan pateri aloi dengan kadar beban yang ditetapkan sebanyak 0.5 mm/min. Keputusan menunjukkan daya kekuatan penyambungan bagi pateri mengandungi lapisan Cu poros adalah lebih tinggi pada kadar 10 - 20 MPa berbanding pateri kawalan pada setiap suhu pematerian iaitu bagi satu-satu tempoh masa pematerian. Lapisan pada Cu poros ini telah memberi ruang laluan kepada cairan aloi sebelum menghasilkan mekanisme cengkaman antara aloi dan Cu poros. Pembentukan lapisan sebatian antara-logam (intermetallic compound, IMC) yang terbentuk di permukaan penyambungan juga jelas mempengaruhi daya kekuatan penyambungan ini. Walau pun lapisan sebatian antara-logam pada permukaan subtrat SAC305/Cu adalah nipis pada tempoh masa 60 s pada semua sampel, ianya meningkat 1 μm bagi setiap 20°C kenaikan

suhu pateri bagi kedua-dua sampel kawalan dan yang mengandungi Cu poros pada tempoh masa suhu 180 s dan 300 s. Selain daripada itu, ujian rintangan haba (thermal aging test) telah dilakukan untuk mengetahui kesan pemanasan ke atas kekuatan penyambungan dan struktur aloinya. Sampel yang telah dipateri di simpan di dalam oven pada suhu 150°C dengan tempoh 100, 200 and 500 jam. Keputusan menunjukkan bahawa kekuatan penyambungan menurun dengan signifikan dengan meningkatnya tempoh penyimpanan. Keadaan ini adalah disebabkan oleh pelumatan butiran kecil atom (grain coarsening) yang tehasil daripada tindak balas atom didalam aloi dan Cu poros. Dominasi rekahan berlaku pada permukaan Cu poros/aloi SAC305. Kajian ini telah memberikan maklumat asas berkenaan prestasi mekanikal dan rintangan haba terhadap pateri aloi bebas Pb dengan penambahan lapisan Cu poros.

ACKNOWLEDGEMENTS

In The Name of Allah, the Most Beneficent, and the Most Merciful.

Undertaking this PhD has been a truly life-changing experience for me which would not have been possible without the support and guidance I have received from many people.

First, I would like to express my sincere gratitude to my supervisor Prof. Mohd Hamdi Abd Shukor and my co supervisor Dr. Farazila Yusof for the continuous support throughout my Ph.D study, for their excellent guidance, patience, motivation, and imparting of immense knowledge. Thank you for providing me with an excellent atmosphere for doing research, supporting my attendance at various conferences, and helping me in all the research and writing of this thesis.

Special thanks to Prof. Emeritus Tadashi Ariga from Tokai University for his encouragement and supervisory role in providing me knowledge and sharing his valuable experience to widen my research specifically in the soldering field. Without his precious guidance it would not have been possible to conduct this research until the end.

Further I greatly appreciate to Prof. Mutoh Yoshiharu and Assoc. Prof. Miyashita Yukio from Nagaoka University of Technology, Japan, who provided me an opportunity for attachment at their laboratory as an exchange student. Thank you for offering a friendly and cooperative atmosphere at the laboratory and access to the research facilities during my stay in Japan.

I also gratefully acknowledge the funding received from the Postgraduate Research Fund, (PPP, PG129-2012B), Fundamental Research Grant Scheme (FRGS, project number FP062-2015A) and University Malaya Research Grant, (UMRG, RP035A-15AET) for this research work. I am also grateful for the financial support from the

Malaysia Ministry of Higher Education under the MyBrain15 program and scholarship from the JASSO Student Exchange Support Program.

I am indebted to all the staff at the Centre of Advanced Manufacturing and Material Processing (AMMP Centre, University of Malaya), the lab assistants and the technicians I have worked with for the support and cooperation given during the experiments. Not to forget all my fellow lab mates at Nagaoka University of Technology and especially at University of Malaya for the friendships, love and unyielding support. It would be impossible to mention all who have assisted me through throughout the research work and during thesis writing.

Finally, I thank my parents and family members for supporting me throughout all my studies. Thank you for always believing in me and encouraging me to follow my dreams. To everybody else who accompanied me on this beautiful PhD journey, THANK YOU!

TABLE OF CONTENTS

LIST OF FIGURES

LIST OF TABLES

LIST OF SYMBOLS AND ABBREVIATIONS

LIST OF SYMBOLS

%	:	Percentage
>	:	More than
°	:	Degree
°C	:	Degree Celcius
μm	:	Micrometer
2θ	:	2 theta
A	:	Area
at.%	:	Atomic perncentage
D	:	Diffusion coefficient
D_0	:	Diffusion constant
F	:	Load
g	:	Gram
h	:	Hour
J	:	Joules
K	:	Kelvin
kJ	:	Kilojoules
kV	:	Kilovolt
mm	:	Milimeter
Mm/min	:	Milimeter/minute
mol	:	Mole
MPa	:	Mega Pascal
ppi	:	Pore per inch
Q	:	Activation energy

R	:	Gas constant
s	:	Second
t	:	Time
T	:	Temperature
W_{as}	:	Weight of porous Cu after submerged in water
W_d	:	Weight of porous Cu in dry condition
W_s	:	Weight of porous Cu while submerged in water
wt.%	:	Weight percentage
σ	:	Stress

LIST OF ABBREVIATIONS

ASTM	:	American Society for Testing and Materials
CuKα	:	Radiation
DSC	:	Differential Scanning Calorimetry
EDS	:	Energy Dispersive X-Ray Spectroscopy
EPA	:	Environmental Protection Agency
EU	:	European Union
IMC	:	Intermetallic Compound
IPC	:	International Printed Circuit
JIS	:	Japanese Industrial Standard
OM	:	Optical Microscope
PCB	:	Printed Circuit Board
Q	:	Activation Energy
RoHS	:	Restriction of Hazardous Substance
SEM	:	Scanning Electron Microscope
TLP	:	Transient Liquid Phase

WEEE : Waste Electronic and Electrical Equipment

XRD : X-Ray Diffraction

LIST OF APPENDICES

CHAPTER 1: INTRODUCTION

1.1 Background

Soldering technology has become essential for the practical interconnection and packaging of electronics devices and circuits. Tin-lead (Sn-Pb) solder alloys have been used extensively in the assembly modern electronics circuits. A solder alloy commonly utilized in the field is a eutectic composition of Sn-37wt.%Pb owing to several advantages, namely ease of handling, low melting temperature of 183°C and good workability and ductility (Katsuaki Suganuma, 2001).

However, in the 1950s the United States Environmental Protection Agency (EPA) deemed Pb as one of the 17 chemicals posing the greatest threat to human beings and the environment (Abtew & Selvaduray, 2000). The European Union (EU) requirements on waste electronic and electrical equipment (WEEE) and the Restriction of Hazardous Substance (RoHS) directive stated that electronic products sold to European consumers must not contain any Pb compounds as of 1st July 2006. It is thus not surprising that efforts to develop Pb-free solders have been ongoing till today (Pang, Xu, Shi, Zhou, & Ngoh, 2004).

In the pursuit for Pb-free solders several potential alloys have been developed, with the majority of alloys containing Sn as the primary component. Sn-based solder alloys are a suitable choice as they exhibit excellent wetting and spreading properties, and are non-toxic and easily accessible. Alloying Sn with copper (Cu) and silver (Ag) appears to produce a potential Pb-free candidate.

A Sn-Cu based alloy has been widely applied for wave soldering in the assembly of electronic devices (Matsumoto & Nogi, 2008). The Sn-Cu binary alloy has a eutectic composition of Sn-0.7wt% Cu, which is cheaper than most other candidate alloys. However, the tensile and shear strengths of Sn-Cu eutectic solder alloys are lower

compared to other Pb-free solder alloys. Small amount of silver (Ag) have been subsequently added to Sn-Cu eutectic solder alloy to improve its mechanical properties. Ag is selected for its capability to promote good wetting characteristics and excellent joint strength (El-Daly & Hammad, 2011). In addition, Ag has been extensively used in the electronics industry as protective coating and for its high electrical conductivity.

A combination of Sn-Ag-Cu (SAC) solder alloys is thus recommended to replace the traditional Sn-Pb solder alloy. On account of the high Sn concentration, SAC solder alloy exhibits a high rate of interfacial reaction rate between Sn and Cu. This results in a high Cu-Sn intermetallic compound (IMC) formation rate, leading to the degradation of the solder joint. Therefore, the addition of a fourth element to SAC solder alloy has in fact been proposed to improve its properties. Rizvi et al. showed that adding small amount of bismuth (Bi) into Sn-Ag-Cu solder alloy had improved the performance of solder joint (Rizvi, Chan, Bailey, Lu, & Islam, 2006).

Despite all developments thus far, there is a requirement for high-temperature solder material suited for advanced technological applications; for instance in the automotive and transportation industries. Recent developments in these industries have created a demand for electronic components that can withstand high temperature conditions. This demand has consequently prompted researchers to seek potential Pb-free solders for use in the assembly of heat-tolerant electronic components.

Meanwhile, some studies have shown that cellular structures like metal foam or porous metal can serve as a heat transfer medium in semiconductor application, where in actual practice high thermal resistance of the system is crucial (Yang, Chung, Lee, Chiang, & Wong, 2013). Thus, porous Cu metal which is known for its high thermal conductivity was applied to the soldering process in the present study to assess any favorable effects

that it may have on the solderability characteristics and heat tolerance performance of solder joints subjected to long periods of high temperature regime.

1.2 Problem Statement

Several related studies have proven that the SAC combination appears to be the most promising alternative candidate for the Pb-free solder alloy owing to its superior comprehensive properties (Hu, Xu, Keer, Li, & Jiang, 2016; Tu, Yi, Wu, & Wang, 2017; Yu, Lee, Chen, & Duh, 2014). Although numerous studies have addressed the mechanical behavior and microstructure defects of SAC Pb-free solder in different testing conditions, more work is necessary to overcome the disadvantages of the SAC solder alloy, such as poor creep rupture and low elongation (Wu, Xue, Wang, Han, & Wang, 2016).

Sn-3.0wt.%Ag-0.5wt.%Cu (SAC305), a well-known SAC solder alloy, was selected for the present study because it is recognized as potential Pb-free solder for current use in the assembly of electronic devices and circuits. Despite the solder's widely acknowledged reliability, one of its limitations is the tendency for excessive intermetallic compound (IMC) in the interfacial reactions. Possible improvements to solderability characteristics, particularly the joint strength of the SAC305 solder alloy, could be achieved through various means such as modifying the solder contents and/or altering the soldering configurations. Hence, the optimal process conditions must be taken into account when designing a soldering process modification.

In addition, uneven solder joints thickness may occur in some instances, possibly due to substrate tilting in one of the soldering stages (Lu, Bailey, & Mills, 2015). Because of the damaging effect of substrate tilting, it is important to stringently control soldering during the manufacturing process. However, there is still no recognized solution to overcoming this tilting configuration problem.

Apart from modification to the solder alloy compositions, another approach to enhance the performance of solder joint is by improving the soldering technique. Despite no to-date reports on the introduction of porous Cu in soldering technology, it is postulated that further improvement in solder manufacturability would be achieved with the addition of porous Cu interlayer in the solder alloy, such as tilting problem. However, uncertainty remains regarding the suitability of porous Cu when added to the SAC305 solder alloy and to be applied in assembly operation for long hours in mid-high temperature regime (possibly above 150°C). Besides, the lack of reports on the utilization of porous Cu metal, especially in soldering has prompted the present investigation.

1.3 Research Objectives

The main objective of the present research is to improve the performance characteristics of a SAC305 Pb-free solder joint by modifying the physical soldering process through incorporating a porous Cu interlayer in the solder configuration. In order to gain a profound understanding of how the added porous Cu interlayer improves the solderability of a SAC305 solder joint, the focus of this research is on the following objectives:

1) To investigate the porosity effect of porous Cu interlayer on SAC305 solder joint on tensile strength and interfacial microstructure development.
2) To study the reaction layer's formation behavior based on the microstructural features and elemental composition of a SAC305 solder joint with an added porous Cu interlayer.
3) To study the effects of isothermal aging treatment on tensile strength and microstructural properties of a SAC305 solder joint SAC305 solder joint with an added porous Cu interlayer.

1.4 Scope of Research

In this research, two different porous Cu interlayers, namely 15 ppi (pore per inch) (P15) and 25 ppi (P25) were used to reinforce a SAC305 solder joint. A porous Cu interlayer and a SAC305 solder alloy were set in a sandwich configuration and were then joined to a Cu substrate. For comparison purpose, a SAC305 solder joint without an added porous Cu interlayer was also prepared and tested as the control sample. Soldering for each treatment was carried out at three temperatures, i.e. 267ºC, 287ºC and 307ºC, each at three holding times, i.e. 60 s, 180 s and 300 s.

The solder joints modified in this study were subjected to standard testing in order to evaluate their joint strength as determined by tensile testing. The modified solder joints also underwent isothermal aging treatment to study their stability when exposed to elevated temperatures. The samples were aged at 150°C for 100 h, 200 h and 500 h. The aged solder joint was subjected to standard testing similar to the as-soldered joint to evaluate the joint strength as determined by tensile testing.

The microstructural characteristics of the as-soldered and aged solder joints after tensile testing were observed through fractography in order to determine their failure behaviors. It is also important to understand the formation of the IMC layer created from the interfacial reaction of the solder alloy with the reinforced porous Cu interlayer during the soldering process. Hence, the cross-sectional morphology of the soldered samples was observed using an optical microscope, and the elemental composition was analyzed. Finally, the crack propagation in the fractured sample was assessed closely to understand the reaction mechanism of porous Cu and molten solder during both soldering and aging treatment.

1.5 Overview of the Thesis

The work documented in this thesis is organized as follows:

Chapter 1 provides background information on the research, problem statement, research objectives, research scope and organization of the thesis.

Chapter 2 delivers a review of past and recent studies related to Pb-free soldering and applications of porous metal in joining technology. The literature review was accumulated from research journals, books, patents and other reliable sources.

Chapter 3 outlines the research work plan. This includes a presentation of the materials used for soldering, the soldering process preparation, experimental parameters for soldering and thermal aging as well as the various characterization and analysis equipment used in the study.

Chapter 4 presents the results of the mechanical testing experiments, data analysis of the fracture morphology and elemental composition, and an analysis of the effects of porous Cu on the interfacial reactions of solder joints of both as-soldered and aged samples.

Finally, the general conclusions based on the study findings are presented in Chapter 5. The strengths and limitations of the overall study together with suggestions for further research are also put forward.

CHAPTER 2: LITERATURE REVIEW

2.1 Introduction to Soldering Technology

Soldering is a relatively longstanding technology. Various topics on soldering technology have generated a great deal of interest, particularly in the electronics assembly industry. Modern soldering technology development involves solder compositions as well as joining processes enhancements. However, any advancements in soldering technology must be responsive to new regulations and in accordance with present legislation, mainly as a result of concerns regarding health and the environment. All key aspects related of soldering technology will be discussed in detail in this chapter.

2.1.1 Soldering and It's Application

Solder joint bonding entails more than adhesion or mechanical attachment. This joining method can produce smooth-edge surfaces at the peripheral connections of joints. The soldering process involves metal joining using a molten filler metal that wets the surface joint, leading to the formation of metallic bonds at the filler and joint material interface (Humpston & Jacobson, 2004). The filler metal, solder alloy, has a melting temperature below 450°C. This differentiates soldering from brazing, both of which essentially have the same bonding mechanism, except that under the agreed classification, the melting temperature of filler alloy in brazing is above 450°C. During soldering process, the material to be joined is not melted. Rather, the molten solder reacts with a small amount of base material or substrate metal and wets the interface by forming intermetallic compound (IMC), hence facilitating metallurgical bonding.

Solder alloys are regularly classified as either soft or hard solders. Soft solders normally consist of alloys containing lead (Pb), tin (Sn), indium (In), bismuth (Bi), antimony (Sb), or silver (Ag) (Ag, Kg, & Chaussee, 1999). In practice, most soft alloys melt at temperatures below 450°C, usually between 180°C and 300°C. Pb-free solders

such as Sn-based alloy, tend to be stiffer, harder and less ductile compared to soft solders. Hard solders often contain metals such as gold (Au), zinc (Zn), aluminum (Al), or silicon (Si) and are meant for elevated temperature applications. Most hard solders are categorized as high-temperature solder materials.

The practice of soldering actually began 5000 years ago in Mesopotamia and was later used in Egypt (K Suganuma, 2003). It became much more popular 1000 years later when tin (Sn) was discovered as a soldering material. Traditionally, solder was primarily used in the structural joining of metals, particularly in the production of household pieces and for joining metal pipes. By the 20^{th} century, the metallurgical science had advanced to designating solders for electrical, plumbing and structural applications as well as sheet metal construction in automotive and transportation technology. The evolution has continued until the present time, with soldering now being considered the most applicable technique for the joining or interconnection of electrical components in electrical or electronic devices and the assembly of printed circuit boards (PCBs). This means solder joints have a dual function of serving both mechanical and electrical connections.

A typical soldering process involves four main components;

1. Substrate metal.
2. A type of flux.
3. Solder material.
4. Heat source.

The substrate metal comes into contact with the molten solder prior to IMC layer formation. The correct solder alloy for use in soldering is determined by the substrate metal itself, on which the wettability of the molten solder alloy is greatly dependent. Several types of metals can easily react with molten solder to form strong chemical and

physical bonding. During the soldering process, a flux is used to eliminate minor surface oxidation and to prevent further oxidation of the base metal's surface. Many kinds of flux are available, each including two basic parts: chemical and solvent. The chemical comprises the active portion, while the solvent is the carrying agent. The solder material is the alloy employed to facilitate solvent action, which generates the bond between base metals. Solder joint quality depends strongly on the combination of elements, solder alloy type and form. The intended application, the base metals used and the soldering method employed are equally important in determining the effectiveness of solder joints.

Eutectic alloys are often regarded as having the best spreading characteristics, which is one of the most frequent reasons cited for selecting them in preference over hypoeutectic and hypereutectic compositions. The often observed superior spreading of eutectic alloys compared with off-eutectic alloys of the same system is explained by the different melting characteristics in the two cases. An alloy with eutectic composition melts instantly, after which molten alloy spreading is driven, by the interaction with the substrate. In the case of a non-eutectic filler metal, melting, wetting and spreading commence before the alloy is entirely molten and it tends to be somewhat viscous. Under such conditions, filler movement is relatively sluggish. By the time the alloy is completely molten, the filler will have partly alloyed with the substrate and the driving force for spreading diminished. When completely molten, eutectic alloys are also less viscous than adjacent compositions.

In the electronics industry, soldering remains the leading method of establishing an interconnection medium. The electrical attachment of different components normally involves simple mechanical joints and general operational procedures. Solder joints utilized in the electronics industry are expected to fulfil the following criteria (Tu, 2007):

i. High compatibility with the metal (especially with respect to alloying behavior and melting points).
ii. Relatively good electrical conductivity.
iii. Workability to ensure the industry can use low-cost and reliable solder joints rapidly.

In microelectronics PCB assembly, various microelectronic subcomponents are mounted onto the PCB and solder materials are applied in various stages of the assembly sequence. First, solders provide the electrical and mechanical connections between the silicon die and the bonding pad and also function as paths for heat dissipation. This stage is commonly referred to as Level 1 electronic packaging. Abtew et al. provided a detailed schematic account of a standard electrical assembly as shown in Figure 2.1 (Abtew & Selvaduray, 2000).

In Level 2 electronic packaging, the components are mounted on the PCB, as in the case of small outline integrated circuit (SOIC) application. A typical assembly established for SOIC is shown in Figure 2.2. In this instance, the soldering process involved is called reflow soldering, whereby heat is applied to melt the solder alloy. Upon the molten solder solidification, a solder joint is formed.

Ultimately, many factors need to be considered when conducting research on soldering reliability. The reason is that solder alloys are expected to function as encompassing electrical, thermal and mechanical interconnections in real practical applications.

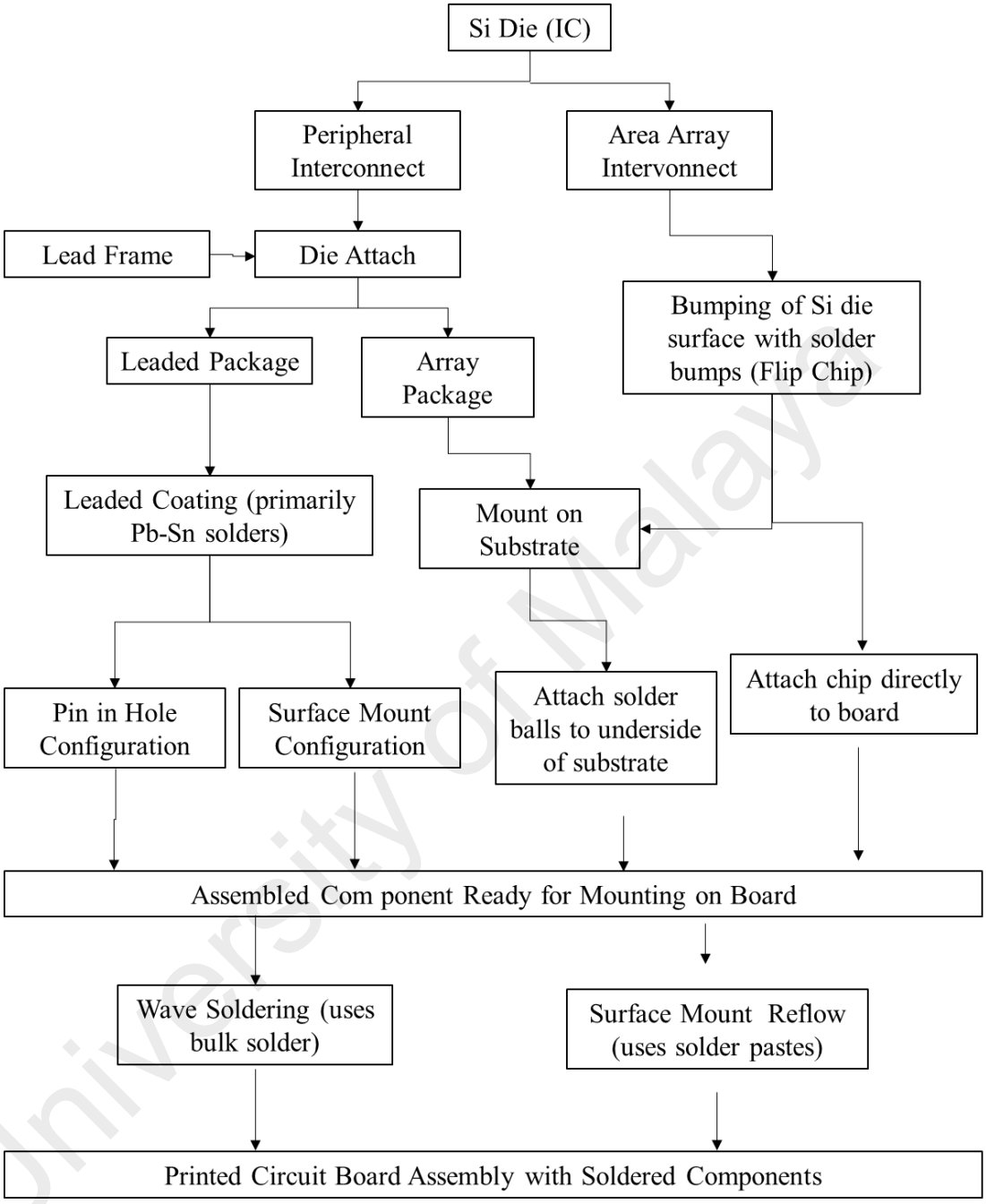

Figure 2.1 : Overview of soldering application to electronic components (Abtew & Selvaduray, 2000)

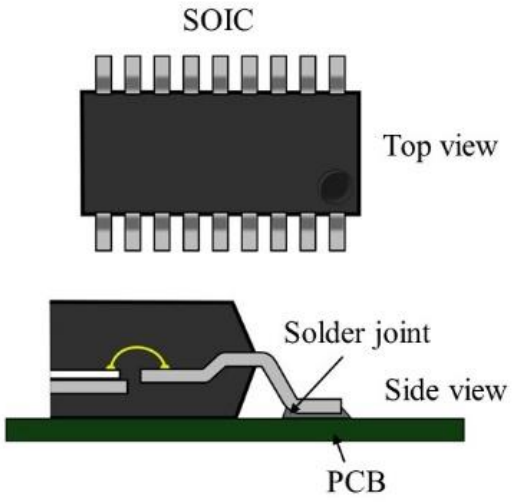

Figure 2.2 : Illustration of typical SOIC

2.1.2 Manufacturability Issues Related to Soldering

Currently, the development of electronic devices, such as notebook computers, smart phones and electronic gadgets is synchronized with industrial needs, whereby the hardware with all complicated functions must be durable. The electronics industry has been coping with changes and consumer needs by offering electronic device miniaturization at the same time attempting to meet the required reliability.

As pointed out earlier, the main purpose of soldering technology is to achieve the advanced interconnection reliability for electronic parts not only to facilitate adequate electrical paths but also to carry the mechanical loads. In terms of mechanical stability, the resultant solder is required to attain high strength, good hardness and good fatigue life in order to ensure extended electronic circuit lifetime. Furthermore, the solder have cost-saving characteristics without jeopardizing the other properties. However, soldered joint strength (under mechanically or thermally caused fatigue) is quite limited compared to other joining methods such as welding, brazing and even adhesive bonding.

Power electronics contain power semiconductor devices, substrates, interconnectors, chips, etc. The soldering technique is employed to attach directly bonded Cu substrates to the baseplates. Here, solder joints not only function as structural support for substrates but also as a heat exchange medium between the semiconductor device and the baseplate. The thermal energy generated in semiconductor devices flows through the substrate to the baseplate. Hence, the solder joint quality may influence the heat dissipation within the devices.

In general, solder joints in many electrical devices are exposed to elevated temperature conditions. When devices are subjected to being switched on and off, the electrical circuit undergoes repeated heating and cooling cycles that could lead to thermo-mechanical fatigue of the solder joints. This is due to the stress arising from the coefficient of thermal expansion (CTE) mismatch between the solder alloy and substrate. Besides, high frequency mechanical impact can occur to solder joints, where the electronic components are mechanically attached in heavy equipment such as equipment used in the transportation industry (Sharma, Jang, Kim, & Jung, 2017).

Among other factors, the solder interconnection thickness may affect the solder joint's lifetime (Lu, Tilford, Bailey, & Newcombe, 2007). Solder joint thickness is dependent on the solder volume applied, but an adequate solder volume alone does not guarantee solder joint quality. Manufacturing defects like voids or uneven solder thickness may arise. The causes for uneven solder thickness may be due to substrate/baseplate bending, or the substrate tilting relative to the baseplate due to the solder applied. Uneven assembly results in delamination at the substrate interface caused by stress concentration at the thinner part, as shown in Figure 2.3 (Hayashi, Izuta, Murakami, Uegai, & Takao, 2002). Therefore, it is worth making an effort to find a solution to the substrate tilting problem in practical soldering applications. It is believed that reinforcements in composite solder

alloys and modifications to the soldering technique may improve the reliability of solder joints.

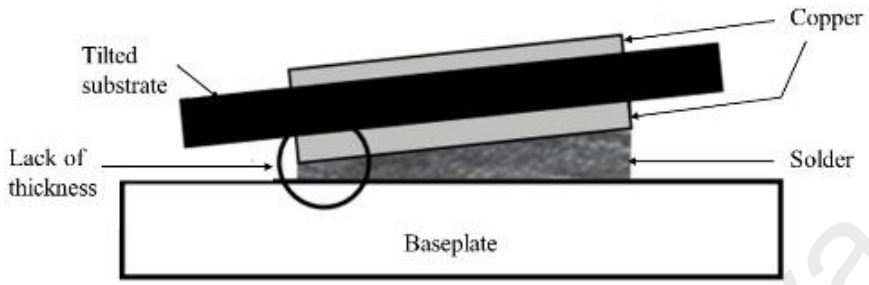

Figure 2.3 : Uneven solder thickness between the substrate and baseplate in power electronic module (Hayashi, Izuta, Murakami, & Uegai, 2002)

2.1.3 Environmental and Health Issues

For many years traditional solder alloys containing Pb have been widely used in the assembly of electric and electronic parts. However, Pb-based solders are hazardous to the environment and human health. This has led the European Restriction of Hazardous Substances (RoHS) directive to impose legislative initiatives to ban Pb from all electronic products (Ogunseitan, 2007). On the same note, the US Environmental Protection Agency (EPA) has also cited Pb compounds as being among the top 17 chemicals posing the greatest threat to human life and the environment (Anderson, 2007; Katsuaki Suganuma, 2006).

The accumulation of Pb in the body to critical levels can have adverse health effects. Lead binds to proteins and degrades body functions. It can also result in nervous and reproductive system disorders, slowing down neurological development and decreasing hemoglobin leading to anemia and hypertension (Monsalve, 1984.).

In landfills, approximately 60 000 tons of Pb are estimated to have originated from electronic wastes, particulary from solder joints (Humpston & Jacobson, 2004). Rainwater that becomes acidic at these landfills will leach into ground water, eventually making its way into water supplies meant for human and animal use. Figure 2.4 illustrates how Pb from electronic products leaches into groundwater and the effect of water pollution on human beings.

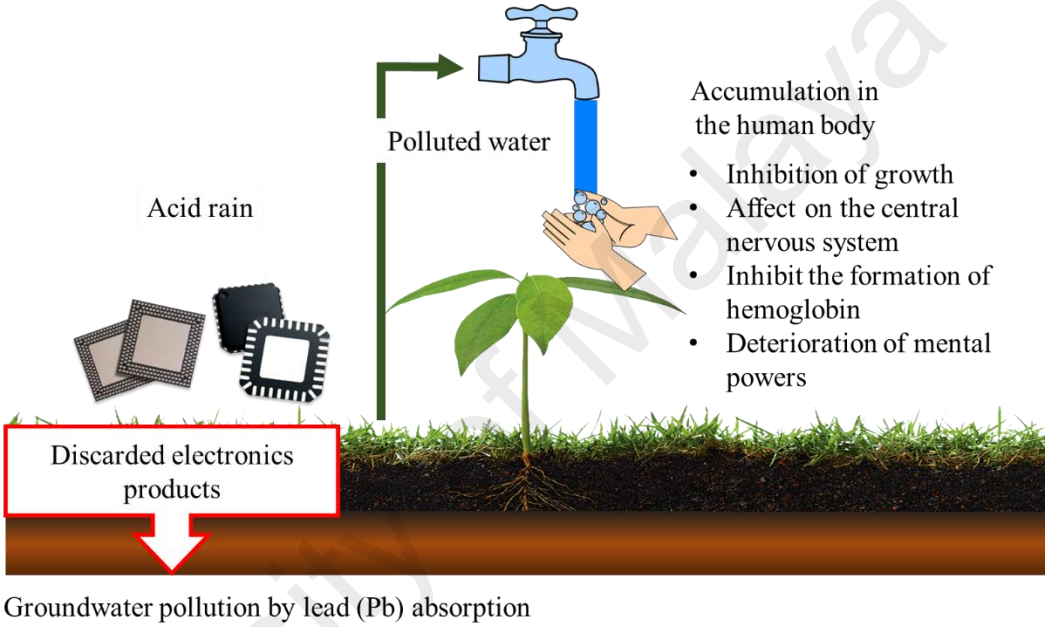

Figure 2.4 : Illustration of Pb contaminated water leached from electronic waste

A potential source of occupational exposure is in the electronics industry, especially where wave soldering is carried out. Most scum formed during wave soldering can be refined to pure metal for reuse, while the remaining 10% represents waste. It has been shown that workers risk their health if they inhale Pb haze or dust generated by scum due to oxidation at the molten solder surface (Tukker, Buist, Oers, & Voet, 2006). This has prompted the Resource Conservation and Recovery Act (RCRA) to classify this waste as hazardous and propose special handling and disposal (Vann, Musson, & Townsend, 2006).

To counter these problems, Japan has enforced recycling rules for home electrical appliances effective from April 2001. This was followed by European and Asian countries in 2003. The promotion of recycling home appliances leads to enormous volumes of discarded electrical items. This brings the issue of toxicity into landfill, where the stringent treatments procedure for recycling is imposed which consequently increase the recycling cost. This matter has motivated researchers to seek environmentally and human safe alternatives to toxic Pb-based solders. Pb-free technology development in future electronics packaging has been taking place as a result, which will be discussed further in the following section.

2.2 Pb-free Soldering

There is no standard definition of Pb-free solder because the minimum Pb content allowed by legislation in a particular country differs from others. US specifications permit less than 0.2% Pb mixed in the solder alloy for for electronics applications. Manufacturers receive tax benefits upon reducing the Pb-based solder used. In European countries, 0.1% Pb is allowed according to RoHS effective on July 1, 2006 (Ogunseitan, 2007).

Figure 2.5 displays the implementation plan to restrict Pb usage in electrical and electronic products around the world. In the year 2000, Pb-free solder mountings started being used in the automotive industry. Nissan is a pioneer company in using Pb-free solders for their mass-produced keyless entry system PWB.

In general, solder alloys must satisfy two basic requirement: i) the ability to wet and bond to metallic terminals on components and substrates and ii) have an adequate melting point for reflowed when attaching components to PCB, yet be robust enough to avoid any ill effects due to operating temperatures in the field. Other important characteristics to be considered are listed in Table 2.1.

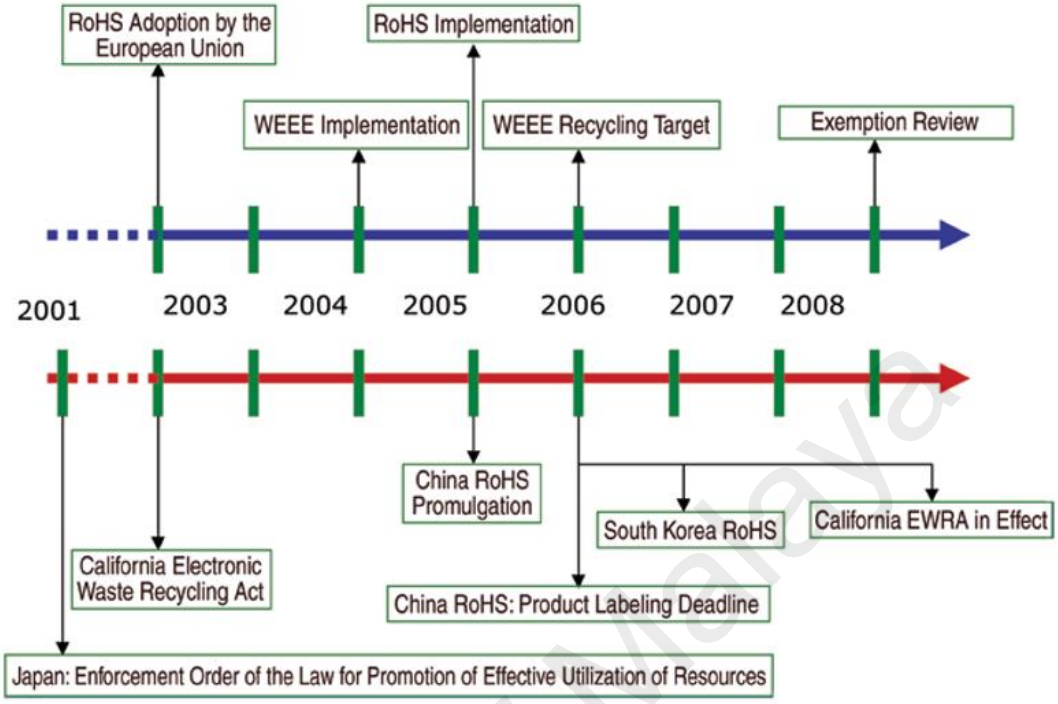

Figure 2.5 : Timeline of regulations on restricting Pb usage in the electrical and electronic industries. The blue arrow refers to the European Union and the red arrow represents the United States and Asia (Ogunseitan, 2007)

Table 2.1 Pb-free solder alloy characteristics

Characteristics and criteria of Pb-free solder
• Not toxic
• Available in sufficient quantities to meet current and future requirements
• Sufficient electrical and thermal conductivity
• Adequate mechanical properties : strength, toughness, fatigue and creep resistance
• Affordable

2.2.1 Low-temperature Pb-free Solder Alloy Candidates

When attempting to replace the traditional Sn-Pb solder alloy, it is crucial to ensure that the replacement candidate's properties are comparable to those of the Sn-Pb solder (see Appendix A). With a melting eutectic temperature of 183°C, the Sn-Pb binary solder has been utilized extensively as an alloy with soldering conditions compatible with most substrate materials and devices (Abtew & Selvaduray, 2000). Sn-Pb solder joints are therefore the benchmark for any solder alloy development. It must be stressed that in many electronic packaging applications, the reflow soldering alloy that is compatible with most places of solder joints must have a melting point below 260°C. Higher processing temperatures promote complications during circuit manufacturing such as damage to components, which are temperature-sensitive.

One of the base materials that have received much attention in Pb-free solder development is tin (Sn)-based solder. The ability of Sn to wet and spread on a wide range of substrates has allowed it to become the main component of most Pb-free solder alloys used in electronic applications. Numerous investigations on adding various single elements to form binary Sn-based solders have been carried out. The most notable amongst them are silver (Ag), bismuth (Bi), copper (Cu), zinc (Zn), indium (In) and antimony (Sb), which are found to generate promising Pb-free solder alloys when added to Sn-based solder (Fallahi, Nurulakmal, Arezodar, & Abdullah, 2012; Kim, Lee, Lee, & Kang, 2014; Rizvi, Chan, Bailey, Lu, & Islam, 2006).

Earlier studies indicate that the Sn-0.7wt.%Cu solder alloy combination has been introduced to industrial production due to the constituent elements' availability and low-cost manufacturing. When attaching a Cu substrate, the solder forms large Sn-rich dendrites that intersperse to form an IMC layer. Researchers have realized that the eutectic or near-eutectic microstructure can be modified to improve the solder alloy

quality by adding a trace element. Therefore, small reinforcements such as Ni have been added to suppress eutectic Sn dendrite growth and consequently constraining IMC layer growth (Nogita, Read, Nishimura, Sweatman, & Suenaga, 2005). The refinement of primary Sn dendrites and eutectic Sn–Cu microstructure can improve the solder's mechanical properties. Figure 2.6 illustrates optical micrographs of (a) Sn-0.7wt.%Cu and (b) Sn-0.7wt.%Cu with Ni added and solidified after heating at 300°C. Although this modification improves the microstructure, this alloy has a high melting point (227°C) and the authors did not mention actual effect of Ni addition on the solder joint's mechanical properties.

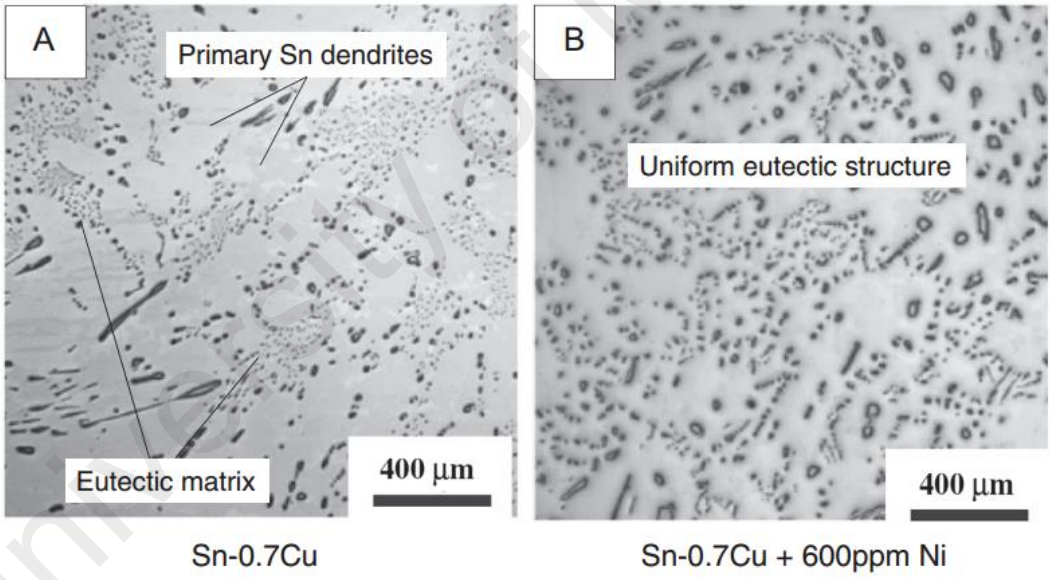

Figure 2.6 : Optical micrographs of Sn-0.7Cu and effect of Ni added to Sn-0.7Cu (Nogita, Read, Nishimura, Sweatman, & Suenaga, 2005)

From a melting temperature point of view, the eutectic Sn–Zn solder alloy is considered another potential candidate for substituting Pb-based solders. The melting temperature of Sn-Zn solder alloy is 198°C compared to 183°C of Pb-Sn solder alloy.

However, the Sn-Zn solder was found to have poor wettability due to Zn oxidation. Various elements such as Ag, Cu or Bi have individually been added to the Sn-Zn alloy to improve the resistance to oxidation so as to achieve superior wetting properties (Mayappan, Ismail, Ahmad, Ariga, & Hussain, 2006). Figure 2.7 shows the relationship between the contact angle and soldering temperature of Sn–9wt.%Zn and Sn–8wt.%Zn–3wt.%Bi Pb-free solder alloys compared with the Sn–40wt.%Pb control sample. A ternary solder alloy of Sn-Zn-Bi provides better wetting properties at higher temperatures. Researchers have found that adding Bi reduces the surface tension of Sb-Zn alloy (Bukat, 2010). Research has been on-going over the past two decades to identify the most suitable alloy combination that satisfies all the necessary properties of a solder for application in microelectronic assembly and electrical components.

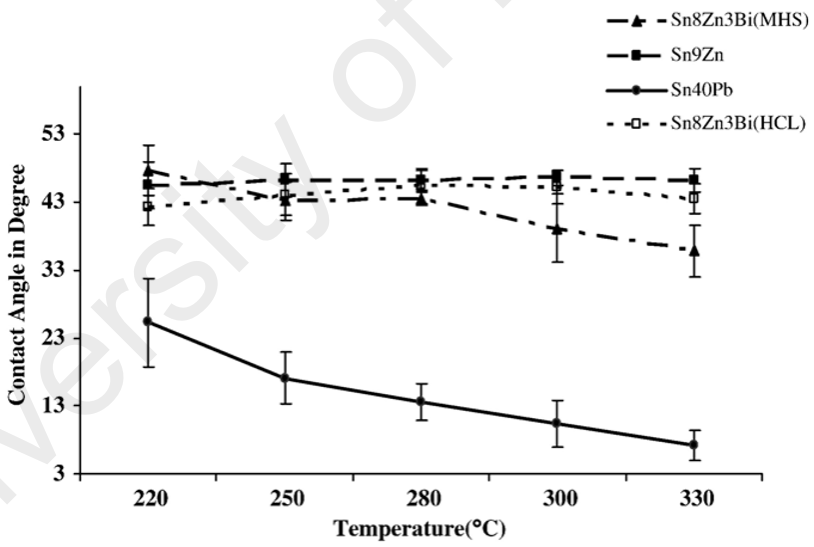

Figure 2.7 : Temperature effect on the contact angle of Sn-40Pb, Sn–9Zn and Sn–8Zn–3Bi solder alloys (Mayappan, Ismail, Ahmad, & Ariga, 2006)

Another potential alternatives to Sn-based solders is Sn-Ag solder alloy, which has a melting temperature of 221°C (Fu Guo, 2006). Studies on the eutectic alloy with the Sn-3.5wt.%Ag composition have demonstrated good joint strength together with excellent

wettability when applied to the Cu substrate, and high resistance to creep (Gao, Takemoto, & Nishikawa, 2006). The microstructure of this alloy has a Sn-Ag eutectic mixture and a primary β-Sn phase, which precipitates within intermetallic Ag_3Sn as shown in Figure 2.8. The Ag_3Sn IMC phase appears in the form of thin platelets that develop due to the solidification behavior variation in the Sn-3.5 wt.%Ag system (Vianco & Rejent, 1999). Despite the Sn-Ag solder alloy having notably good properties, it has been shown that much greater improvement could be achieved by adding small amounts of Cu (Lin, Srivatsan, Wang, & Kovacevic, 2006). Another study demonstrated that the addition of 0.5wt.%Cu particles helped the Cu dissolve completely in the Sn-dominant solder alloy. Under normal soldering conditions, the presence of Cu in the Sn-Ag solder alloy produced Cu_6Sn_5 and Cu_3Sn IMCs. This new Sn-Ag-Cu (SAC) Pb-free solder combination has better wetting and mechanical properties such as high creep resistance compared to other Sn-based solders (Guo, Lucas, & Subramanian, 2006). Solder joint mechanical properties can also be enhanced by controlling the cooling rate throughout the soldering process. This is because the cooling rate during solder joint solidifications is influenced by the joint size, how fast the heat source is removed from the joint and the environment surrounding the joint. Thus, it is crucial to have a good understanding of the relationship between the microstructural development, the cooling rate and mechanical properties of a solder joint. The SAC ternary eutectic composition of solder alloys has thus generated great interest and several researchers have reinforced the basic Sn-Ag solder alloy by varying the Cu element percentage.

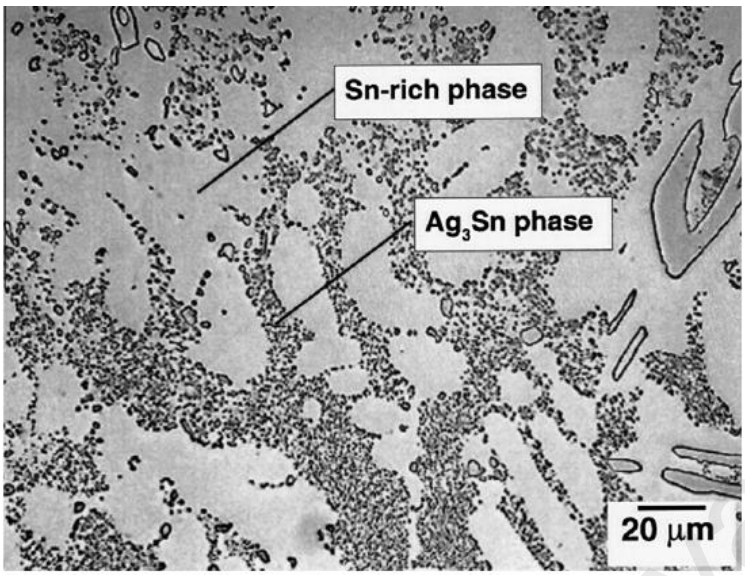

Figure 2.8 : Typical microstructure of eutectic Sn-3.5wt.%Ag solder alloy (Vianco & Rejent, 1999)

When using the solder alloy with a composition of three elements (ternary system) it is beneficial to refer to a phase diagram to determine the liquidus and solidus temperatures, and extract information on intermetallic phase formation (Kattner, 2002). According to the Sn-Ag-Cu phase diagram in Figure 2.9, SAC Pb-free solders are located in the Sn-rich corner within the Sn-(2.0-4.0wt.%Ag)-(0.5-1.0wt.%Cu). Most current Pb-free solder alloys are based on this Sn-rich corner (Moon, Boettinger, Kattner, Biancaniello, & Handwerker, 2000). Suganuma reported that the eutectic composition of the SAC ternary alloy is around that of the Sn-3.0wt.%Ag-0.7wt.%Cu solder alloy (Katsuaki Suganuma, 2006). Later on, an attempt was made to study the effect of adding Cu to SAC Pb-free solder alloys on the tensile properties (Shohji, Osawa, Matsuki, Kariya, Yasuda, & Takemoto, 2008). The study showed that the tensile strength of the solder joint is sensitive to the addition of Ag and Cu. The tensile strength increased with an increase in Ag and Cu amount. It was concluded that the eutectic SAC or the near-eutectic alloy appears to be at least comparable to the eutectic Sn-Pb solder alloy.

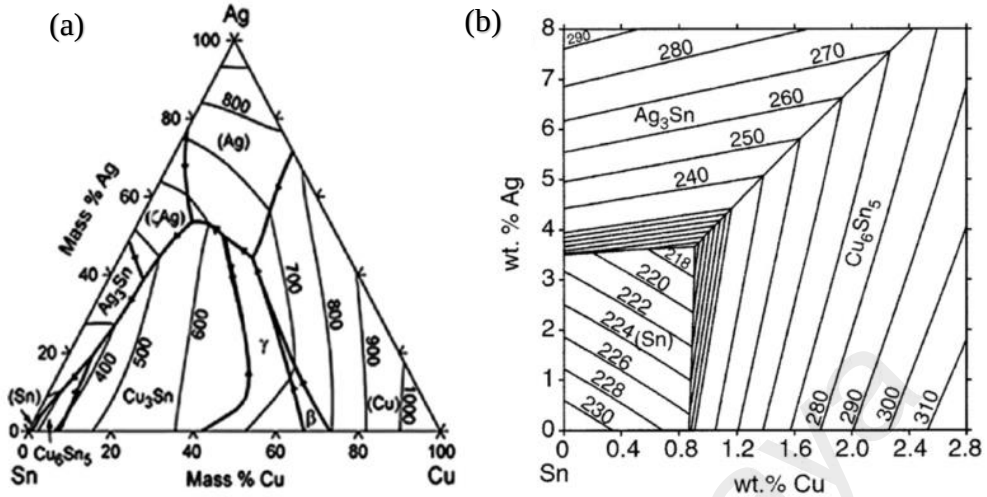

Figure 2.9 : Phase diagram of (a) Sn-Ag-Cu ternary eutectic reaction and (b) Sn-rich corner (Moon, Boettinger, Kattner, & Biancaniello, 2000)

It is well-known that the interfacial microstructure of IMC in solder joints greatly affects the mechanical properties. It has also been noted that IMC is generally brittle in nature. IMC particle sizes is influenced by the undercooling behavior during solidification. A suitable thickness of IMC that form at the interface between solder and the substrate provides interfacial adhesion and excellent solder joint reliability (Guo, Choi, Lucas, & Subramanian, 2001). However, excessive intermetallic phase population will degrade solder joint reliability. Several attempts have been made to suppress IMC growth in the SAC solder alloy. It seems that further readjusting the SAC solder alloy by reducing the Cu content and substituting it with Co, Fe, Zn, Ni, and Al can control the growth of IMC and eliminate joint brittleness as well (Anderson, Walleser, & Harringa, 2007).

In another development, it was found that adding Ni, which is actually positioned on the left of Cu in the periodic table (see Appendix C), to the SAC solder alloy does not trigger IMC thickness expansion and the size of grains as-reflowed and after thermal aging are unaffected (Amagai, 2008). Other studies have indicated that the reaction

between the molten solder and Ni layer results in the formation of two IMC namely $(Cu,Ni)_6Sn_5$ and $(Ni,Cu)_3Sn_4$ at the joint interface. It was observed that $(Ni,Cu)_3Sn_4$ IMC comprise a thin and continuous layer while $(Cu,Ni)_6Sn_5$ IMC represents a discontinuous layer as shown in Figure 2.10 (Xia, Xie, Lu, & Chang, 2006; Yoon, Kim, & Jung, 2005). Such understanding is very important in relation to determining the appropriate thickness of IMC and the correct alloy material combination to be used in real applications.

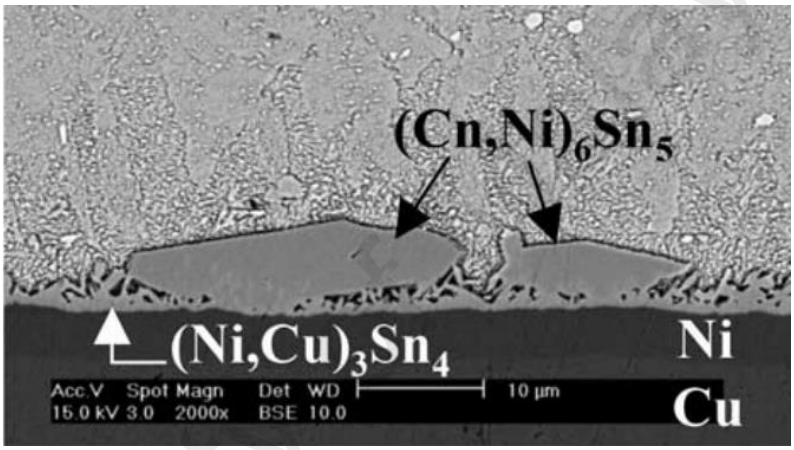

Figure 2.10 : SEM micrograph of SAC-Ni reflowed at 255°C for 10 minutes (Yoon, Kim, & Jung, 2005)

On the other hand, it has been reported that the addition of Al to SAC significantly affects IMC formation by reducing Sn and Cu activity after prolonged reflow (Kumar, Foudzer, Chan, Sharif, & Wong, 2010). During SAC-Al solder alloy solidification, two types of IMC form in the bulk solder: a thinner η-Cu_6Sn_5 phase and a layer of η_2-AlCu IMC. Upon reacting with the Cu substrate, the IMC transform into δ-Al_2Cu_3 IMC to reduce the growth of η-Cu_6Sn_5 and ε-Cu_3Sn IMC. This consequently improves joint strength. It is postulated that Al in SAC solder contributes to controlling the development of a fine IMC microstructure after prolonged reflow time.

In addition, various studies have demonstrated that Pb-free solders containing Co exhibit better shear ductility, improved solder quality, inhibited excessive formation of an IMC layer and reduced IMC growth (Amagai, 2008; Cheng, Gao, Nishikawa, & Takemoto, 2009). The IMC of $(CuCo)_6Sn_5$ forms when Co atoms substitute the Cu element in the Cu_6Sn_5 IMC of a SAC/Cu solder joint. Even a trace amount of Co nanoparticles (as low as 0.03wt.%) are capable of inducing beneficial changes to IMC growth at the joint interface. This phenomenon is similar to Ni addition because both elements have the same atomic radius. However, $(CuCo)_6Sn_5$ is thermodynamically unstable compared to $(CuNi)_6Sn_5$ IMC due to the weak driving force between Sn and Co to form an IMC layer. The search for appropriate Pb-free solder alloy combination with various base elements and reinforcements of the low-temperature solder alloy is ongoing. The aim is for the candidate alloys to satisfy the requirements of replacing traditional Sn-Pb alloy.

2.2.2 Mid-High Temperature Solder Alloy Candidates

To date, high-power electronic systems, such as in energy production systems, aerospace technologies, the automotive industry and telecommunication equipment involve operation at specific but higher temperatures (Figure 2.11). From a packaging perspective, there are a few crucial requirements for all advanced electronics applications. Among the requirements are the ability to withstand high electrical current, dissipate large amounts of heat, manage thermal expansion and tolerate stresses in order to achieve high reliability and economical servicing. Besides, the soldering materials must be environmentally friendly. Power electronic packaging requires the use of solder alloys that can withstand high temperature exposure (Suganuma, Kim, & Kim, 2009). The challenge with manufacturing high-temperature solders is then in their application at the first interconnection level during assembly in electronic devices.

Figure 2.11 : High-reliability solder alloys in high power electronic systems

Previously, Pb-based solder alloys, namely Pb-Sn and Pb-Ag with over 85wt.% Pb content were popular solder materials for mid-high temperature soldering applications. For instance, the common combinations of Pb-based high-temperature solders were Pb-5wt.%Sn and Pb-10wt.%Sn, with melting ranges of 308-312°C and 275-302°C, respectively. However, manufacturers must limit the usage of the solder alloy containing Pb since Pb is highly toxic, harmful to human health and the environment, and has been restricted by law.

One of the Pb-free solder candidates for coping with higher performance and temperatures like in automotive industry under-bonnet applications is the Zn-Al solder alloy. Zn-Al solder alloy records solidus and liquidus temperatures of about 370°C and 470°C, respectively (Kang, Sung, Jun, & Yun, 2009). Although, this alloy has poor creep resistance at higher temperatures. Kim et al. reported that adding of 2-3wt.%Cu to Zn–Al alloy increases strength and hardness (Kim, Kim, Kim, Kang, & Suganuma, 2008). The microstructure of Zn-Al-Cu solder alloy consists of a primary ε-phase, dendritic η-phase, and eutectic α-η phases. The eutectic α-η phases in the microstructure increase with increasing the Cu content volume, resulting in enhanced Vickers hardness and tensile

strength. These properties further improved when the Cu content is increased (Kang, Sung, Hun, & Yun, 2009). Nonetheless, Zn application in electronic packaging remains unclear due to its susceptibility to oxidation and corrosion, mainly during IMC layer formation.

Another Pb-free solder option that is commonly utilized as a medium-high temperature solder alloy is Au-based alloys. The Au-Sn solder alloy has great mechanical (strength and creep resistance) and thermal properties. It can also be reflowed without flux during soldering (Yoon, Noh, & Jung, 2010). Chidambaram et al. observed that the microstructure of Au-Sn consists of a brittle Au-5wt.%Sn phase (ζ phase) as shown in Figure 2.12 (Chidambaram, Hattel, & Hald, 2011). However, weaknesses of Au-based alloys are that Au is expensive, enormous IMC are formed, and the ζ phase is brittle.

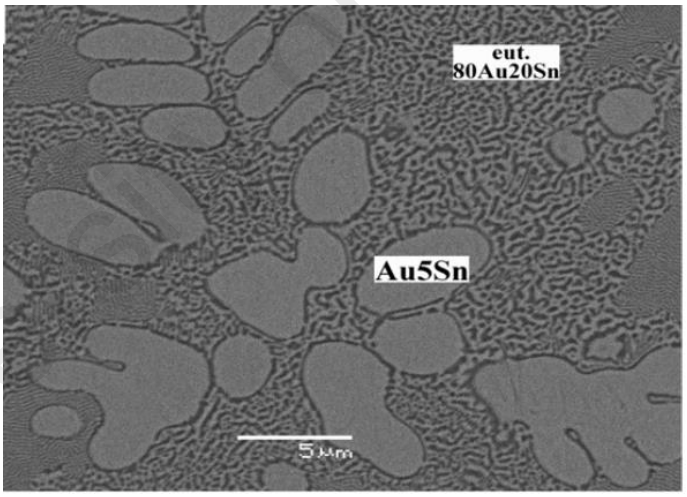

Figure 2.12 : SEM micrograph indicating the Au-5wt.%Sn phase in Au-Sn solder alloy (Chidambaram, Hattel, & Hald, 2011)

Despite the proposed Pb-free high-temperature solder candidates, the higher melting temperature of solders during the joining process remains a critical issue. It is known that high soldering temperature is important for wetting behavior. Thus, low-temperature solders do not really provide advantages in selecting a solder alloy. However, temperature

is considered a major factor influencing function in the base component or solderability. Because some electronic components (such as capacitors, connectors or power semiconductor devices) cannot presently withstand an increase in reflow temperature, it is believed that modifying or developing processing conditions to incorporate heat-resistant components is suitable. This can in fact be considered as another key factor in promoting Pb-free soldering.

2.3 Sn-3.0wt.%Ag-0.5wt.%Cu (SAC305) Pb-free Solder Alloy

Selecting a proper solder alloy facilitate good wetting, spreading or flow, as well as a neat finished surface. A large number of Pb-free solder alloys have been investigated intensively in order to achieve superior characteristics. It has been reported that Japanese companies are a strong driving force behind Pb-free manufacturing and accelerate Pb-free solder usage. Among numerous lead-free solders, Sn-based lead-free solder alloys seem very promising. The US International Printed Circuit (IPC) Association has reviewed Pb-free solder alloys candidates and recommended near-ternary eutectic Sn-3.0wt.%Ag-0.5wt.%Cu (SAC305) solder alloy to electronic producers (Wu, Yu, Law, & Wang, 2004). Since then, SAC305 has received much attention regarding Pb-free solder alloy development, as it is appropriate for most packaging applications in any temperature regime (Chen, Yu, Mei, Li, & Chen, 2014; Cheng, Gao, Nishikawa, & Takemoto, 2009; Mei, Chen, Guo-Quan, & Chen, 2012).

2.3.1 Solidus and Liquidus Temperature

From a manufacturing perspective, the melting/liquidus temperature is the first and foremost important factor in soldering. Soldering temperature is one of the most sensitive parameters in achieving quality soldered joints. Characteristically, soldering is conducted at temperatures 30°C above the melting point, or 20-40°C above the alloy's eutectic or liquidus temperature (Abtew & Selvaduray, 2000). The required operating temperature

in some assembly equipment, particularly in the automotive industry, is up to 175°C, which is relatively high compared to many other equipment. Therefore, the mechanical stability of the joint is degraded when the melting point approaches elevated temperatures. In addition, particularly die attachment in power semiconductor packaging requires a melting point of 280°C or higher (Liu, Lee, & Bachorik, 2013).

The solidus and liquidus temperatures of SAC305 solders of 217°C and 227°C respectively, which make them ideal for use at high operating temperatures (Kanchanomai, Miyashita, & Mutoh, 2002; Shnawah, Sabri, Badruddin, Said, & Ariga, 2013). Figure 2.13 presents differential scanning calorimetry (DSC) graphs that reveal the melting and solidification points of SAC305 solder alloy (Shnawah, Sabri, Badruddin, Said, & Ariga, 2013).

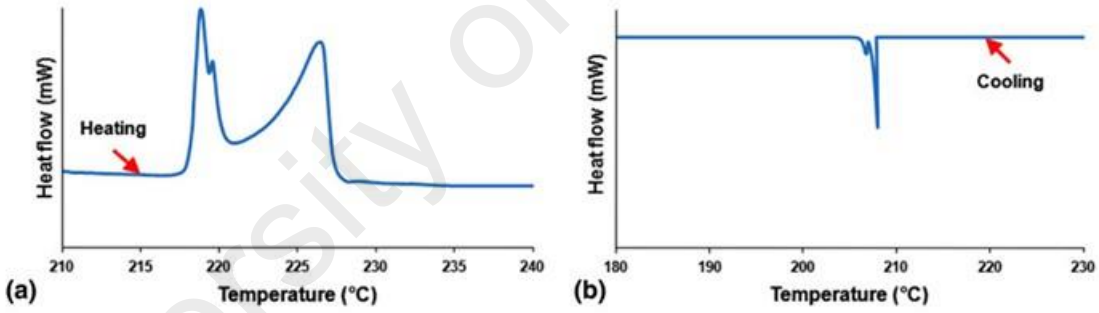

Figure 2.13 : DSC profile of (a) liquidus and solidus temperature, and (b) solidification onset temperature of Sn-3.0Ag-0.5Cu (SAC305) solder alloy (Shnawah, Sabri, Badruddin, Said, & Ariga, 2013)

Figure 2.14 illustrates XRD patterns of SAC305 at selected temperatures during solder heating by Pietriková et al (Pietriková, Bednarˇ, & Duriˇ, 2011). At the diffraction peak of 224°C, the primary β-Sn phase decreased, which indicates it has reached the melting point of the SAC305 solder alloy. A similar diffraction pattern was recorded during a process temperature increase (226–228°C) for β-Sn phase reflection. Much reduced peak

of Ag_3Sn phase was observed at this temperature level because the solder alloy was molten, therefore no crystallization occurred.

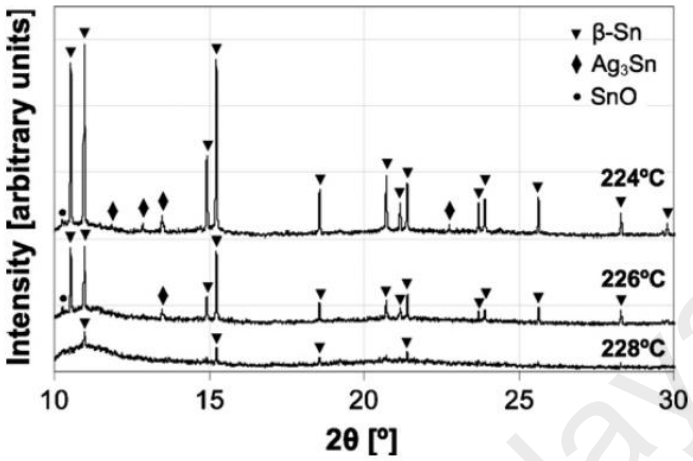

Figure 2.14 : XRD patterns of SAC305 at selected temperatures during solder heating (Pietriková, 2011)

2.3.2 Measurement of Mechanical Properties

In terms of mechanical stability, the solder is required to attain high joint strength, good hardness and long fatigue life. This is to ensure extended electronic circuit lifetime. Studies on mechanical properties are abundant, especially on joint strength. The tensile and shear strengths, creep, and stress relaxation behavior of Pb-free composite solder joints have in fact been widely investigated (Bai, Calata, & Lu, 2007).

Several factors affect the mechanical and electrical properties of solder joints, including the test method used, specimen preparation procedure, specimen geometry, solder volume, solder microstructure, reflow conditions, strain rate employed in the test and many more (Humpston & Jacobson, 2004). Variables such as time and temperature can be manipulated to attain varying joint strengths for one sample. It is noted that the majority of soldered joints in electronic packaging are not made to meet load-bearing requirements but focus is on electrical connectivity and thermal conductivity.

Joint strength in soldering reliability can be measured by tensile stress or compressive (shear) stress testing. The tensile stress, which is normally expressed as MPa, is calculated from the fracture load (F) employed to the test specimen divided by the contact area (A) as in the equation 2.1 bellow:

$$\sigma = \frac{F}{A} \tag{2.1}$$

2.3.3 Formation of Intermetallic Compound (IMC)

During the soldering process, a metal solvent action takes place when the hot molten solder comes in contact with the substrate metal surface (Cu substrate). The solder dissolves and penetrates into the metal interface. The solder and metal molecules then blend to form a new alloy, which is composed of partly substrate metal and partly solder. The solvent action known as wetting forms the intermetallic bond between the two parts as illustrated in Figure 2.15. This intermetallic bond is created from intermetallic compound (IMC) formation.

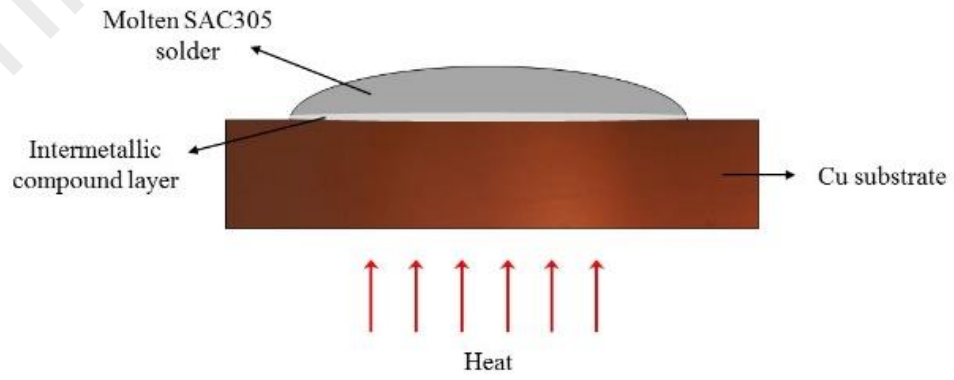

Figure 2.15 : Illustration of molten SAC305 solder wetting the Cu substrate to form an intermetallic compound layer

IMC layer formation is desirable because it provides good metallurgical bonding. A thin, uniform and continuous IMC layer is necessary for good bonding. Without the IMC layers, the solder joint is weak, easy to crack and harmful to electronic interconnections (Nai, Wei, & Gupta, 2009). However, if the IMC layer is too thick, it will degrade solder joints reliability. This is because the IMC are generally brittle and have weak bonding strength, thus promoting structural defects due to mismatching physical properties, such as the thermal expansion coefficient and elastic modulus (Zhang, Xue, Zeng, Gao, & Ye, 2012). Such microstructural formation at the interface must be inhibited within optimization conditions.

The IMC layer reportedly grows proportional to increasing soldering time, whereby the soldering temperature is higher than the melting temperature of the solder alloy (Lee & Mohamad, 2013). In the case of solder joint of SAC305 with Cu substrate (a substrate metal acting as a common conductor), the IMC layer that forms between the solder alloy and the Cu substrate can be divided into two types: Cu_6Sn_5 and Cu_3Sn, as derived from the binary Cu-Sn phase diagram shown in Figure 2.16 (ASM International, 2004).

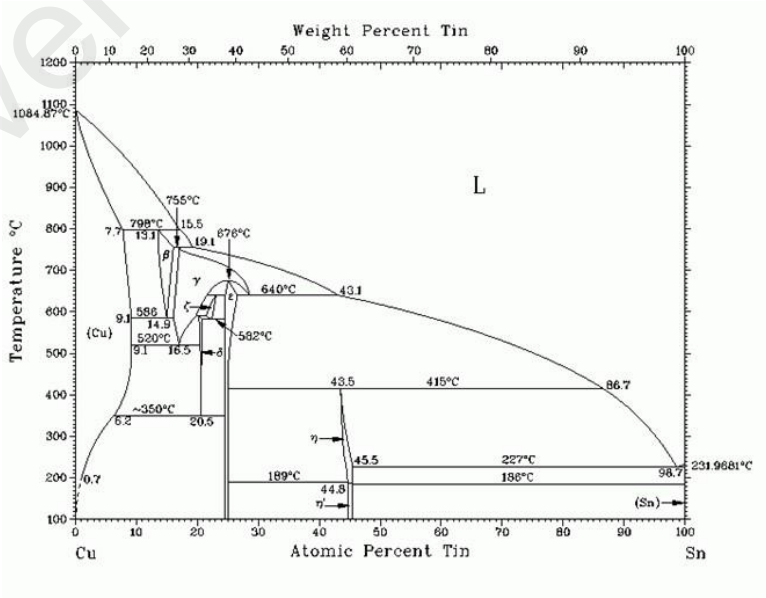

Figure 2.16 : Cu-Sn phase diagram adapted from (ASM International 2004) in determining the IMC phase

Figure 2.17 concisely illustrates the interfacial reaction of SAC305/Cu substrate during soldering. As the melting point of SAC305 is approximately 217°C, the soldering process takes place at around 250°C and above. The solder alloy to wet the Cu substrates is in molten condition, as seen in Figure 2.17(a). The Cu substrate in contact begins into dissolve to the molten solder in this stage to form a super-saturated layer as shown in Figure 2.17(b). The diffusion of Sn atoms through the molten SAC305 towards Cu at the substrate interface will form η-Cu_6Sn_5 (Figure 2.17(c)). Then η-Cu_6Sn_5 continues to grow and the thin ε-Cu_3Sn particle layer nucleates in the middle to make a Cu_6Sn_5/Cu_3Sn/Cu sandwich structure at the contact interface as illustrated in Figure 2.17(d). When the temperature exceeds 375°C, ε-Cu_3Sn gradually becomes the primary phase of the IMC layer.

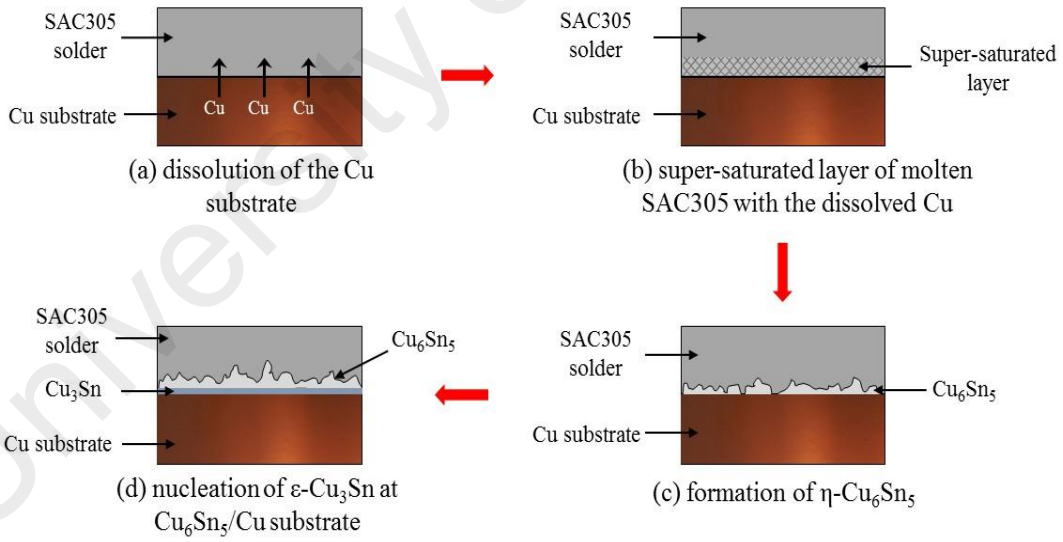

Figure 2.17 : Schematic of the interfacial reaction of SAC305/Cu during soldering

The actual formation of IMC phases is controlled by local thermodynamic equilibrium at the Cu/Sn interface. The Cu_6Sn_5 phase grows into a scallop-like morphology, during the substrate/solder interactions stages to provide a higher driving force for precipitation than the Cu_3Sn phase (Lord & Umantsev, 2005). The thin, planar Cu_3Sn phase underneath the Cu_6Sn_5 phase layer precipitates due to the thermodynamically unstable Cu_6Sn_5 phase which gives rise to the reaction as in the equation 2.2 below (Gao, Takemoto, & Nishikawa, 2006). It may also be contributed from the inter-diffusion of Sn atoms through the Cu_6Sn_5 phase which then react with Cu atoms from the metal substrate as in equation 2.3 below. (Peng, Monlevade, & Marques, 2007). Conversely, the Cu_3Sn phase could dissolve and react with Sn atoms to form Cu_6Sn_5 as in equation 2.4.

$$Cu_6Sn_5 + 9Cu \rightarrow 5Cu_3Sn \tag{2.2}$$

$$3Cu + Sn \rightarrow Cu_3Sn \tag{2.3}$$

$$2Cu_3Sn + 3Sn \rightarrow Cu_6Sn_5 \tag{2.4}$$

The growth of IMC in solder joints is an ordinary diffusion process that is controlled by the inter-diffusion of the substrate and solder element (Li, Qu, Zhao, Zhao, & Ma, 2013). At the beginning of soldering, IMC grows quickly because the formation is controlled by reaction diffusion. Upon IMC formation, further growth is mainly controlled and reduced by grain boundary diffusion. An interfacial IMC layer continues to grow even at room temperature after the solder joint has completely solidified owing to its low activation energy. Figure 2.18(a) and (b) show the cross-sectional microstructure and top-view morphology of the $Cu_6Sn_5/Cu_3Sn/Cu$ substrate multilayer, as observed by Wang et al. (Wang, Gao, Ma, & Qian, 2006). A scallop-type Cu_6Sn_5 and uniform Cu_3Sn phase layers are detected in the cross-sectional view. A rougher surface

and more crystalline grains are recorded in the top view morphology of Cu_6Sn_5 IMC phase.

In high temperature storage conditions, the IMC growth behavior has been shown to follow a volume diffusion mechanism with IMC thickness increasing proportional to the time squared. Hence, the IMC layer thicken and the Cu_6Sn_5 morphology changes from a scalloped structure to a planar layer (Harcuba & Janeček, 2010; Zhang, Xue, Zeng, Gao, & Ye, 2012). In contrast, the Cu_3Sn phase layer remains even and planar but increases in thickness with increasing aging temperature and time.

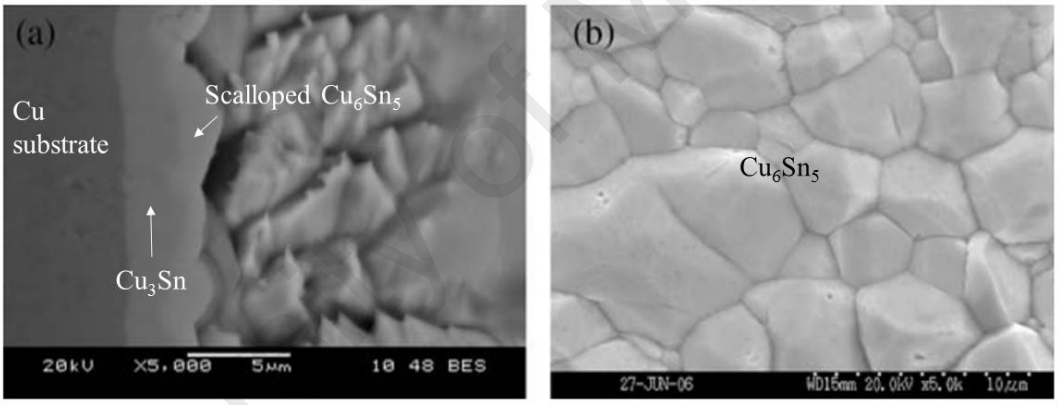

Figure 2.18 : (a) Cross sectional and (b) top view morphology of $Cu/Cu_3Sn/Cu_6Sn_5$ (Wang, Gao, Ma, & Qian, 2006)

2.4 Previous Research on SAC305 Solder Alloy

Some years ago, a proposal was made to study the SAC solder alloy for its suitability as a high-temperature solder alloy (Che, Zhu, Poh, Zhang, & Zhang, 2010). Layers et al. studied the thermal performance of SAC305 as a die-attach material in an elevated insulated-gate bipolar transistor (IGBT) (Layers, Cao, Wang, & Ngo, 2011). Failure usually occurs in the solder sandwiched between the direct bonded copper module and substrate metal when temperature or power cycling load is employed in the IGBT power

module. After the initial crack starts at the solder joint interface, the crack eventually expands. This has become one of the problems that need resolving. Therefore, a novel design involving substrates and a copper base plate is necessary to reduce risks during assembly. However, the major concerns with high-temperature applications are the electrical and thermal conductivity characteristics and long-term mechanical stability of the interfaces formed with the module and substrate metal at high temperature operation. Figure 2.19 shows a typical die bonding arrangement in a power module semiconductor where the solder alloy is applied.

The melting point of SAC305 is around 220ºC and a higher reflow temperature of at least 250ºC is required (George, Das, Osterman, & Pecht, 2011). However, the rapid growth of IMC between solders and the contact metallization on both semiconductor devices result in brittle fracturing of the joints. Therefore, a composite solder alloy can be enhanced by adding other elements to improve the solder alloy performance to be appropriate for high power applications (Chen, Yu, Mei, Li, & Chen, 2014; Li, Agyakwa, & Johnson, 2012).

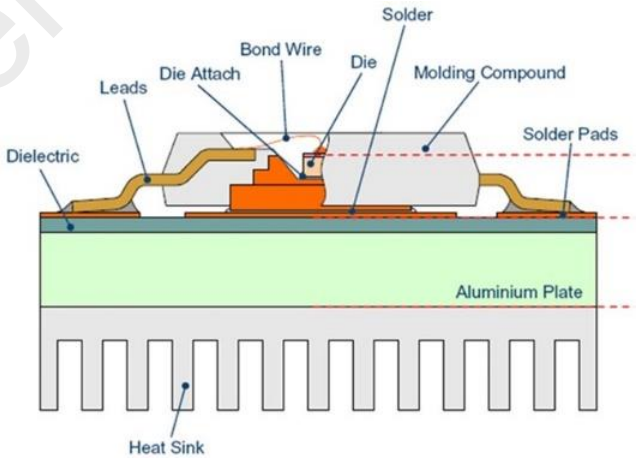

Figure 2.19 : Graphical Presentation of Die Bonding in a Typical Power Package (Zheng, Ngo, & Lu, 2015)

2.4.1 Enhancement of composite SAC305

The composite approach was developed mainly to enhance service performance, including service temperature capability. In other words, the aim is to re-engineer the composite solder microstructure and homogenize the solder joint deformation in order to improve the mechanical properties of the solder joint, such as creep and thermo-mechanical fatigue resistance.

Appropriate joint strength of solder joint in electrical products is essential to meet the performance requirements of the interconnections. A quarternary solder system with a fourth element added to the SAC305 solder matrix is a principal consideration in achieving enhanced solder joints. The system should also fulfils certain conditions for enhanced solder joint service performance. Though the intention of adding another element is to improve the mechanical properties, the added reinforcement should not affect the electrical properties and manufacturability of interconnections adversely, and the solder alloy's melting point should not be modified. However, the addition may efficiently ameliorate the service temperature of the base solder material by enhancing the thermo-mechanical fatigue features of the solder alloy (Guo, 2006).

Various particulate reinforcements have been tried in engineering a composite solder. For example, some researchers studied re-engineering Pb-free composite solders by adding nanoparticles. The technique is meant to strengthen the composite solder by particle diffusion which may increase the resistance to solder deformation through hindering dislocation motion and resisting the grain boundaries sliding tendency in the solder matrix (Guo, 2006). Chellvarajoo et al. re-engineered composite SAC305 solder alloy by adding iron nickel oxide (Fe_2NiO_4) nanoparticles to improve the solder joint's reliability (Chellvarajoo, Abdullah, & Samsudin, 2015). The researcher reported that IMC growth degraded by increasing the percentage of Fe_2NiO_4 in the SAC305 solder matrix

joined to Cu substrate. When the Fe_2NiO_4 nanoparticle percentage was raised, the newly formed nanoparticle bonds inhibited the entrance of Cu molecule hence retarding IMC growth. However, the optimum efficiency on the mechanical properties was not discussed.

El-Daly et al. added SiC nanoparticles to SAC305 solder alloy to refine the microstructure of the composite-based solder (El-Daly, Desoky, Elmosalami, El-Shaarawy, & Abdraboh, 2015). The SiC nanoparticles enhanced the nucleation rates of the IMC phases and refined the β-Sn matrix due to the homogeneous dispersal of SiC nanoparticles (Figure 2.20). Additionally, SAC305 with SiC nanoparticles added exhibited dislocation interactions within the particles, which interrupted the dislocation motion to improve the mechanical strength.

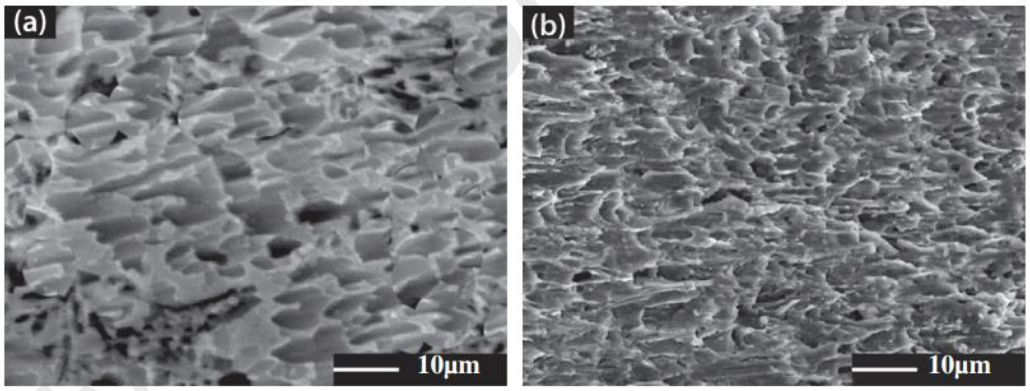

Figure 2.20 : Fractography of (a) SAC305 and (b) SAC(305)-0.7SiC solder alloys (El-Daly, Desoky, Elmosalami, & El-Shaarawy 2015)

Nanoparticle addition to SAC305 with the various advantages has attracted much interest, especially in the academic field. However, there are still no reports of practical solder joint technology application where the Pb-free solder properties requirements are fulfilled (Wu, Xue, Wang, Lie, & Han, 2016). Therefore, at present, innumerable studies

regarding SAC305 solder enhancements are ongoing vigorously to broaden knowledge of Pb-free solder joint technology.

Meanwhile, the melting behavior of Pb-free solder alloys in high-temperature operation is crucial. In many instances, industries have defined the melting temperature range for elevated-temperature operation for electronic products between 270ºC and 350ºC (Kim, Lee, Lee, & Kang, 2014; Sharif, Lim, Made, Lau, & Phua, 2013). The SAC305 solder alloy is often recommended for general purpose applications of devices operating at usual temperatures of around 57°C (Yao & Basaran, 2013). As mentioned above, the SAC305 solder alloy with an appropriate reinforcement will amplify the joint reliability and strengthen the solder joint. For these reasons, SAC305 may presently be considered as a suitable alloy for both general purpose soldering and systems operating at high temperatures (Wang, Wang, & Ke, 2014).

Chen et al. investigated the performance of soldered SAC305 joints in high-temperature tests compared with sintered nanosilver joints (Chen, Yu, Mei, Li, & Chen, 2014). The study revealed that SAC305 solder joints exhibit greater elongation than nanosilver joints during shear strength testing. It can be deduced that SAC305 joints have superior ductility behavior due to the excellent viscosity properties. This finding is significant because a solder with good ductility, which is relevant at the component level, is a must under static loading. Under dynamic loading, ductility plays a key role in structural response, which is associated with energy absorption. In other words, the better ductility a solder has, the stronger is the ability to absorb energy and the higher the resistance to failure (Yu, Lee, Chen, & Duh, 2014). However, SAC305 solder joints tend to crack easily due to the arisen of IMC formation along the joint interface.

An attempted has been made to reinforce composite SAC305 solder with carbon-based of fullerene (FNS) nanomaterial in terms of physical and mechanical properties tested at

250°C~280°C (Chen, Wu, Liu, Xia, & Liu, 2015). It was found that adding a suitable amount of FNS can effectively improve the mechanical properties of solder joints. The notable enhancements in joint strength and microhardness after FNS nanoparticle addition were on account of the microstructural refinement and homogenous dispersion of FNS nanoparticles in the solder matrix. Furthermore, the FNS nanoparticles mitigated the negative effect of thermo-migration on the microstructure, hence rendering the modified material a potential solder material for use under extreme service conditions. However, the key point that needs to be understood is that reinforcements do not alter the melting point of the solder alloy but may efficiently augment the service temperature of solder materials.

2.4.2 Aging Treatment

There is a growing demand for solder joints in electronic interconnections that can remain stable under extreme conditions, such as elevated-temperatures, impact loading and thermal burdens. The focus is still on finding suitable Pb-free solders. In general, electronic devices such like those in telecommunication electronic products experience -55°C to 100°C during operation. In critical applications, for instance in the automotive industry where under-the-hood and engine-mounted electronics typically experience many thermal cycles, operating temperatures can reach up to 165°C and higher (Gayle, Becka, Badgett, Whitten, & Pan, 2001; Puttlitz & Stalter, 2004; Shen, Cao, Zhai, Zhao, & He, 2014). Exposure to temperature and electrical stress throughout the running time can easily lead to IMC layer development. Due to the brittle nature of the IMC layer, excessive IMC layer thickness will badly degrade solder joint bonding strength, thereby reducing the reliability of electronic devices (Shohji, Osawa, Matsuki, Kariya, & Yasuda, 2008). Accordingly, solder alloy reinforcement particularly to control the IMC layer formation is being investigated extensively.

As highlighted above, it is been reported that Pb-free solder alloys such as the SAC alloy with a high melting point are potential candidates for high temperature applications (George, Das, Osterman, & Pecht, 2011; Huangl, Lee, Li, & Chen, 2000). However, not many studies have been done to evaluate the performance of Pb-free solder at 150°C. In high-temperature storage, IMC growths has been shown to follow a volume diffusion mechanism with IMC thickness increasing proportional to the time squared. An attempt has been made to restrain IMC layer growth during isothermal aging by adding Zn and nano-TiO_2 to Sn-3.5wt.%Ag-0.5wt.%Cu solder alloy (Tang, Li, Chen, & Pan, 2014). According to the study, the researchers believe that Cu–Sn IMC formation during aging can be controlled by volume diffusion.

Hu et al. studied in detail IMC formation and the fractography of SAC305/Cu solder joints after aging treatment at 150°C for various durations through single-lap shear testing with a constant displacement rate (Hu, Xu, Keer, Li, & Jiang, 2016). The morphology of interfacial IMC changed from scalloped shape to planar shape with longer aging time as shown in Figure 2.21. It was concluded from the study that Cu-Sn IMC phase formation is controlled by the diffusion mechanism, as the growth after aging treatment displayed a linear function of the square root of aging time. The flattening of the solder/Cu_6Sn_5 IMC interface during isothermal aging contributed to the shear joint strength reduction.

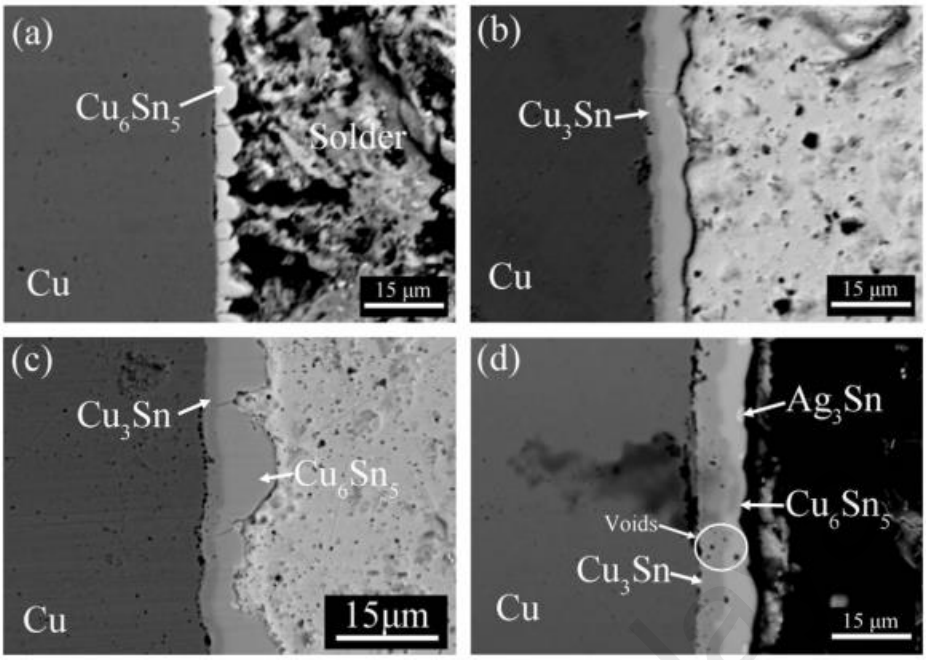

Figure 2.21 : Cross-sectional morphology of SAC305/Cu interfaces aged at 150 °C for, (a) 48 h; (b) 144 h; (c) 240 h; (d) 456 h (Hu, Xu, Keer, & Li, 2016)

Introducing an adequate amount of a rare earth (RE) element to the SAC305 solder alloy may effectively improve the solder joint's reliability during isothermal aging treatment. It has been found that RE elements have a crucial role in microstructural refinement and thinning the IMC layer. Tu et al. investigated the effect of RE Cerium (Ce) addition on the microstructure and tensile strength of a SAC305 solder joint (Tu, Xi, Yu, & Wang, 2017). They proved that the shear strength of the SAC305 solder joint with Ce added improved, as observed in the as-soldered and aged samples (summarized in Figure 2.22). The existence of an appropriate amount of Ce in the solder alloy aggregated the Ag_3Sn IMC particles on the IMC layers surface. These Ag_3Sn IMC hindered the IMC layer growth, and acted as small linking skeletons between Cu_6Sn_5 particles to strengthen the solder joint. However, in the study, increasing the Ce content to >0.15wt.% did not improve the ductility behavior, due to the increasing amount of brittle and rougher $CeSn_3$ particles. As so much attention has previously been directed to the actual effects of aging

on solder joint strength, it is worthwhile investigating the mechanism of IMC growth during aging process and at the same time its effect on solder joint reliability in other attempts of SAC305 solder alloy enhancement.

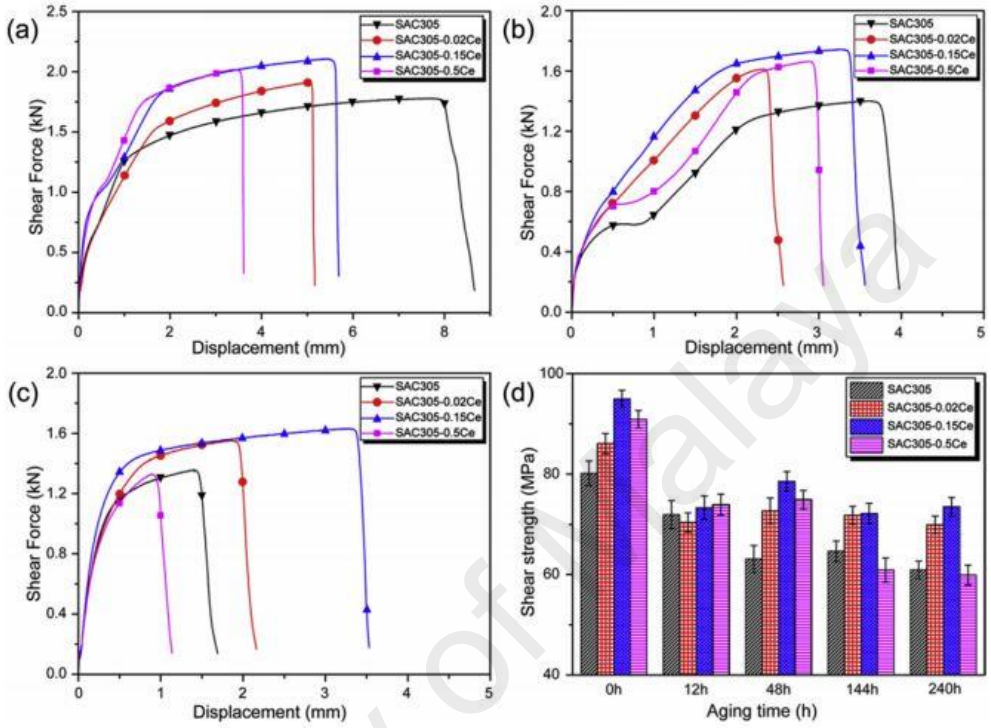

Figure 2.22 : Shear test of SAC305 solder alloy with x-Ce element added and joined to Cu after isothermal aging for different times of (a) 0 h, (b) 48 h, (c) 240 h. Figure (d) is a statistical graph of strength with aging time for different SAC305-xCe/Cu solder joints (Tu, Yi, Wu, & Wang, 2017)

2.5 Soldering Technique Modification

Another approach to advance the performance of solder joints is by modifying the in-situ joining method. The technique employed in the soldering process should be compatible with standard processes in industrial applications.

2.5.1 Metal Composite Preforms

Some studies address adding an interlayer structure in the joining technique, especially for dissimilar bonding. One instance is in transient liquid phase (TLP) bonding that is an

established joining technique for die bonding in high-temperature electronic system applications. In conventional methods, a thin layer of a low melting point metal serves as the interlayer material for effective bonding in the TLP process. Liu et al. developed a new composite preform using a Ag core layer in the TLP bonding process (Liu, Lee, & Bachorik, 2013). The joint had a longer life-time and IMC growth was reduced with this technique. However, the joint had low tensile strength due to the voids formed at the joint interface.

In another study, a new technique was proposed where an interlayer structure is utilized for dissimilar bonding in joining. Yang et al. reported that using Ti and Ni interlayers enhance the contact reaction for ceramic joining (Yang, Lin, He, Wei, & Xing, 2014). Adding Ti-Ni interlayers apparently increases interfacial region hardness.

2.5.2 Substrate Metallization

Currently available processes for a high-power module on a direct bonded copper substrate with die requires the additional step of metallizing the die back side and the substrate material (Drevin-Bazin, Lacroix, & Barbot, 2013). One of the most common base materials for die and substrate material metallization is gold (Au)-based material. Although Au-based materials such as Au-20wt.%Sn are currently used in high-temperature soldering applications, they are very expensive and exhibit poor workability and wetting.

2.5.3 Porous Metal Interlayer

Porous copper (Cu) or Cu foam is considered a potential material in various engineering fields due to its desirable properties, including excellent thermal conductivity, light-weight material, sound absorber and high liquid and gas permeability (Banhart, 2001). In view of the advantages of porous Cu, researchers recommend this interlayer type as prospect reinforcement in applying joining technology applications.

Another means of advancing Sn-Ag-Cu (SAC) solder alloy performance is to add porous metal to the joint material. Porous metal is preferred because it has excellent thermal conductivity and can serve as interconnections (Thewsey & Zhao, 2008). Porous metal for high-temperature joining was utilized in a study by Zaharinie et al. (Zaharinie, Moshwan, Yusof, Hamdi, & Ariga, 2014). The technique increased the mechanical properties of the braze joint when a Cu/Ni porous metal interlayer was added during the braze joining of metal and ceramic by altering the thermodynamic activity near the ceramic portion of the sapphire site. This led to the formation of ductile IMC for better joining. It was also proven that the Cu/Ni porous composite interlayer can significantly absorb residual stress left from cooling, resulting in successful joining. Despite such promising findings regarding brazing, the use of a porous metal interlayer has not been attempted in solder joining.

Based on elemental selection criteria and consideration discussed earlier, another approach to enhance the reliability of Pb-free solder is to modify the physical process of soldering by utilizing a porous Cu interlayer in a Pb-free Sn-3.0wt.%Ag-0.5wt.%Cu solder joint. Degischer et al. have also reported that metallic foams with attractive mechanical, electrical, acoustic, and thermal properties have been applied in cooling electronic components, jet engines, adsorption chillers, sound absorbers, and compact heat exchangers (Degischer, 2002).

2.6 Summary

This chapter presented an overview of various issues, past investigations and current technology pertaining to various aspects of soldering encompassing Pb-free solder alloys, Pb-free solder enhancements, IMC formation, microstructural determination and the solderability of low and mid-high temperature solder alloys. These aspects are also discussed in relation to isothermal aging of solder joint. Research findings thus far are not

sufficient to meet the requirements for acceptable solder joint quality and feeble joining is still exhibited due to some drawbacks with reliability. As a different approach to alloy development for solving problems and obtaining high quality solder joints, the concept of a porous metal interlayer in soldering applications has been introduced. Therefore, the expected outcome of this research is a porous interlayer that provides a good mechanical properties on solder joining.

CHAPTER 3: RESEARCH METHODOLOGY

3.1 Introduction

This chapter introduces the details of the procedures designed for this research work. Pb-free solder alloy SAC305 was the solder material used to join Cu substrates. A porous Cu interlayer was added in the middle of the joined part in order to study the effect of adding an interlayer on the solder joint. The solder joint without a porous Cu interlayer addition was the control sample. The overall flowchart of the methodology for the research work is given in Figure 3.1, which includes the sample preparation method, sample evaluations, and characterization techniques. For each treatment, data analysis was done to make comparison with the control sample. In addition, mechanical testing and microstructural observations were also performed on the solder joints under two conditions, namely as-soldered treatment and aging treatment.

3.2 Substrate Metal

Copper is widely employed for contact metallization in conventional electronic assembly (Zhang, Xue, Zeng, Gao, & Ye, 2012). In the present study, Oxygen-Free High Conductivity (OFHC[1]) Cu with high purity (99.99 wt%) was used as the substrate metal. Figure 3.2 illustrates Cu rod as substrate with 8 mm diameter and 25 mm length.

3.3 Solder Material

The solder material utilized in this study is Sn-3.0wt.%Ag-0.5wt.%Cu (SAC305), manufactured by Nihon Handa Co., Ltd. (Tokyo, Japan) in paste form. Figure 3.3 and Figure 3.4 represent the solder paste physical and particle morphologies respectively, observed under SEM. The average particle size of the SAC305 was 15-50 μm.

[1] Registered trademark of Phelps Dodge Specialty Copper Products.

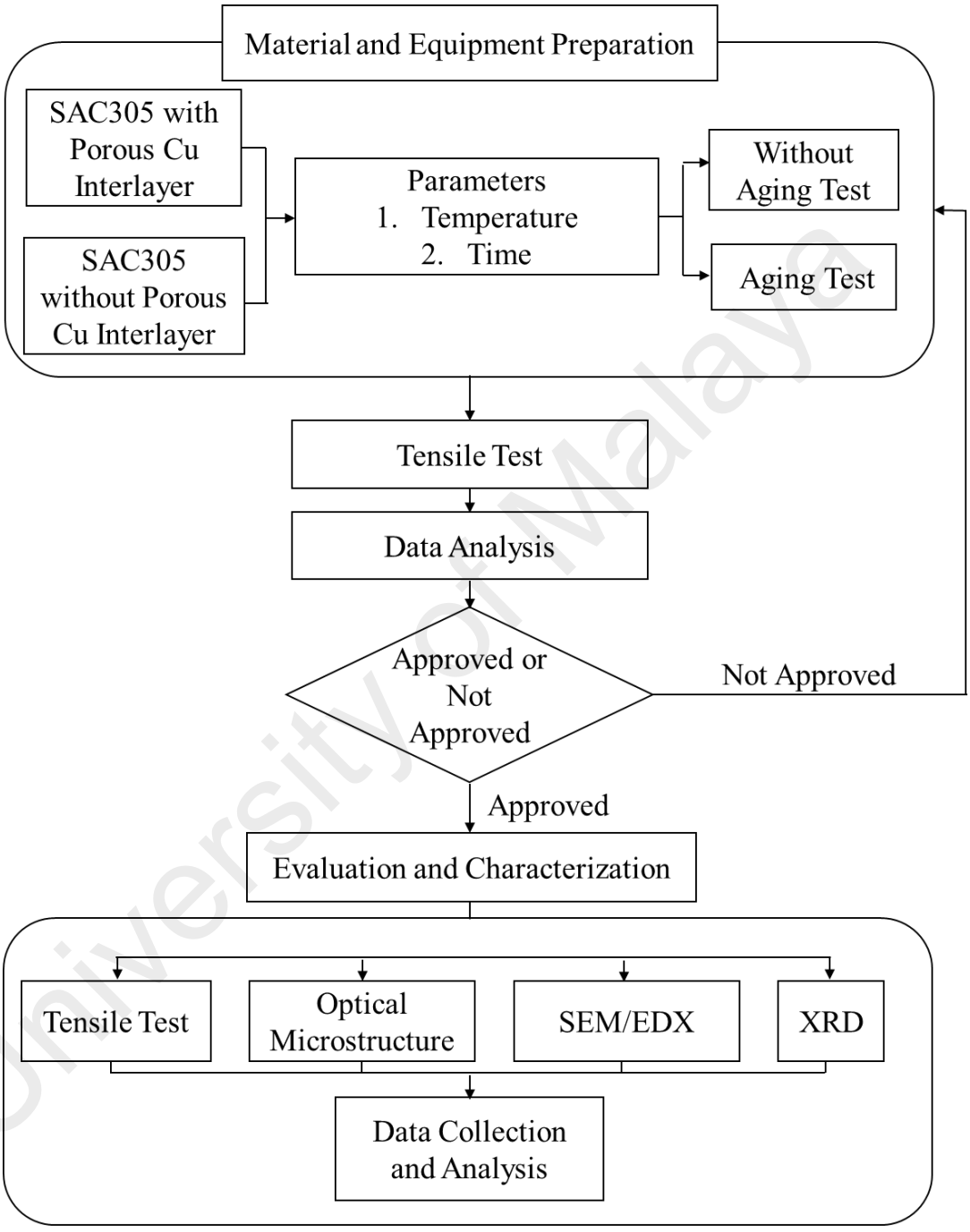

Figure 3.1 : Research work flow chart

Figure 3.2 : High purity OFHC copper rods (99.99% purity)

Figure 3.3 : Solder paste of Sn-3.0wt.%Ag-0.5wt.%Cu (SAC305)

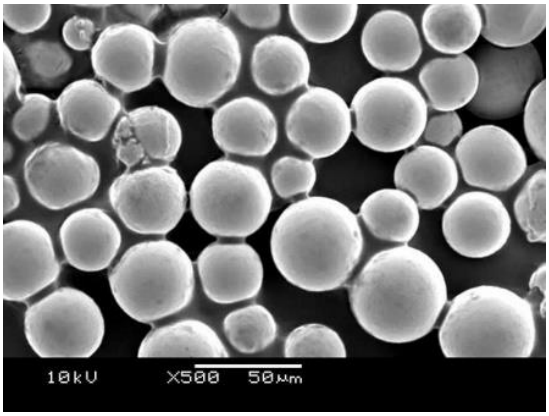

Figure 3.4 : SEM micrograph of typical particle morphology

Details of the chemical composition and general properties of the SAC305 solder alloy are listed in Table 3.1 and Table 3.2, respectively.

Table 3.1 Chemical composition of SAC305 solder alloy (wt%) (Yamakawa, 2013)

Solder alloy	Cu	Ag	Bi	Fe	As	Ni	Pb	Sb	Sn
Sn-3.0Ag-0.5Cu	0.516	3.083	0.011	0.002	0.005	0.001	0.022	0.015	Bal.

Table 3.2 Mechanical properties of SAC305 solder alloy (Kanchanomai, Miyashita, & Mutoh, 2002)

Solder alloy	Melting temperature, °C	Tensile strength, MPa	Young's modulus, MPa	Hardness, HV
Sn-3.0Ag-0.5Cu	217	50.6	54	13.3

3.4 Porous Cu Interlayer

A porous metal with closed-cell structure was placed in between two joining materials in order to study its effect on the solder joint. In this study, porous Cu was selected owing to its excellent conductivity and ability to react with molten solder at the atomic level that facilitate good chemical bonding between Cu and Sn. Figure 3.5 shows an as-received porous Cu interlayer piece. Two types of porous Cu interlayer were used and denoted by 15 ppi (pores per inch) (P15) and 25 ppi (P25). The pore size was smaller at higher ppi values.

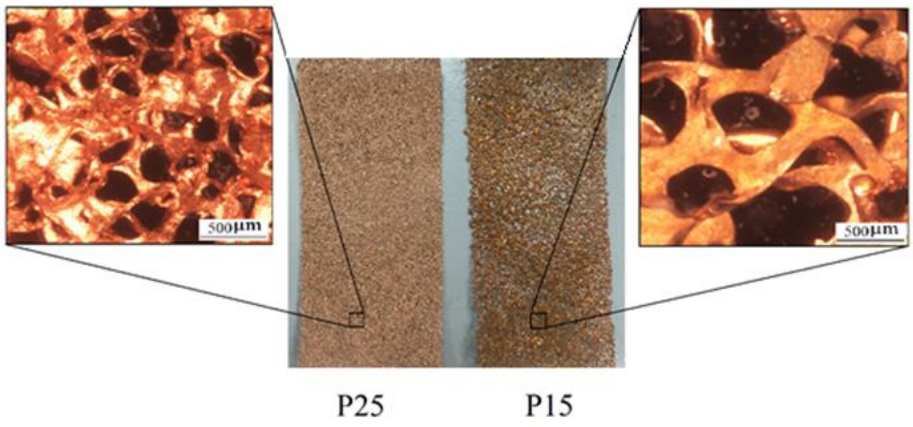

Figure 3.5 : Porous Cu interlayer

3.4.1 Uniform Thickness Interlayer

It is necessary for a solder joint to have an appropriate gap distance for good solderability. Therefore, a thin solder joint was obtained by simply providing a uniform, thin interlayer before reassembling it in the middle of the solder joint. The thicknesses of as-received P15 and P25 porous Cu interlayers were 1.23 mm and 1.53 mm, respectively. The interlayers were rolled manually with a solid cylinder as illustrated in Figure 3.6, to obtain uniform layers with 100 μm thickness. The rolled porous Cu was then cut into circular pieces with 8 mm diameter.

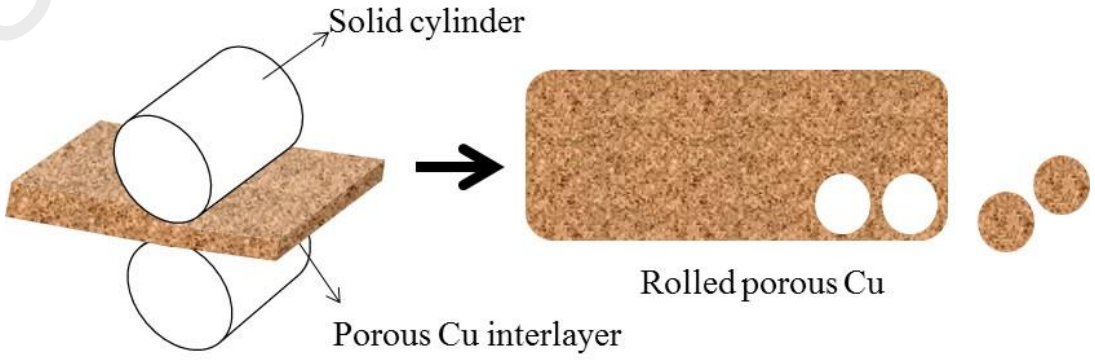

Figure 3.6 : Schematic illustration of porous Cu rolling by using a solid cylinder

3.4.2 Porosity Measurement

The porosity of porous Cu interlayer affects the penetration behavior of the molten solder during soldering process. The porosity percentage of the porous Cu interlayer (before and after rolling) was determined by water immersion technique based on Archimedes' principle using an electronic balance (Shimadzu AY220, Japan) equipped with a density meter kit.

The following formula was derived to calculate the porosity percentage:

$$P(\%) = \frac{W_{as} - W_d}{W_{as} - W_s} \times 100 \quad (3.1)$$

where;

P = percentage of porosity

W_d = weight of porous Cu in dry condition

W_s = weight of porous Cu while submerged in water

W_{as} = weight of porous Cu after submerging in water

3.5 Soldering Pre-treatment

Prior to conducting soldering, the Cu rods were first cleaned with ethanol to remove any substrate contaminants. The SAC305 solder alloy (0.1 g) and rolled porous Cu interlayer formed a sandwich-like layer between the ends of the Cu rods to be joined. The configuration is illustrated in Figure 3.7. A solder joint without a porous Cu interlayer was also prepared as the control sample.

The prepared solder joint was clamped using a fabricated jig to hold the sample during heating. The clamping features are crucial to the soldering process to ensure proper solder joint to be joined properly. In addition, a 234 N load was imposed at by the upper jig to obtain a constant joined solder layer during soldering process as shown in Figure 3.8. The soldered sample was then machined lightly to remove excess solder solidified around the joining part, as shown in Figure 3.9.

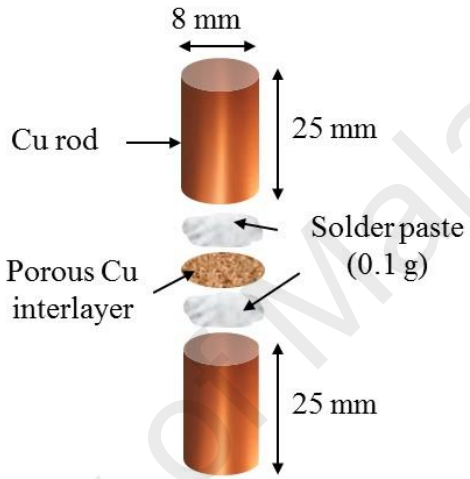

Figure 3.7 : Solder joint configuration

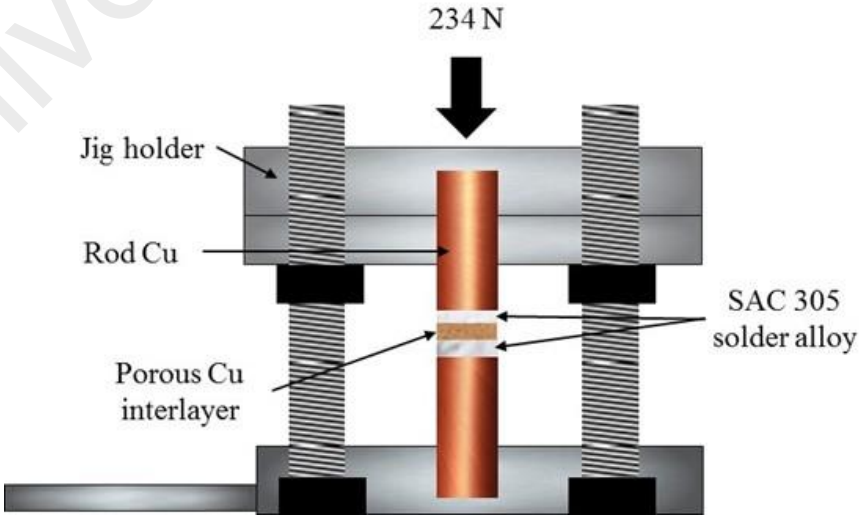

Figure 3.8 : Jig to hold the solder joint during soldering

Figure 3.9 : Soldered sample after soldering process

3.6 Soldering Process

The following sections describe the soldering procedures carried out in the laboratory.

3.6.1 Furnace Setup

Soldering process was conducted in a furnace equipped with argon gas and setup based on the Japanese Industrial Standard, JISZ 3191: 2003 (Japanese Standard Association, 2003.). According to this standard, the furnace was placed on a movable trolley while the soldered sample was fastened in the jig holder to avoid movement during solder solidification upon soldering completion. A schematic view and the actual figure of the movable furnace setup in compliance with JISZ 3191 are shown in Figure 3.10 and Figure 3.11, respectively.

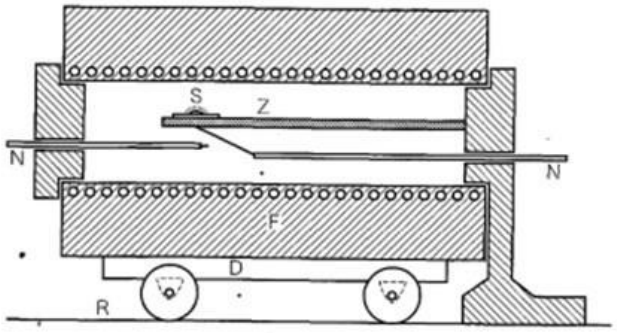

A（フラックスを用いる場合）

F：電気炉　内径φ60×300
Z：試料受台
S：試験片
N：熱電対
D：くるま付台
R：移動用レール

Figure 3.10 : Schematic diagram of JISZ 3191: 2003 furnace for soldering process (Japanese Standard Association, 2003)

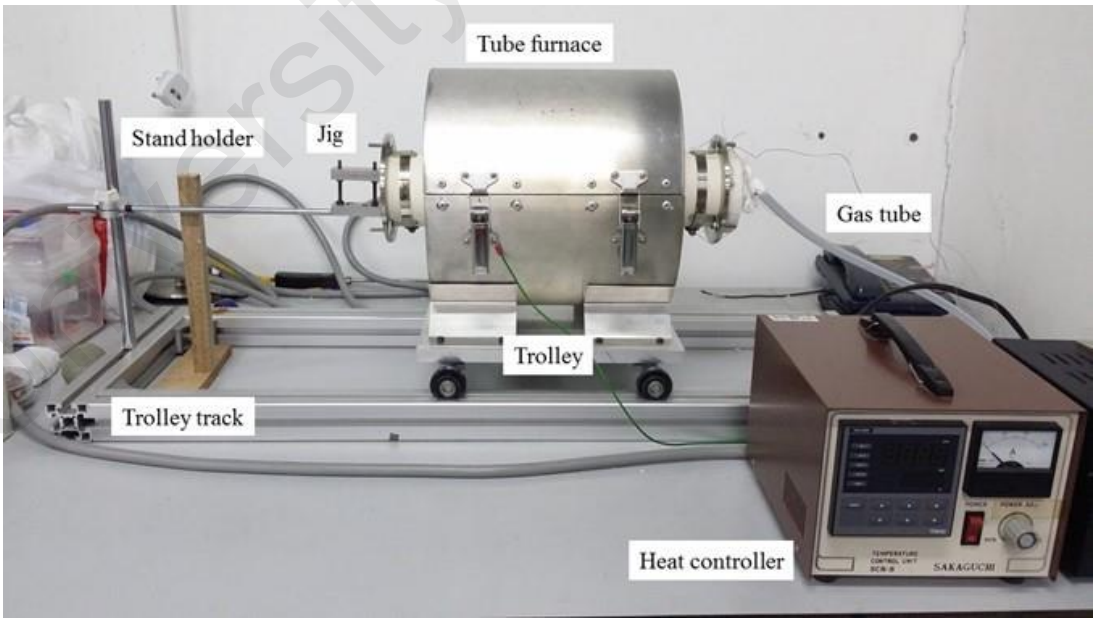

Figure 3.11 : Actual furnace setup

3.6.2 Soldering Process Parameters

The melting point of SAC305 is 217°C and soldering is carried out at 40°C above the melting point (Wang, Gao, Ma, & Qian, 2006). Three soldering temperatures, i.e. 267°C, 287°C and 307°C were adopted for joining SAC305 and porous Cu. Much higher temperature, 307°C is chosen in order to investigate the solder joint performance when added with porous Cu as compared to without porous interlayer addition.

The solder joints heating times were set at 60 s, 180 s and 300 s. The soldering was prolonged to 300 s to accommodate additional heating on porous Cu to study the effect on solder joint ability. The soldering process was carried out in an inert argon atmosphere to prevent oxidation. After soldering was completed, the solder joints were cooled naturally. Table 3.3 presents summary of the experimental parameters.

Table 3.3 Parameter settings for soldering process

Parameters	Settings
Soldering temperature (ºC)	267, 287, 307
Soldering time (s)	60, 180, 300
Porosity (ppi)	No porous, P15, P25

3.6.3 Isothermal Aging Treatment

Soldered parts in electronic packages can be exposed to high temperatures caused by ambient temperature or heat dissipated from packaged devices. An isothermal aging test was performed to investigate effect of heating on the solder's strength and microstructure. All samples at soldering temperatures of 267°C, 287°C and 307°C and all holding time of 60 s, 180 s and 300 s were used in the study. The joined samples were arranged in a heat-resistant container for 100 h, 200 h and 500 h aging at 150°C in the oven as shown

in Figure 3.12. The setting parameters for the thermal aging test are summarized in Table 3.4.

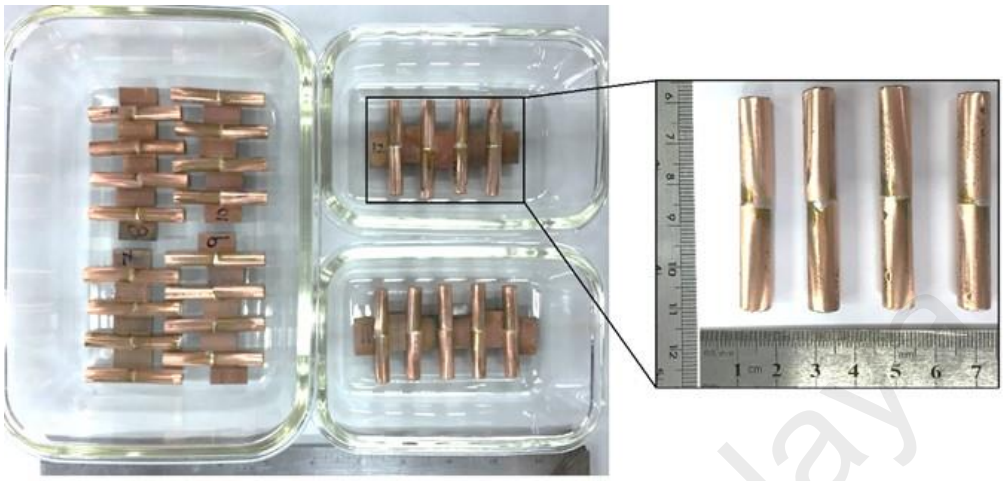

Figure 3.12 : Arrangement of solder joint specimens for isothermal aging treatment

Table 3.4 Parameter settings for the isothermal aging test

Parameters	Setting conditions
Isothermal aging time (h)	100, 200, 500
Isothermal aging temperature, (ºC)	150
Porosity (ppi)	P15, P25

3.7 Joint Strength Evaluation

Mechanical properties of the as-soldered and aged SAC305 solder joint sample soldered with a porous Cu interlayer were evaluated by measuring the joint tensile strength of the specimens. The tensile test was carried out at room temperature with an Instron® Corporation Universal Testing Machine (Model No. 3369, Norwood, MA, USA) with a crosshead speed of 0.5 mm/min. The joint strength was calculated by dividing the maximum force with contact area between Cu rod and solder alloy as in

equation (3.2). The exact contact area for each sample was measured after every tensile test from an image captured by an optical microscope. The joint strength results were determined from the average value of three different samples with each setting parameter.

$$\sigma = \frac{F}{A} \tag{3.2}$$

Where ;

σ = joint strength

F = maximum force

A = contact area

3.8 Microstructural Analysis

The microstructural analysis of the solder joint involved observing the cross-sectional area and fractured surface of the test sample for each parameter. Cross-sectional analysis was done to observe the interfacial reaction at the joining area of the SAC305 solder alloy with a porous Cu interlayer. The solder joint fractography (surface and cross-section) after tensile testing was examined to study the failure behavior.

3.8.1 Cross-sectional Analysis

The solder joint samples were cut perpendicular to the joint using a high-speed cutting machine. The prepared samples were then placed in epoxy in molding cups. After mounting the specimens, they were ground with 800, 1000, 1500 and 2000 grade abrasive sandpaper and then polished to a final finish using diamond suspension of 6, 3 and 1 μm

particle size. The selected cross-sectioned soldered joint samples were etched in a mixture of 90 volume% hydrochloric acid and 10 volume% methanol for 10 s to reveal the interfacial reaction microstructure.

3.8.2 Optical Microscope

The microstructure of the solder joint was observed at low and medium magnification with an optical microscope (OM, Olympus, Tokyo, Japan) to visualize the overall morphology of the fractured surface.

3.8.3 Scanning Electron Microscope (SEM)/Energy Dispersive X-Ray Spectroscopy (EDS)

The morphology of the cross-sectioned and fractured surfaces was examined by SEM (Crest System (M) Sdn. Bhd., Eindhoven, The Netherlands) equipped with an EDS analyzer (Crest System (M) Sdn. Bhd., Eindhoven, The Netherlands). The samples were scanned with a digital SEM at high magnification of up to 2000x using acceleration voltage of 15 kV. EDS was utilized to determine the elemental composition of the interfacial reaction layer.

3.8.4 X-Ray Diffraction (XRD) Analysis

The dominant element on the fractured surface was determined by X-Ray Diffraction (XRD, PANalytical Empyrean, DKHS Holdings (Malaysia) Bhd., Almelo, The Netherlands) analysis. The scanning angle ranged between 0° to 90° with orientation of 2θ. In X-ray diffraction, a crystal is mounted and gradually rotated while being bombarded with X-rays. The X-rays are directed at the sample and the diffracted rays are collected. The XRD graphs obtained are compared with existing patterns of different phases so that the crystal phase can be determined.

3.8.5 Differential Scanning Calorimetry (DSC)

DSC analysis was carried out to determine the effect of porous Cu interlayer addition on the thermal characteristics of the SAC305 solder alloy. The soldered part of the solder alloy joined with porous Cu were scraped to obtain samples of around 20-40 mg. The DSC experiments were performed in a purified argon gas atmosphere, from ambient temperature up to 300°C with a scanning rate of 10°C/min.

3.8.6 IMC Thickness Measurement

ImageJ software (National Institutes of Health, Maryland, USA) was used to measure the average thickness of the IMC layer formed along the interface. The picture taken by SEM was loaded into a computer equipped with ImageJ software. This software measured the total area of the IMC layers. The thickness of the IMC layers was then obtained by dividing its area by the length.

3.8.7 Activation Energy of IMC Growth

The various IMC growth kinetics are endorsed by the difference in IMC growth rates, which are controlled by the diffusion rates (Zeng, 2009). Meanwhile, the interface energies of the solder/IMC control the grain coarsening and IMC nucleation kinetics. The interfacial IMC layer after solder joint solidification continues to grow uniformly due to its low activation energy (Dutta, Kumar, & Subbarayan, 2009).

For the diffusion-dominant mechanism, controlling the isothermal growth of the IMC layer should reportedly follow a parabolic equation of the square root of time, which is expressed as follows (Nishikawa, Takemoto, Kifune, Uetani, & Sekimori, 2004)

$$d = d_0 + \sqrt{kt} \tag{3.3}$$

where d is the IMC layer thickness measured from SEM images (mm), d_0 is the initial thickness (μm), t is the aging time (s) and k is the growth rate constant of the diffusion

coefficient of Cu in the solder matrix. The *k* value can be determined from the slope of the linear regression plotted from the average IMC thickness (d-d_0) versus $t^{1/2}$.

Meanwhile, the activation energy for the IMC growth is determined using the Arrhenius relationship:

$$k = k_0 \exp(-\frac{Q}{RT}) \tag{3.4}$$

where k_0 is the pre-exponential diffusion constant (m^2s^{-1}), Q is the activation energy (kJ mol^{-1}), R is the gas constant (8.31 J mol^{-1} K^{-1}), and T is the absolute temperature (K). The activation energy value, Q is determined from the slope of the straight line obtained by taking the natural logarithm of equation (3.5) expressed as follows:

$$\ln k = \ln k_0 - \frac{Q}{RT} \tag{3.5}$$

The kinetic parameters of IMC layer growth determined by plotting the measured thickness as a function of exposure time at the given temperatures. This provides a linear relationship between the IMC layer thickness and the square root of holding time, as described in equation (3.3). The activation energy of IMC growth, Q, can then be calculated by taking the natural logarithm derived from the Arrhenius equation (3.5).

CHAPTER 4: RESULTS AND DISCUSSION

4.1 Introduction

This chapter presents the data and discussion of the experimental results obtained from Sn-3.0wt.%Ag-0.5wt.%Cu (SAC305) solder joint with an added porous Cu interlayer. The results and discussion will focus on the joint strength of soldered samples, microstructural observation, elemental analysis of the interfacial reactions and IMC growth observation. The discussion pertaining to solder joint performance will be divided into two sections: as-soldered (before aging) and aged (after aging) solder joints.

4.2 Macroscopic Structure of Porous Cu Interlayer

Magnified side and surface views of P15 and P25 porous Cu interlayers before and after rolling conditions are shown in Figure 4.1 and Figure 4.2, respectively. The pores before and after rolling are all not simply round in shape like a sphere. Various sizes and shape of pores are observed. Pores may also overlap with one another. The pores remained distinct even after rolling except they are more compressed and compacted. The rolling of porous Cu into a very thin layer was intended to facilitate a homogeneous joint layer by reducing the joint gap between the solder alloy and the Cu substrate. The solid parts of porous Cu are recognized as solid cell walls (Thewsey & Zhao, 2008), whilst the empty spaces represent pores. The average thickness of the solid cell walls for P15 and P25 are 0.26 mm and 0.06 mm, respectively while the pore size after rolling for P15 and P25 are 0.3 mm and 0.1 mm, respectively.

4.3 Verification of porosity percentage

Porous interlayers are normally characterized by the pore diameters, which correlates with the interlayer porosity (volume of pores divided by the total volume of solid and void spaces) (Nawaz, Bock, & Jacobi, 2012). The characteristic feature of the porous

	Before rolling	After rolling
Side view	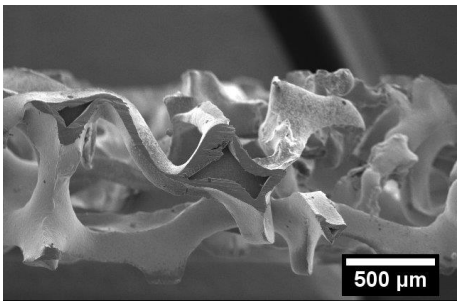	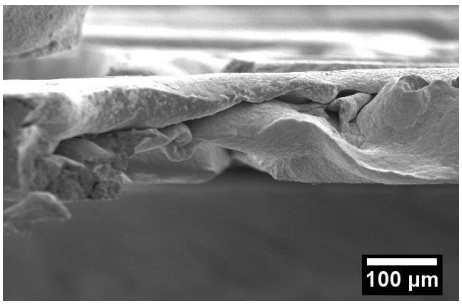
Surface view	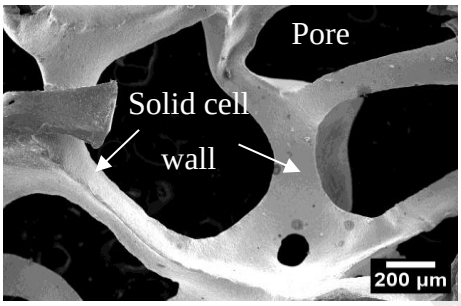	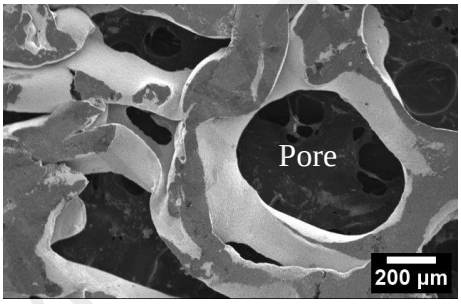

Figure 4.1 : Pore size and interlayer thickness of P15 porous Cu interlayer before and after rolling

	Before rolling	After rolling
Side view	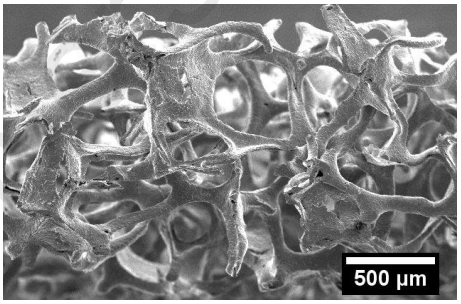	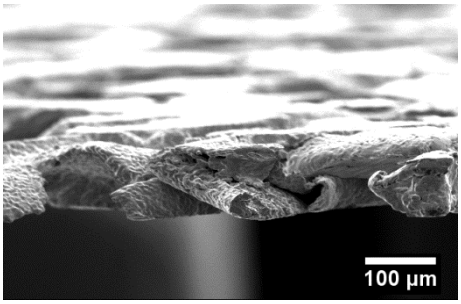
Surface view	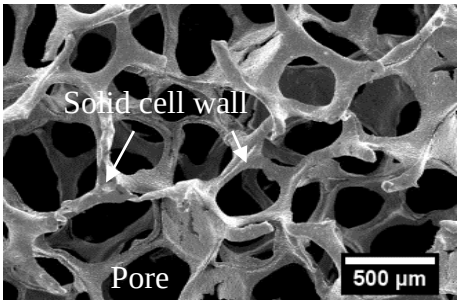	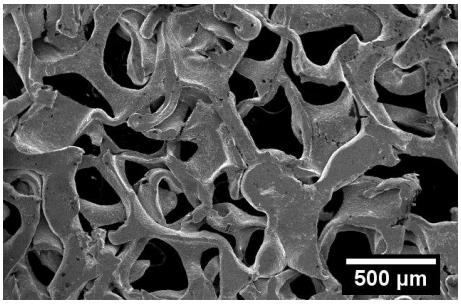

Figure 4.2 : Pore size and interlayer thickness of P25 of porous Cu interlayer before and after rolling

interlayer have an important role in the penetration of the molten solder alloy during the soldering process. Both experimental and theoretical porosity percentages of porous Cu used in this study are presented in Figure 4.3.

The experimental values were measured using a technique based on Archimedes' principle, while the theoretical values were calculated according to the pore density formula. Table 4.1 lists the percentage difference of porosity between experimental and theoretical values. The difference of 5.4% for P15 and 2.1% for P15 (both at before rolling) were obtained within the acceptable error limit arising from reading of equipment during running of experiment. It can be concluded that although the porosity of porous Cu decreased after rolling, the act of rolling on porous Cu interlayer into a thin layer did not change the porosity percentage in relation to the theoretical value.

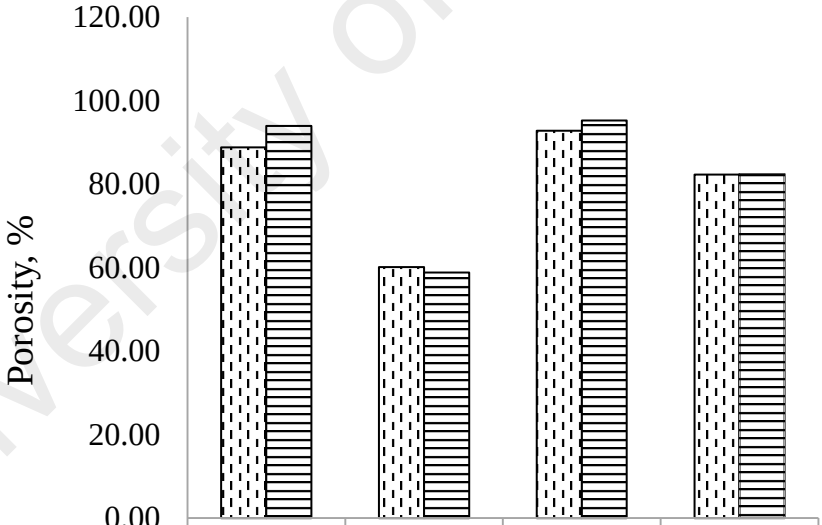

	Before, P15	After, P15	Before, P25	After, P25
Experimental	88.83	60.13	92.82	82.31
Theoretical	93.92	58.85	95.24	82.42

Figure 4.3 : Experimental and theoretical measurements of the porosity percentage of pre-rolled and post-rolled porous Cu interlayers

Table 4.1 Percentage differences between experimental and theoretical measurements

Before, P15	After, P15	Before, P25	After, P25
5.40%	2.10%	0.02%	0.00%

4.4 Melting Point Characteristics

The melting characteristics of the composite solder alloy were investigated using differential scanning calorimetry (DSC). The samples were first heated from ambient temperature up to 300°C at a heating rate of 10°C/min followed by cooling to ambient temperature. Figure 4.4 shows the onset melting temperatures of the SAC305 solder alloy with added (a) P15 and (b) P25 porous Cu interlayers, respectively. It was found that the onset transformation temperature for which represents the melting point, does not change markedly for both types of porous Cu. The porous Cu interlayers were not melted during heating at 300°C and did not exhibit significant changes in DSC profiles. The profile shows the melting point of the SAC305 alloy at 217.8°C.

4.5 Tensile and Microstructural Properties of As-soldered Sample

The solder joint performance after the soldering process involving tensile strength, microstructure analysis and effect of porous Cu interlayer addition to a SAC305 for as-soldered sample are presented in the following subsections.

4.5.1 Tensile Properties

Among several methods of verifying solder joints reliability, tensile testing is considered the most important method as it assists in determining the fracture behavior and joint strength of the solder joint. It is well-known that soldering temperature and time have significant roles on solder joints reliability.

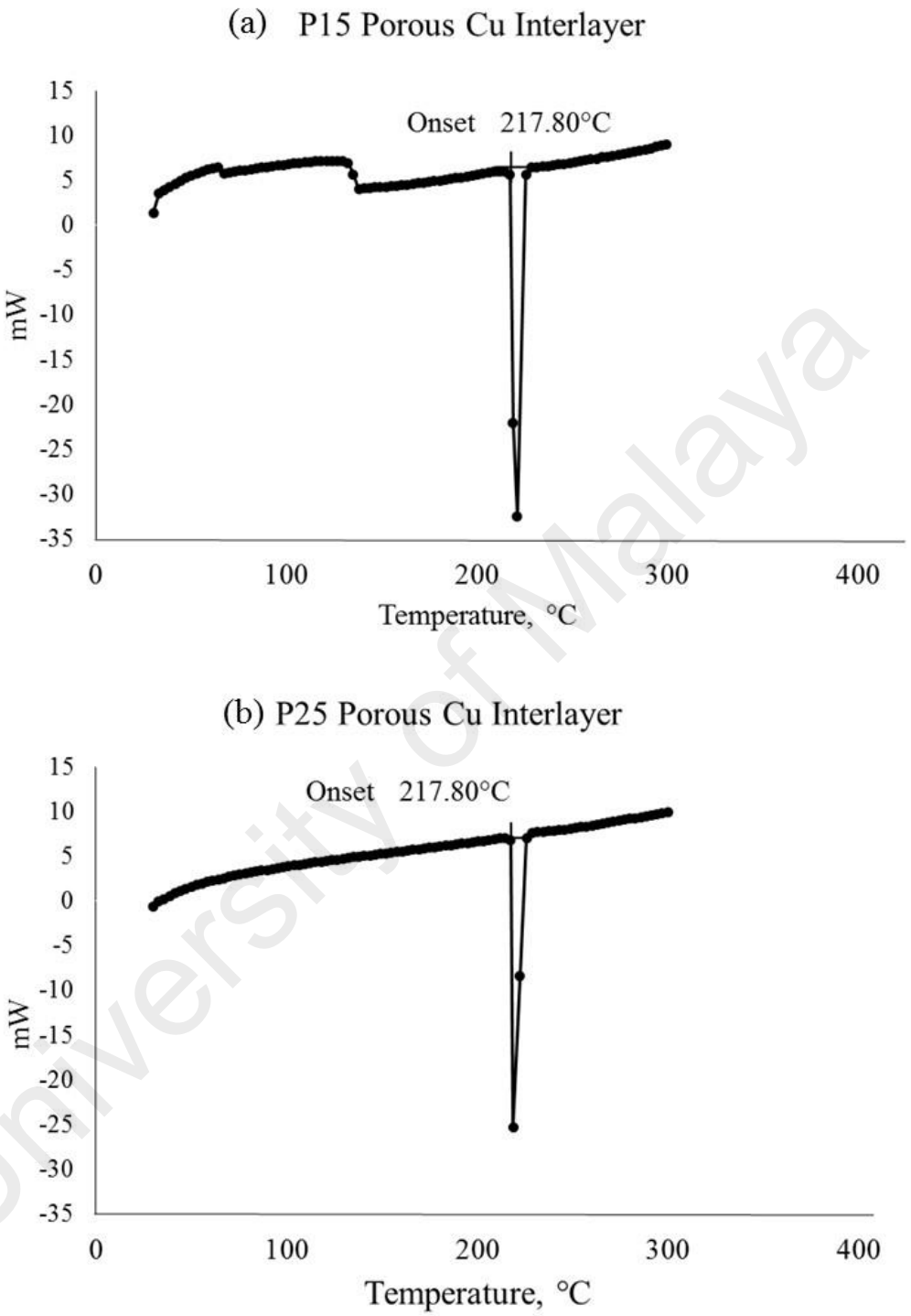

Figure 4.4 : DSC profiles of SAC305 solder alloy with added (a) P15 and (b) P25 porous Cu interlayer

After a solder alloy was melted, it reacts with the Cu substrate and the porous Cu interlayer. These reactions are also referred to as wetting, which produces bonding within the interfaces. In the present study, the tensile strength of solder joints at various time and temperature were evaluated using a universal test machine with crosshead speed of 0.5 mm/min at room temperature. The strength was calculated as the maximum tensile load (F) divided by the area (A), using equation (3.2) presented in Chapter 3. The error bars represent the maximum and minimum values of the three joint strengths measured for each soldering process parameters.

Figure 4.5 presents the effect of soldering time and porosity on tensile strength at 267°C soldering temperature. The strengths observed at each soldering time appeared in decreasing order as follows: P25 solder joint > P15 solder joint > without porous solder joint. It was observed that the strength of solder joint with porous Cu (P15 and P25 porous Cu) increased with longer soldering time. For solder joint with no porous, the tensile strength shows minimal increment of ~38 to 40 MPa, was recorded at each soldering time. The tensile strengths of solder joint with P25 were 5 to 10 MPa higher at each soldering time than the solder joint with P15 porous Cu. Meanwhile, the tensile strength for the solder joint with P15 were 5 to 10 MPa greater than the solder joints without porous Cu at each soldering time. The highest strengths of 48 and 50 MPa were observed for the solder joints with P15 and P25 porous Cu addition respectively, both at 300 s.

Tensile testing was also conducted on joints soldered at 287°C. The results obtained are presented in Figure 4.6. The strengths observed at each soldering time were in the following strength decreasing order: P25 solder joint > P15 solder joint > without porous solder joint. Similarly, the strengths of solder joint with porous Cu (P15 and P25 porous Cu), increased with increasing soldering time. The tensile strengths recorded for the solder joint without porous Cu ranged from 33 to 38 MPa at the three soldering times

applied. The highest strength of 51 and 46 MPa were observed for the solder joints with added P25 and P15 porous Cu, respectively; also at a holding time of 300 s.

The investigation continued for 307ºC soldering temperature in order to observe the reactivity of porous Cu with solder alloy when subjected to a higher temperature. Figure 4.7 presents the results obtained. At 307°C, no clear-cut trend was observed as for 267°C and 287°C soldering temperatures, where the strength was in the order : P25 solder joint > P15 solder joint > without porous solder joint at both temperatures. Instead, it was observed that P25 had slightly lower strength than P15 soldered at 60 s and 300 s. The joint strengths for samples without porous Cu were observed at 36-40 MPa. The highest strengths were recorded at 51 MPa for P25 with porous Cu addition (at 180 s) and at 54 MPa for P15 with porous Cu addition (at 300 s). P25 porous Cu at 300 s was taken as having approximately the same strength as at 180 s.

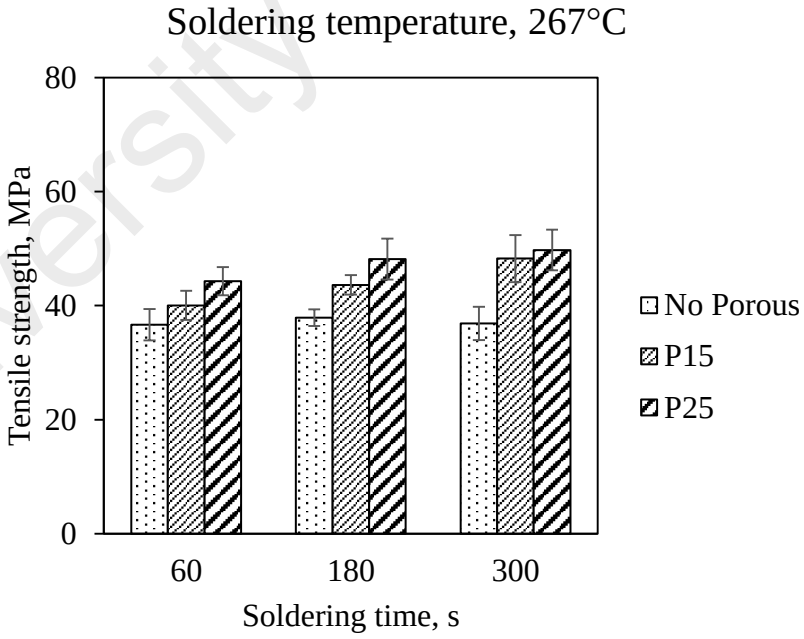

Figure 4.5 : Effect of soldering time and porosity on tensile strength after soldering at 267°C

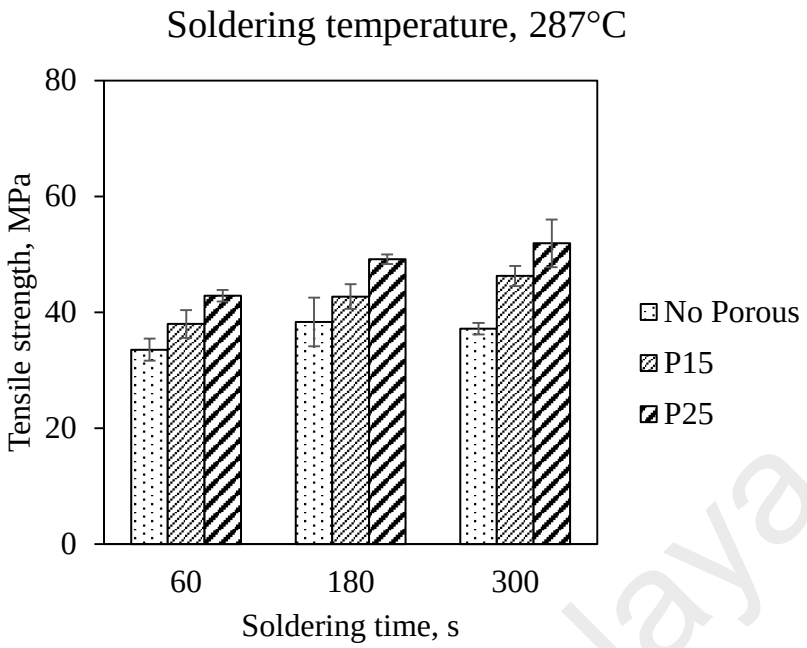

Figure 4.6 : Effect of soldering time and porosity on tensile strength after soldering at 287°C

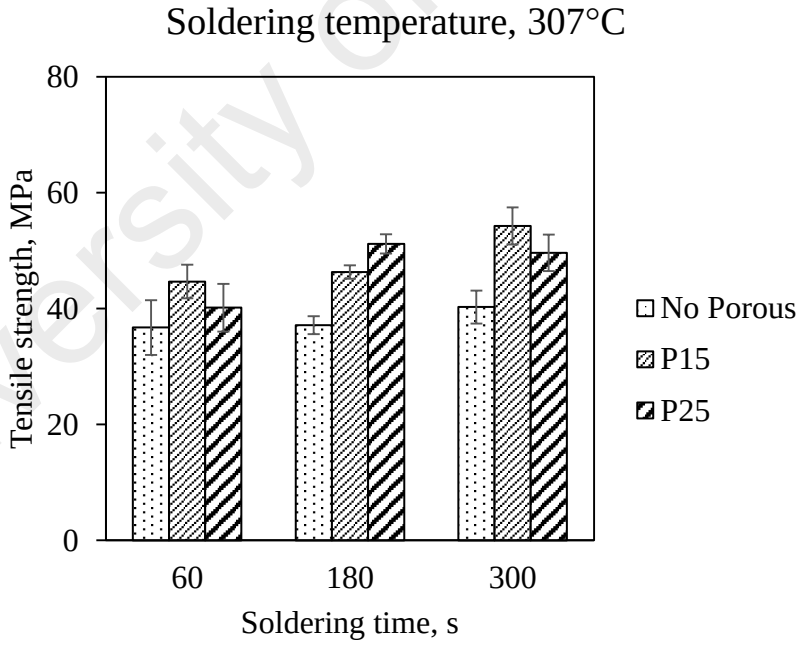

Figure 4.7 : Effect of soldering time and porosity on tensile strength after soldering at 307°C

Table 4.2 summarized results obtained in Figure 4.5 to 4.7. According to the results within the range of soldering temperatures carried out in the present study, increasing the temperature from 267°C to 307°C results in a slight increase in tensile strength for the solder joint without porous at each corresponding soldering time.

Table 4.2 Summary of tensile strength for as-soldered solder joint

Porous Cu	Soldering Temperature, T (ºC)	Soldering Time, t (s)	Tensile Strength, MPa
No Porous	267	60	36.64
		180	37.88
		300	36.88
	287	60	33.55
		180	38.33
		300	37.18
	307	60	36.74
		180	37.14
		300	40.26
P15	267	60	40.03
		180	43.63
		300	48.25
	287	60	37.98
		180	42.72
		300	46.27
	307	60	44.66
		180	46.31
		300	54.26
P25	267	60	44.27
		180	48.15
		300	49.74
	287	60	42.86
		180	49.16
		300	51.11
	307	60	40.16
		180	51.13
		300	49.63

It also appears that increasing the soldering temperature from 267°C to 307°C generally improved the strength of solder joints with porous Cu interlayer, at all

corresponding soldering times. P25 porous Cu had values about 5-10 MPa higher than P15 porous Cu at each corresponding soldering time (except at 307°C when P25 porous Cu show slightly lower strength than the corresponding P15 porous Cu at 60 s and 300 s soldering times). The data further indicates P15 porous Cu had strength 5-10 MPa higher than samples without porous Cu at each corresponding soldering time. This means that overall, the addition of P15 and P25 porous Cu resulted in strength increment of 10-20 MPa compared to solder joints without porous Cu added.

Overall, the results demonstrates the three soldering temperatures produced 40-54 MPa strengths for joints with two porous Cu types added. A closer analysis of the data shows that 11 out of 18 solder joint samples with either porous Cu interlayer type added obtained strength values above 45 MPa. Basically, these 11 samples are considered to have surpassed the optimum strength values of solder joints used in electronics devices, as advocated by Kim et al. at strength of 45 MPa (K. S. Kim, Huh, & Suganuma, 2003). Furthermore, the highest strength values obtained from the above study for either P25 or P15 porous Cu are also comparable with the joint strength in die-attach bonding using composite preform recorded at 50 MPa, as reported by Liu et al. (Liu, Lee, & Bachorik, 2013). Details on the failure mechanism arising from tensile testing will be discussed in the following subsection.

4.5.2 Fractured Surface Analysis

The fracture behavior of a solder joint is not only affected by the solder configuration but also by the alloy microstructure. It is typical for solder joint failure to occur at the solder/IMC interface near the solder region. Studies have shown that crack initiation occurs at the solder/IMC interface, which is near the inside of the solder and the inner IMC as analyzed by SEM (Rzepka, Hofer, Simon, Meusel, & Reichl, 2002). In this study, the fractured surfaces after tensile testing were analyzed using SEM to understand the

effect of porous Cu addition to the solder joint on the fracture mode. The failure modes observed include the ductile mode, brittle mode as well as mixed modes, which involve both brittle and ductile failure. Mixed modes are either classified as quasi-ductile or quasi-brittle. A mode is quasi-ductile if the failures exhibits ductile behavior and quasi-brittle if the failure passed through the interfacial region (Nguyen & Kim, 2014).

4.5.2.1 Surface Morphology

The fractured surface analysis results demonstrate that the morphological features of the fractured surfaces determined by SEM appeared similar for all solder joint samples with added porous Cu. Furthermore, the differences in the strength obtained for all samples with porous Cu addition were not too large, with values within the 45–54 MPa range. Thus, the results from specimens at 307°C soldering temperature and 300 s holding time were selected as favorable results for tensile strength evaluation for the purpose of the present discussion. The results are compared with those obtained for the control sample with a corresponding soldering temperature of 307°C and holding time of 300 s.

Figure 4.8 shows the fractured surface of the control sample soldered at 307°C, 300 s holding temperature after tensile testing. The overall fractured surface as in Figure 4.8(a) displays the brittle mode failure because the fractured solder does not indicate any plastic deformation. Small voids are noticeable at the fractured surface. The failure behavior observed is in fact similar to that observed for SAC305 under high-speed shear impact loading as reported by Nguyen et al. (Nguyen & Kim, 2014). At higher magnification of the selected area, the surface appears mostly flat as shown in Figure 4.8(b). The elements present at the interfaces together with their respective phases determined from EDS analysis are listed in Table 4.3. The flat area, marked with A in Figure 4.8(b), indicates fractures that occurred at the IMC interface. However, a small ductile deformation is visible in the residual solder area marked with B. It is believed that the joint strength of

the control sample was influenced by this Sn matrix residue inside the SAC305 solder alloy. C represents an area with dominant SAC solder alloy elements.

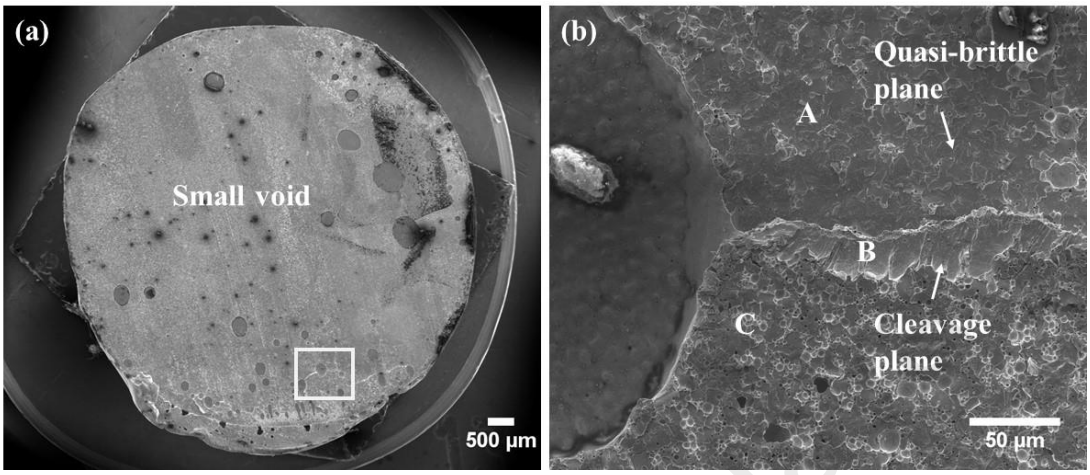

Figure 4.8 : Fractured surface of solder joint without porous Cu at 307°C and 300 s: (a) overall, (b) magnified view of the rectangle marked in (a)

Table 4.3 EDS analysis at marked spot in Figure 4.8(b)

Spot	Element (at. %)			
	Cu	Ag	Sn	Phase
A	58.24	(0.37)	41.39	Cu_6Sn_5
B	2.08	1.57	96.35	Sn
C	4.23	13.02	82.76	Sn-Ag-Cu

In contrast it is observed that solder joints with P15 porous Cu have a rougher fractured surface (Figure 4.9(a)). A broken porous Cu interlayer was observed on the fractured surface after tensile testing. This finding is somewhat similar to that reported by Shirzadi et al. from a study involving metal foam. The authors identified in their study a cup and cone-like structure of metal foam at the fractured surface (Shirzadi, Zhu, & Bhadeshia, 2008) . A higher magnification of the fractured surface in Figure 4.9(b) indicates that the failures occurred at the interface between alloy and porous Cu. This area in fact corresponds to the IMC layer. This means that failure occurred at the interfaces of the SAC305/Cu substrate and the SAC305/IMC layer as well as inside the porous Cu itself.

The fractures manifest as a mixed form of flat, brittle and irregular ductile fractures. Nonetheless, based on a comparison of different surface areas, the ductile forms appear more dominant than the brittle features. This can be explained by the formation of only a Cu_6Sn_5 IMC phase at the boundary between the solder and porous Cu. The phases were confirmed by EDS analysis and are presented in Table 4.4. The development of ductile-brittle failure in the transition area between them is a result of some kind of competition between ductile tearing from porous Cu and cleavage fracture from residual solder. Subsequently, a quasi-ductile mode (marked as D, E and F in Figure 4.9(b)) occurred in solder joints with porous Cu interlayer.

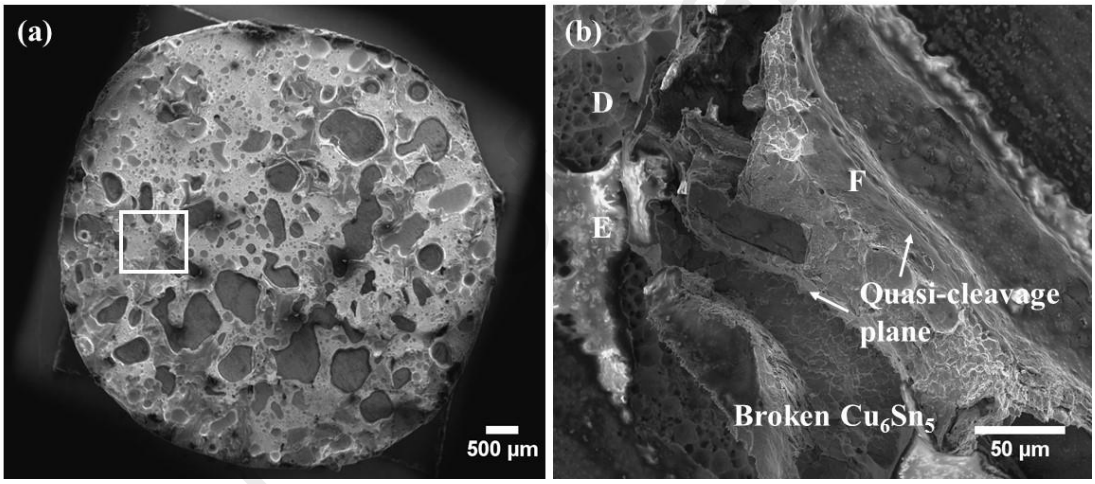

Figure 4.9 : Fractured surface of solder joint with P15 porous Cu interlayer at 307°C and 300 s: (a) overall, (b) magnified view of the rectangle marked in (a)

Table 4.4 EDS analysis at marked spot Figure 4.9(b)

Spot	Element (at. %)			
	Cu	Ag	Sn	Phase
D	31.43	(2.48)	66.09	Cu_6Sn_5
E	58.38	0	41.62	Cu, Sn
F	2.89	2.13	93.98	Sn

On the other hand, solder joint with P25 porous Cu appears to have a less rough fractured surface than P15 porous Cu as shown in Figure 4.10(a). The failures can be

classified as quasi-ductile mode because there is evidence of dimple pattern from ductile fracture and also a smaller brittle surface area could be seen. Under high magnification, the fractured surface comprises ductile and mixed mode failures that occurred mainly at the interfaces of SAC305/IMC and porous Cu/IMC (Figure 4.10(b)). Table 4.5 presents the summary of the EDS analysis of the magnified image in Figure 4.10(b). A broken IMC phase is observed at the boundary of the solder and the broken porous Cu, while residual solder pieces are seen on the surface at spot G. It is also noted that the ductile area from residual solder and porous Cu are dominant over the brittle surface area (marked at H). The higher strength of the solder joint with P25 porous Cu recorded at 307°C and 300 s is likely attributable to this configuration. It can be deduced that to some extent porous Cu has the ability to absorb residual stress. From the fractured surface obtained, it is also probable that porous Cu enhanced the bond reliability. These observation were similarly pointed out earlier by Fang et.al. based on a study on using a Cu metal interlayer (Fang, Zheng, Lou, & Sui, 2001).

In addition, the smaller diameter of pores and thinner solid cell walls in P25 porous Cu (as in Figure 4.2) compared to P15 porous Cu (as in Figure 4.1), facilitated better molten solder penetration into the porous Cu. Subsequently, stronger adhesive bonding formed due to the interfacial reaction observed in spot H. This explains the higher strength values obtained with P25 porous Cu than P15 porous Cu at all three soldering temperatures applied, each for three holding times. The exception is that the P25 porous Cu strengths are slightly lower than P15 porous Cu at 307°C and holding times of 60 s and 300 s. It has been accepted that appropriate IMC amounts resulting from interfacial reactions lead to better joining strength at solder/solid (Cu and porous Cu) interfaces (Humpston & Jacobson, 2004). The optimal thickness of the IMC have to be 1.0 to 4.0 μm to allow for the formation of a scalloped-shaped morphology at the weaving

boundary. This will produce a strong adhesion between the IMC layers and solder or solid interface leading to higher joint strength.

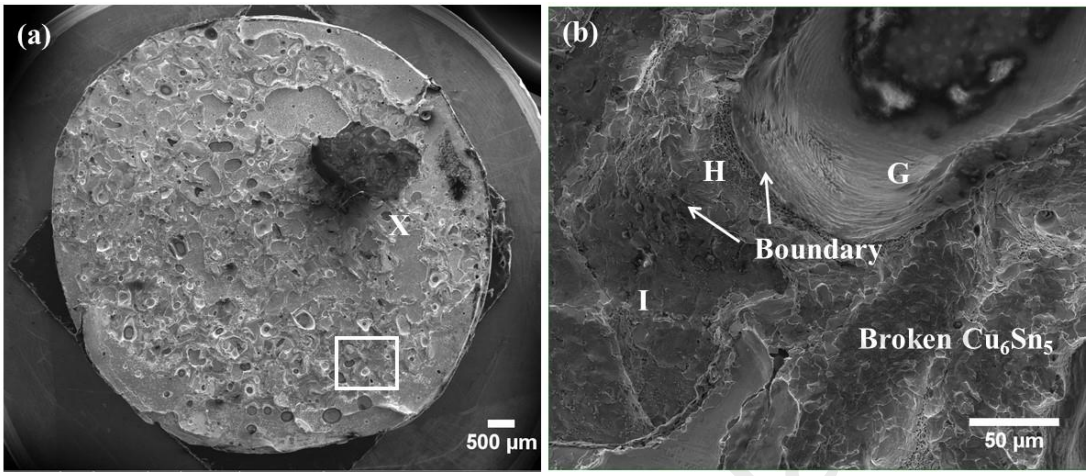

Figure 4.10 : Fractured surface of solder joint with P25 porous Cu interlayer at 307°C and 300 s: (a) overall, (b) magnified view of the rectangle marked in (a)

Table 4.5 EDS analysis at marked spot in Figure 4.10(b)

Spot	Element (at. %)			
	Cu	Ag	Sn	Phase
G	3.71	(1.92)	94.38	Sn
H	57.16	0.29	42.56	Cu_6Sn_5
I	85.17	0.27	14.55	Cu (major)

In addition and as mentioned in the section 4.2, P15 porous Cu has larger solid cell walls than P25 porous Cu. During soldering, it appears there was a portion area within P15 porous Cu where the molten solder could not reach and is only covered by a very thin solder layer. As a result, the bonding strength at the contact area of the solid cell walls is weaker. This explains the generally weaker strength of the solder joint with P15 porous Cu compared to the joint with P25 porous Cu at soldering temperatures of 267°C and 287°C (Figure 4.5, Figure 4.6). The exception being the slightly higher strength of the solder joint with P15 porous Cu than the corresponding solder joint with P25 porous

Cu at higher soldering temperature (307°C) and soldering times of 60 s and 300 s as shown in Figure 4.7. These P15 readings were assumed to fall within the acceptable error limits.

Figure 4.11 shows EDS mapping of Sn, Ag and Cu elements scanned in spot X marked in Figure 4.10(a). Emphasis is on the analysis of Cu element. Cu seems to have remained at the fractured surface, indicating that fracturing occurred in the porous Cu region. It is also observed that bright Cu dimples had arisen from the cleavage fractured surfaces. These phenomena affecting Cu were observed at the wall boundary between the porous Cu and the solder alloy, denoting that cleavage surface mentioned actually developed at the IMC layer. This was the result of the Cu/Sn decohesion with Cu derived from porous Cu while active Sn derived from the solder component. It is believed that existence of these Cu dimples proves that ductile fractures occurred at a slow strain rate during tensile testing earlier on since the fast diffusion of atoms at the interfacial reaction at the interfacial reaction was suppressed. It is also noted that Sn and Ag are present everywhere in the SAC solder alloy joint. Similar findings were reported by El-Daly et al. who showed small amounts of Ag and In added to Sn-0.7wt.%Cu solder had improved the solder joint ductility. In another similar study by Kim et al., with Ni alloy added to SAC305 solder joints, ductile fractures with a dimple pattern was observed during tensile testing under a low strain rate (Kim, Huh, & Suganuma, 2003). For comparative purposes, fracture morphology of solder joint without porous and with P25 at soldering temperature of 287C with soldering time of 60 were shown in Figure 5.1 and Figure 5.2, respectively in APENDIX B.

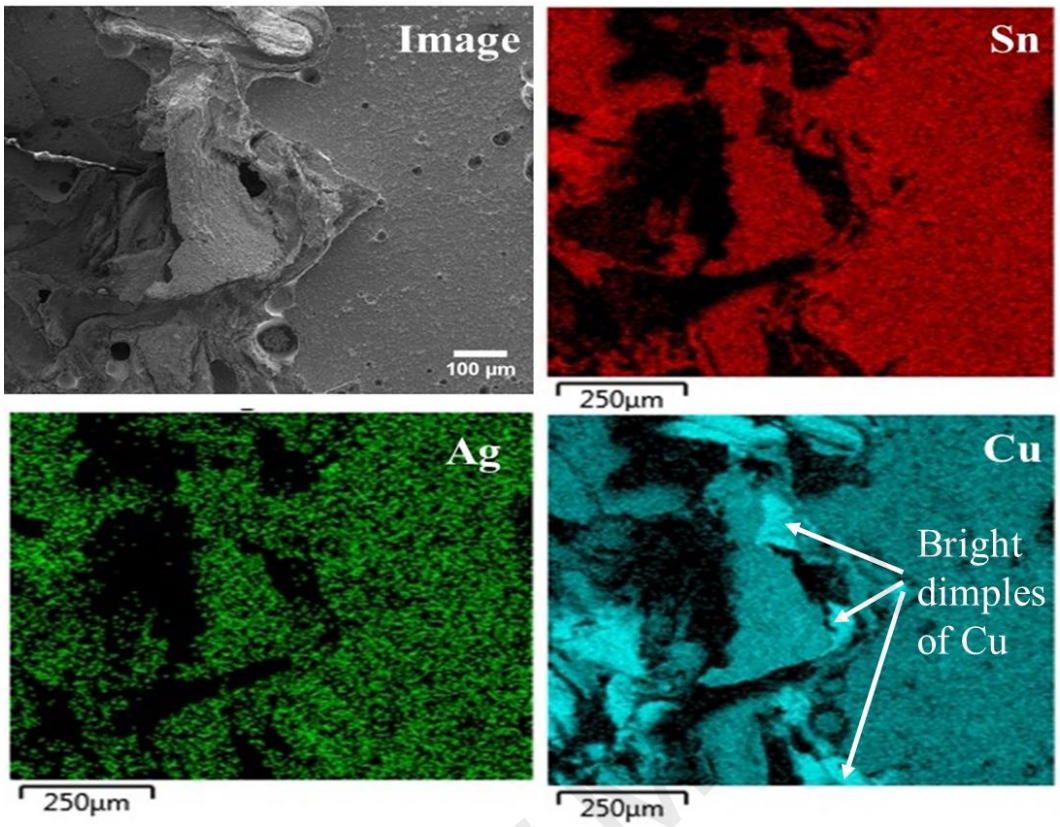

Figure 4.11 : EDS elemental mapping of the selected solder joint with an added porous Cu interlayer

4.5.2.2 Cross-sectional Morphology

Figure 4.12 illustrates SEM photomicrographs of the cross-sections of solder joints with and without porous Cu interlayer. For the control sample, it appears the crack propagated at the IMC/SAC305 interface near the Cu substrate and later expanded along the interface (Figure 4.12(a)). The excessive growth of the uniform IMC layer at the solder interfaces actually weakened the bonding strength of the solder joint.

In the case of solder with added P15 porous Cu, it was found that large segments of their solid cell walls were in contact with each other after being rolled into a very thin layer. Consequently, this apparently caused poor molten solder penetration into the porous Cu, since the passage was limited by blockage from the thicker solid cell wall

structures. Crack propagation could be seen inside SAC305 and the porous Cu, as well as at the porous Cu/IMC interface as shown in Figure 4.12(b).

Despite the smaller pore diameter in P25 porous Cu compared to P15, the thinner solid cell walls of P25 porous Cu had less contact with each other than those of P15 porous Cu, especially after rolling. This facilitated better molten solder penetration to the inner portion of the P25 porous structure. According to Figure 4.12(c), the penetrated molten solder filled the gaps inside P25 porous Cu. The cracks that formed inside the solder are typical ductile fractures, a few of which also occurred at the IMC/SAC305 interface upon stress loading. Cracking also happened inside the porous Cu, resulting in the formation of a cleavage fractured surface as mentioned in section 4.5.2.1.

The differences in the physical properties of solder joints such as thermal expansion also generate interfacial stress. This stress was found to have accelerated the fractures occurring along those interfacial boundaries. It is clear that the availability of porous metal in joining assemblies had clearly reduced the differences in thermal expansion between the interfaces, ultimately preventing crack development in joints (Zaharinie, Moshwan, Yusof, Hamdi, & Ariga, 2014). Therefore, it can be deduced that porous Cu is able to absorb residual stress and can therefore improve the bond reliability of solder joints while simultaneously preventing cracks. Fang et al. studied the use of a Cu interlayer in joining assemblies and reported similar finding (Fang, Zheng, Lou, & Sui, 2001).

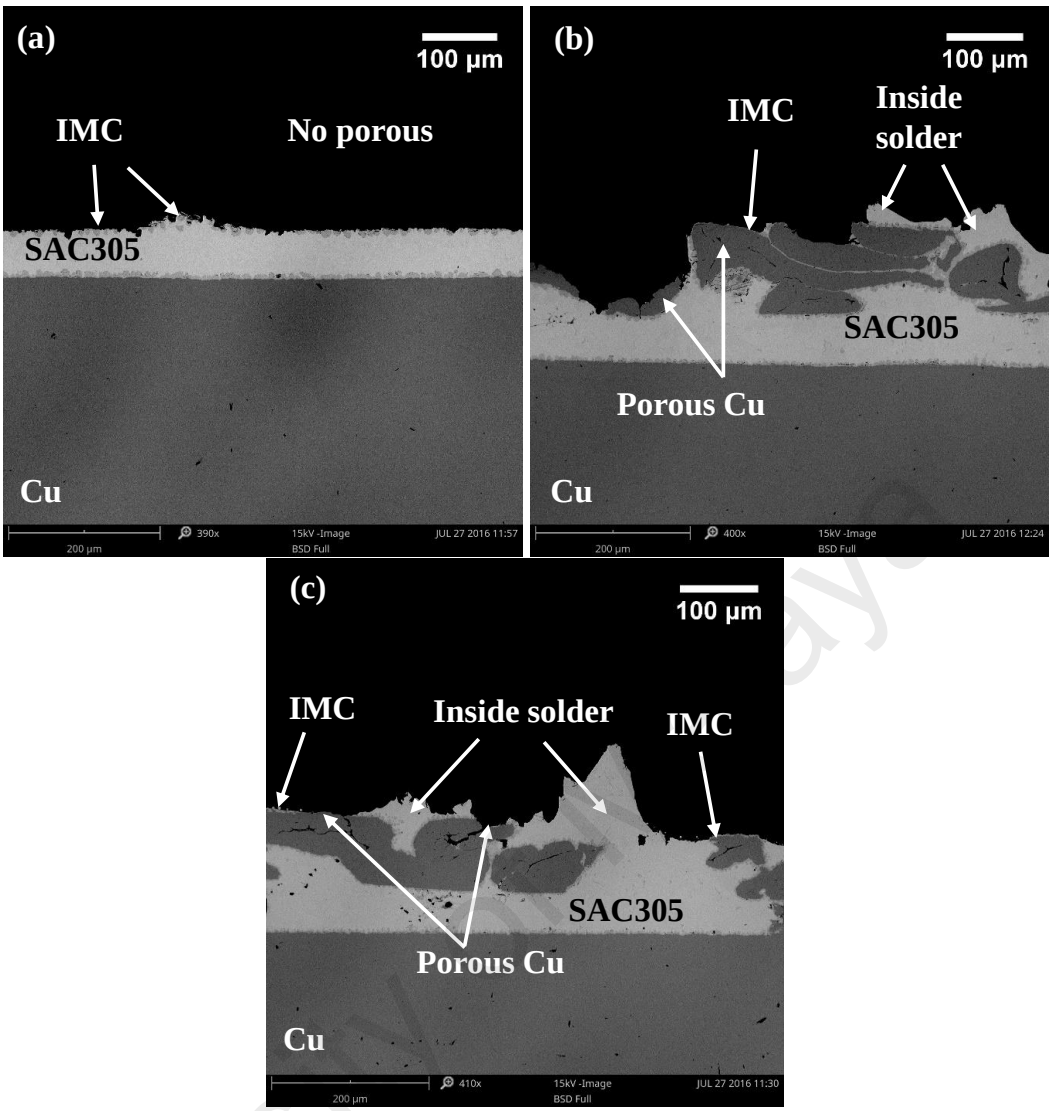

Figure 4.12 : Cross-sectional image of solder joints at soldering temperature of 307°C and soldering time of 300 s after tensile test; for (a) without porous sample, (b) solder joint with P15 and (c) solder joint with P25 porous Cu

4.5.2.3 Crack Propagation

From the fractured surface and cross-sectional morphologies, the possible mechanism of crack propagation is schematically illustrated as shown in Figure 4.13.

For solder joint with no porous addition, the crack occurred at the flat surface which consists of IMC phase as shown in Figure 4.8. In this case, the fracture occurred at Cu_6Sn_5/SAC305 interface, as indicated cross-sectional picture in Figure 4.12(a). It is also

expected that the crack would have occurred in the middle of the solder alloy and propagated slowly inside the solder as illustrated in Figure 4.13(a).

From the surface morphology (Figure 4.9, 4.10 and 4.12(b), (c)), Cu seems to have remained at some parts of the fractured surface. This indicates that the crack occurred at porous Cu itself. Crack was also observed at IMC/SAC305 interface. For solder joint with porous Cu, the fracture at IMC formation was mostly at Cu_6Sn_5/SAC305 interface. Therefore, the fracture mode for solder joint with porous Cu interlayer addition occurred at Cu substrate/IMC, SAC305/IMC interface, and/or in porous Cu itself as shown in Figure 4.13(b). The existence of porous Cu interlayer in solder joint appear to have retarded the crack propagation thus providing the ductile behavior during the tensile testing. This improve the joint strength compared to solder joint without porous Cu addition.

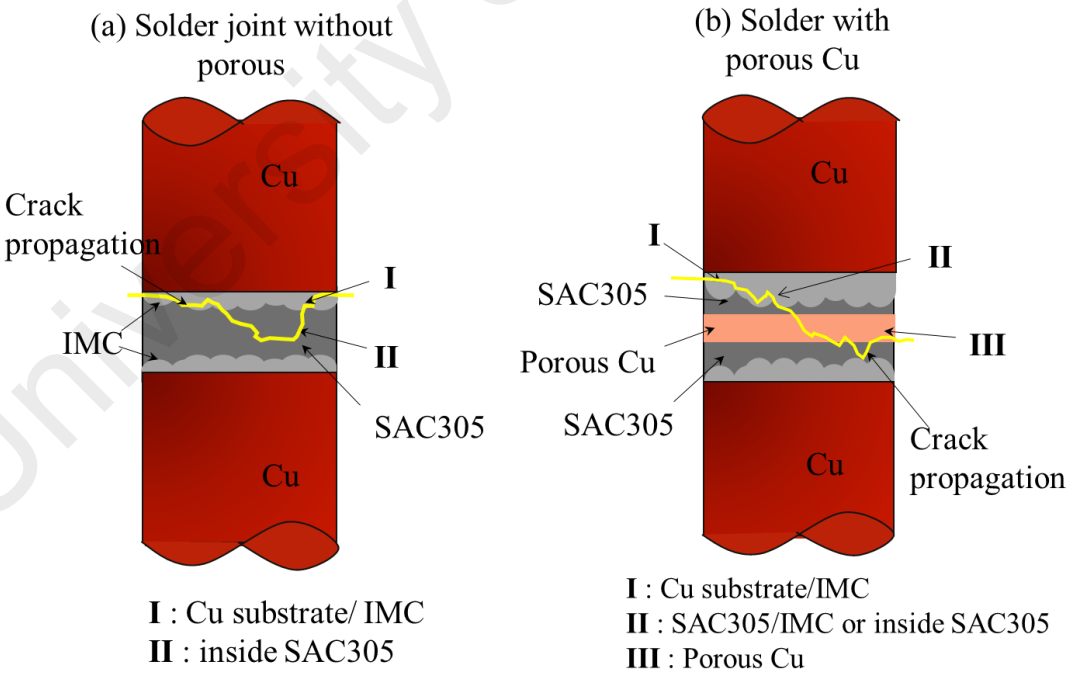

Figure 4.13 : Crack propagation mechanism for the solder joint (a) without porous and (b) with porous Cu interlayer

4.5.2.4 Load-Displacement Curve of Tensile Testing

The relationship between the test load and displacement of every solder joint sample at a constant speed of 0.5 mm/min and at room temperature is shown in Figure 4.14. The points marked x_1, x_2, x_3 are the elongation distances needed to break the solder joint for without porous Cu, with P15 porous Cu and with P25 porous Cu, respectively. It is clear that the elongation of the solder joint increased to a larger extent with the addition of porous Cu compared to the solder joint without porous Cu. The solder joint with higher P25 porous Cu porosity exhibited greater elongation than the P15 porous Cu solder joint. The decreasing elongation trend for the three solder joints is therefore as follows: $x_3 > x_2 > x_1$. It is apparent that the increased disbursement of Cu atoms from porous Cu into the interfacial region during molten solder solidification led to the formation of the IMC layer. The interaction of Cu atoms with IMC from the molten solder possibly restricted the diffusion of atoms, thereby causing increased solder joint motion resistance. These phenomena ultimately generate a plastic behavior of the solder joints (Liu, Wang, Tian, & Chen, 2008; Nadia & Haseeb, 2011).

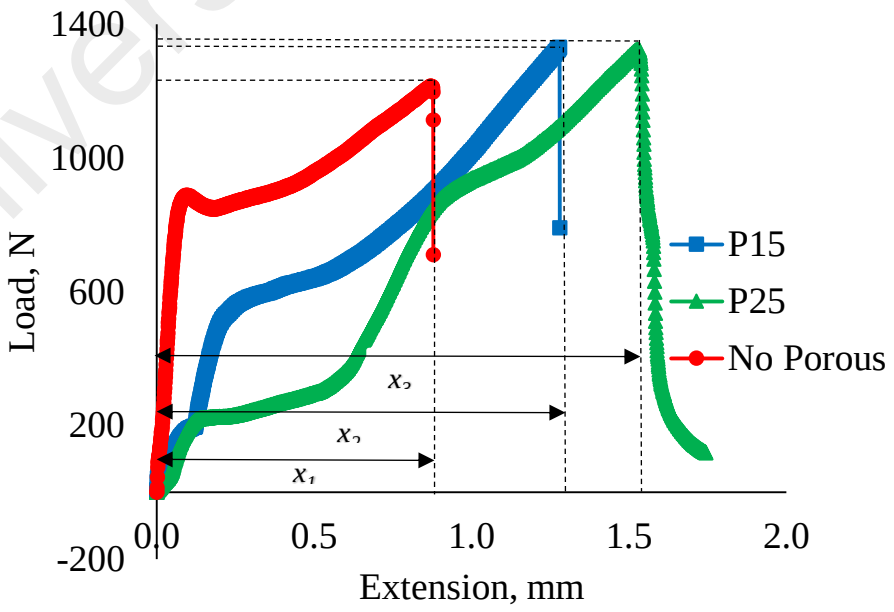

Figure 4.14 : Load-extension curve for solder joints with and without porous Cu soldered at 307°C for 300 s

4.5.3 Interfacial Microstructure Analysis

For interfacial analysis, solder joints were cross-sectioned perpendicular to the interfaces and then prepared according to standard metallographic techniques as described in section 3.8.1. The effect of adding a porous Cu interlayer to SAC305 solder joints on the interfacial microstructure will be elaborated in this section.

4.5.3.1 IMC Layer Thickness

It has been acknowledged that the IMC layer forms and develops at the solder alloy and substrate interface during the soldering process of a solder joint. It is a fact that the IMC interfacial reactions have a role in ensuring effective joining at solder alloy/solid substrate interfaces (Lee, Wang, & Kim, 2007). In the present study, this IMC layer formed at the interface between the SAC305 and Cu substrate as well as between the SAC305 and the porous Cu interlayer, is schematically illustrated in Figure 4.15. The average IMC layer thickness is calculated based on measurements taken at more than five points on one side of the interface where the IMC layer formed.

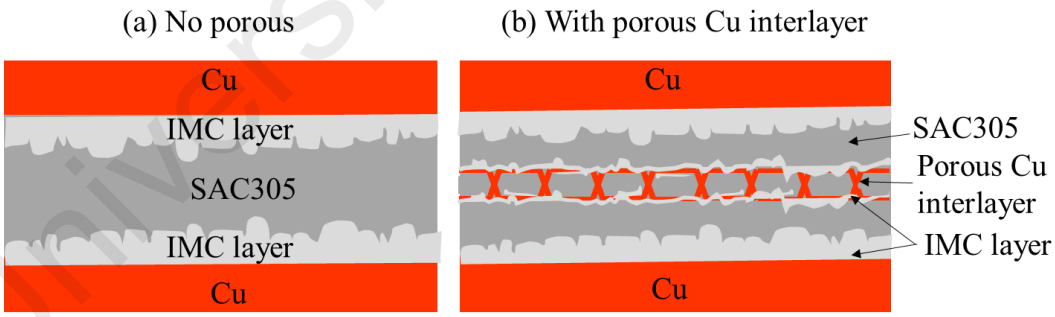

Figure 4.15 : Schematic of IMC layer formation at the Cu substrate/SAC305 and porous Cu/SAC305 interfaces

Figure 4.16 presents the average of IMC layer thickness as a function of soldering temperature for solder joints with and without porous Cu for a soldering time of 60 s. Not much variation is observed in the IMC layer thickness measurements for both interfaces

with increasing temperature at this soldering time. The highest IMC value of 3.42 µm for the solder joint with P25 porous Cu at soldering temperature of 307°C. This corresponds to the strength value of 38 MPa as shown in Figure 4.7, which is considered low for solder joining. This was similarly reported by Li et al., who recorded a SAC-0.1wt.%Re IMC layer thickness of 4.4 µm for joint strength of 43.5 MPa (Li, Shi, Hao, Xia, & Lei, 2009).

The interfacial reaction between porous Cu and the SAC305 solder alloy began active by prolonging the soldering time to over 60 s. At 180 s, the IMC layer thickness developed gradually at both SAC305/Cu substrate interface and SAC305/porous Cu interface, as illustrated in Figure 4.17. The Cu_6Sn_5 IMC layer in the SAC305/Cu substrate interface being more scallop-shaped than the more uniform IMC layers formed at SAC305/porous Cu interface, facilitated a 1.5 to 2.0 µm thicker IMC layer for both solder joints with porous Cu interlayers (P15 and P25) with every 20°C increment in soldering temperature. At the SAC305/porous Cu interface, the molten SAC305 solder alloy may have taken a longer time to react since it first needs to dissolve in the pore spaces of the porous Cu. This molten solder reacts with porous Cu at the atomic level to form a Cu_6Sn_5 IMC layer along the porous Cu interfaces. At 180 s soldering time, it appear that despite the rise in IMC layers in the solder joint with porous Cu, only a minimal increase in joint strength took place. This is because there exists an optimum thickness at which the IMC layer formed will develop an adhesion bonding with the joint interface to provide a good joint (Lee, Wang, & Kim, 2007). It can generally be speculated that the joint strength was enhanced with the addition of a porous Cu interlayer.

The average of IMC layer thicknesses in solder joints with and without porous Cu at prolonged soldering time of 300 s are shown in Figure 4.18. It can be seen that the IMC thickness at the SAC305/Cu substrate interface in solder joints with and without porous Cu exhibit a similar increment pattern, with thickness range of around 3.5-6.8 µm. This

thickness is common for a typical IMC layer at the SAC305/Cu substrate interface, as reported elsewhere (Wu, Yu, Law, & Wang, 2004). The IMC thickness at 180 s and 300 s at the SAC305/Cu substrate interface for both the control sample and with porous Cu (as observed from Figures 4.17 and 4.18) actually increased 1 μm for every 20°C increase of soldering temperature.

From the measurement, it can be assumed that the IMC thickness at the porous Cu/SAC305 interface reached the limit of formation at around 3.0-5.0 μm. The prolonged time of 300 s allowed Cu_6Sn_5 more time to grow at the SAC305/porous Cu interface. The mechanism of IMC layer formation at the interface is similar to that described above. The IMC layer thicknesses measured for joints soldered at the highest temperature parameter offered the highest strengths to the solder joints with P15 and P25 at 54 MPa and 51 MPa, respectively.

It has also been reported that the cooling rate influences IMC thickness along the solder joint interface (Wenge Yang, Felton, & Messler, 1995). The difference in cooling rates might be due to differences in thermal conductivity of the porous Cu interlayer inside the solder joint. In the present study, thermal conduction through the Cu metal during soldering dissipated heat into the molten solder flowing through the pore spaces during cooling. This eventually had a bearing on the solder alloy solidification. The increment in IMC thickness can be attributed to the solidification of molten solder during the cooling phase which ultimately resulted in IMC layer growth.

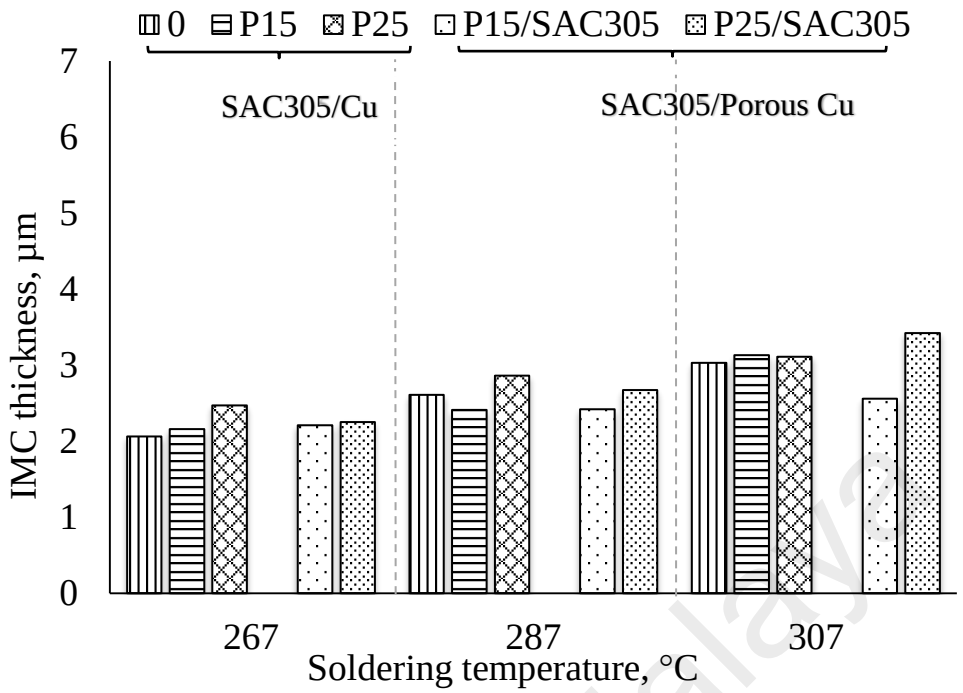

Figure 4.16 : Average IMC layer thickness as affected by soldering temperature for solder joint with and without porous Cu soldered at 60 s

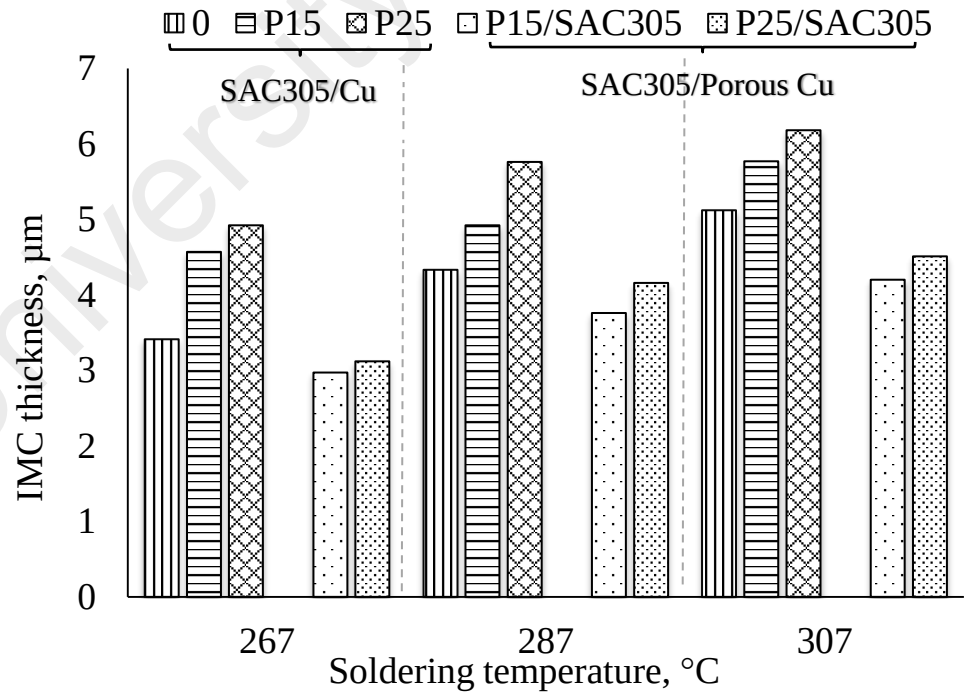

Figure 4.17 : Average IMC layer thickness as affected by soldering temperature for solder joints with and without porous Cu soldered at 180 s

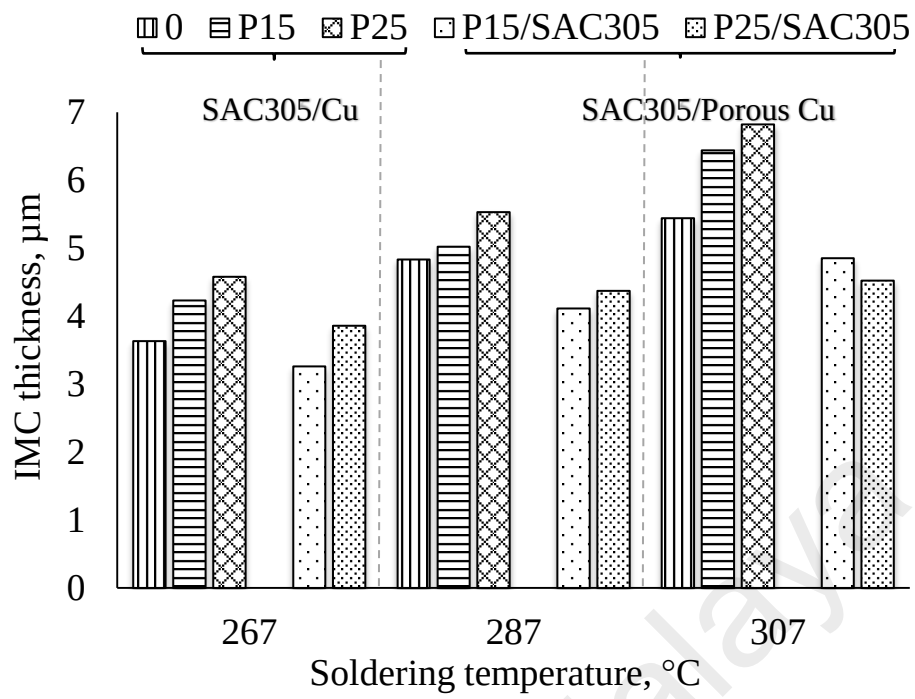

Figure 4.18 : Average IMC layer thickness as affected by soldering temperature for solder joints with and without porous Cu soldered at 300 s

4.5.3.2 Activation Energy in IMC Growth

Generally, the kinetics of IMC growth is diffusion-controlled (Huang, Xiu, Wu, Tian, & He, 2016). This activation energy are for the IMC layer to grow. It results from the dissolution of Cu from substrate, which therefore corresponds to the Cu atomic diffusion. The Cu atoms which have diffused into the solder will be utilized to form the Cu_6Sn_5 IMC.

Figure 4.19 shows the slope of the Arrhenius plot for IMC growth at 300 s soldering time. The calculations of the activation energy for IMC growth at the different interfaces were made from the graph plotted. The estimated activation energies of IMC growth at the Cu substrate/SAC305 interface in solder joints with no porous Cu, P15 porous Cu and with P25 porous Cu were 52.90 kJ/mol, 54.53 kJ/mol and 51.67 kJ/mol, respectively. These values are all approximately the same, indicating that similar reactions probably

occurred at the Cu substrate/SAC305 interface. IMC layer growth involves the diffusion of Sn atoms from the solder alloy and Cu atoms from the Cu substrate into the SAC305/IMC layer interface. This finding is similar to that obtained by Huang et al. for the activation energy of Cu and Sn atoms diffusion for the growth of Cu_6Sn_5 IMC (Huang, Xiu, Wu, Tian, & He, 2016).

Meanwhile, the activation energies for IMC growth at the SAC305/porous Cu interface for P15 and P25 were 51.73 kJ/mol and 20.62 kJ/mol, respectively. The different types of Cu in porous Cu interlayer have different sizes of grains and energy states result in different diffusion rate of Cu into the solder. Most likely, the porous Cu of P25 has high energy state after rolling compared to P15. These values also depend on the diffusion of Cu and Sn atoms through the IMC layer and the amount of atoms transferred across the interface.

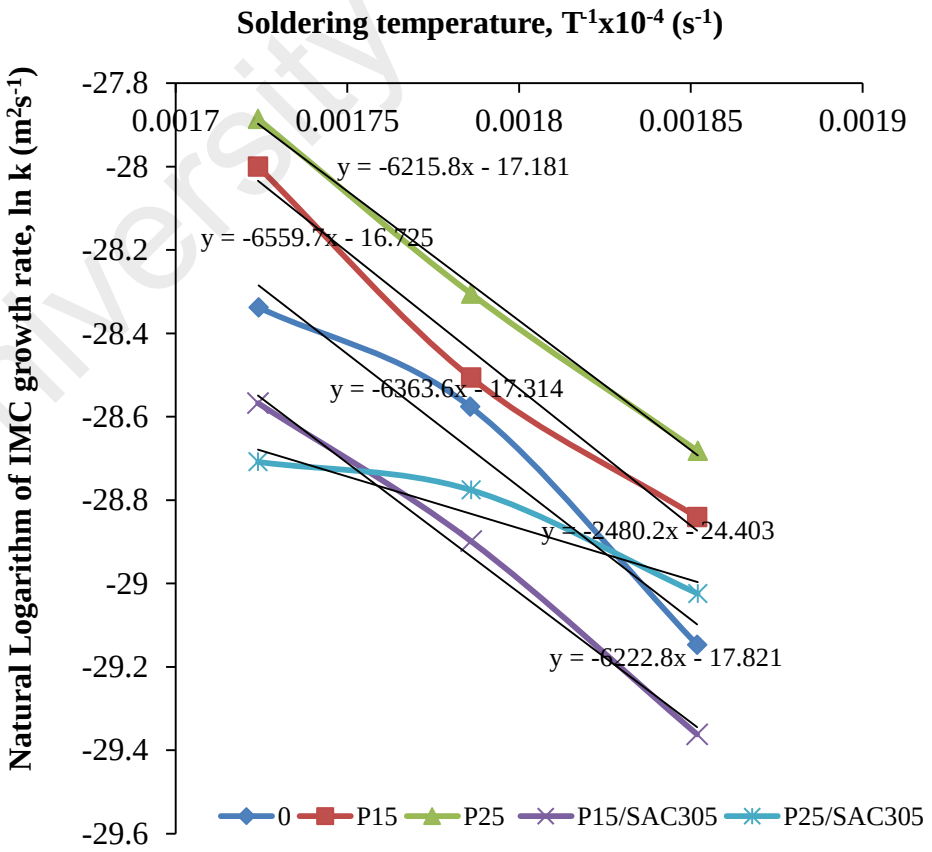

Figure 4.19 : Arrhenius plot of IMC layer thickness in solder joint soldered for 300 s

4.5.3.3 Cross-sectional Morphology

It has been acknowledged that the IMC layer forms and develops at the solder alloy and substrate interface. Thus, it is interesting to observe the cross-sectional morphology to study the effect of a porous Cu interlayer on the SAC305 solder alloy microstructure. Prior to observation, the sample was etched to reveal the microstructure. In the present study, the IMC layer was present at the interface between the solder and Cu substrate as well as between solder and the porous Cu interlayer.

Figure 4.20(a) presents the cross-sectional morphology and IMC formation for the control sample soldered at 307ºC for 300 s. The IMC layer appears rough with scallop-shaped structures, which are confirmed by EDS to be a Cu_6Sn_5, a typical IMC phase when the SAC solder alloy reacts with the Cu substrate. Typical coarse β-Sn dendrites approximately 16 µm in size exhibited from SAC305 with eutectic solidified were also detected. Based on the tensile test results, the joint strength of the control sample was lower compared to the solder joint with both P15 and P25. The situation is as such because the solder joint reliability is weakened by the coarse Sn dendrites in the joint microstructure (Anderson, Cook, Harringa, & Terpstra, 2002). At high SEM magnification, it appears that the Cu_6Sn_5 IMC grew as discontinuous scallop-shaped grains in the molten SAC305 solder resulting in a rough interfacial morphology between the IMC layer and the solder alloy (Figure 4.20(b)). A thin Cu_3Sn layer is observed at the interface between the Cu_6Sn_5 and the Cu substrate. However, the growth of Cu_3Sn IMC was limited by the short diffusion time, therefore most of the time it is difficult to observe. On account of the Cu atoms dissolving from the Cu substrate into the solder alloy, the residual voids left on the substrate and the solder/substrate interface would not be filled up rapidly by the Sn atoms released from the solder alloy. As a result, micro voids are formed in the IMC layer.

In contrast, a typical scallop-shaped and continuous layer of Cu_6Sn_5 IMC was spotted at the interfaces of the porous P15/SAC305 and porous P25/SAC305, as shown in Figure 4.21 and Figure 4.22. Cu is certainly highly adherent to the solder alloy (Guo, Xi, Peng, & Liu, 2007). During the soldering process, the surface energy of the liquid molten solder is lower than at the solid porous Cu surface, allowing a tendency to wet and interact with the P15 and P25 porous Cu interfaces.

As mentioned previously, P15 porous Cu has thick solid cell walls of 0.26 mm. This hinders the penetration of molten solder into the porous Cu as shown in Figure 4.21(a). According to the magnified view as in Figure 4.21(b), continuous Cu_6Sn_5 grew along the thin SAC305/P15 interface inside the porous Cu area. The uneven structure of pores facilitates more channels for the molten solder to penetrate into the internal porous structure. This increases Sn and Cu atoms diffusion and results in the formation of continuous IMC phase at the SAC305/porous interface. However, the width of each scallop-shaped grain was 5% narrower than at the SAC305/Cu substrate interface. As a result, a thicker of IMC layer formed at Cu substrate interface than at porous Cu as measured in Figure 4.16 – 4.18.

Evidently, the reaction between the solder alloy and substrate is desirable to achieve good metallurgical bonding (Zhang, Xue, Gao, Chen, & Yu, 2009). It is also noticeable inside the solder alloy that the dendrite structure of the Sn phase interrupted into finer dendrites which leads to the IMC eutectic dispersion among the inter-dendritic parts. When the solder joint with P15 porous Cu was exposed to high soldering temperature, for example 307°C, the porous Cu had the ability to absorb the heat, which therefore decreased the cooling rate. The nucleation of the intermetallic and β-Sn dendrites became longer and more refined, which is in agreement with Anderson et al.'s findings on doping SAC solder alloy with Fe and Co for microstructural modification (Anderson, Cook,

Harringa, & Terpstra, 2002). The smaller dendrites Sn phase enhanced the solder joint reliability in the joint strength (El-Daly & Hammad, 2011). Thus, greater joint strength was thus observed in solder joints with P15 porous Cu than those without porous Cu addition.

The structure of P25 porous Cu was more compact due to the thin solid walls of 0.06 µm. The smaller pore diameter of P25 porous Cu provided a larger contact area for the interfacial reaction between molten solder and porous Cu to form Cu_6Sn_5 IMC at the porous Cu/SAC305 interface as shown in Figure 4.22(a). Consequently, more diffusion of Cu-Sn atoms occurred at the porous Cu/SAC305 interface as the molten solder was penetrating into the P25 porous Cu as compared to P15 porous Cu, leading to the formation of a more uniform and less-developed scalloped Cu_6Sn_5 IMC structure as can be seen in Figure 4.22(b). As a result, the IMC layer formed was more uniform at the SAC305/P25 interface than at the SAC305/Cu substrate interface. It is also observed that the IMC layer resembled a rough and scallop-shaped structures.

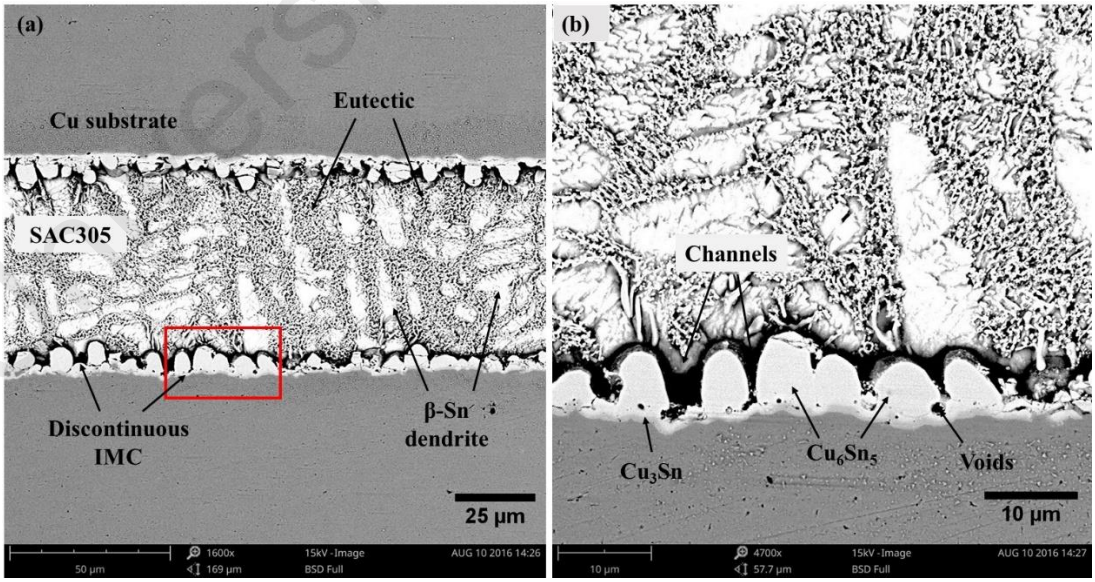

Figure 4.20 : (a) Cross-sectional morphology and (b) high magnification of the red area marked in (a) of a solder joint without porous Cu at 307°C and 300 s

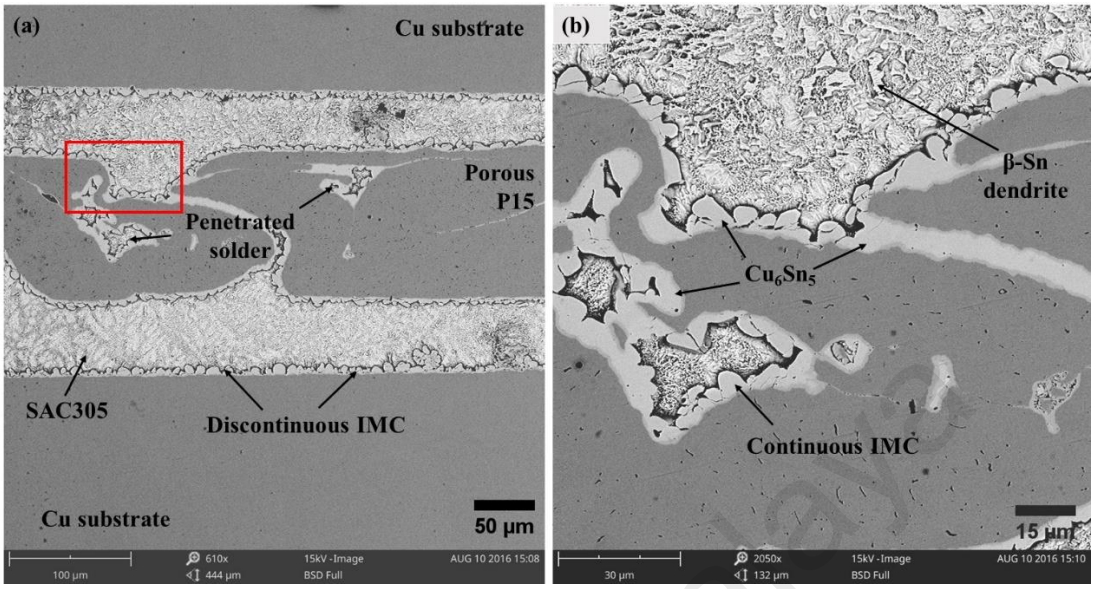

Figure 4.21 : (a) Cross-sectional morphology and (b) high magnification view of the red area marked in (a) of a solder joint with a P15 porous Cu interlayer at 307°C and 300 s

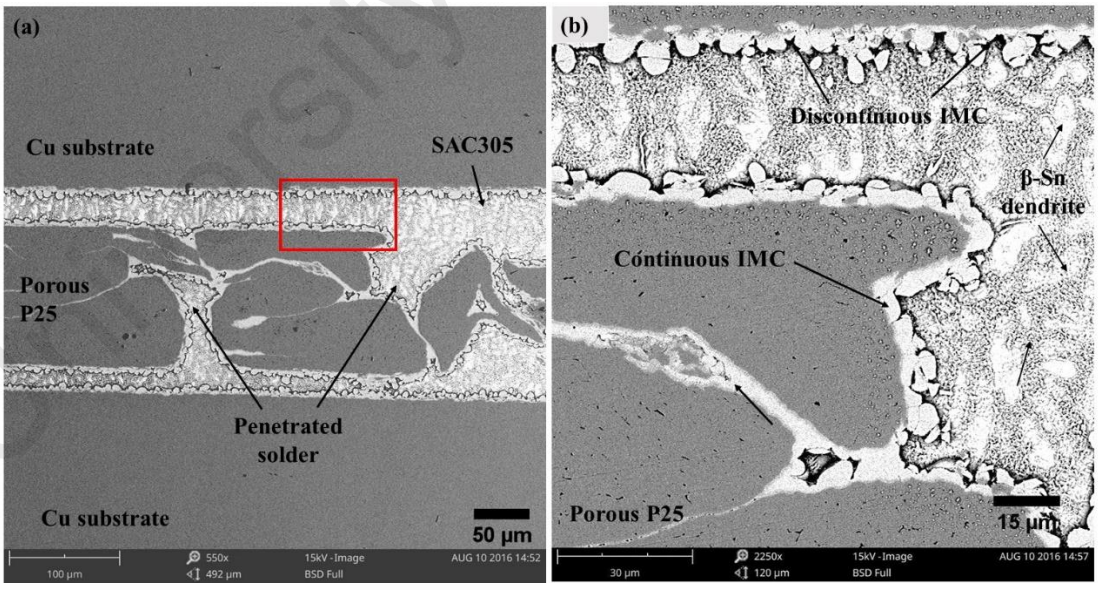

Figure 4.22 : (a) Cross-sectional morphology and (b) high magnification of the red area marked in (a) of a solder joint with a P25 porous Cu interlayer at 307°C and 300 s

4.6 Tensile and Microstructural Properties of Aged Sample

The SAC305 solder alloy selected in the current research is extensively applied in microelectronic assemblies owing to its superior thermal cycling properties. The liquidus point of SAC305 is 217ºC: hence it requires a higher reflow temperature of at least 240ºC, which makes it suitable for use in middle-temperature range applications (Kanchanomai, Miyashita, & Mutoh, 2002). It would also be desirable to develop alternative Pb-free soldering materials which is suitable for high-temperature soldering applications, particularly for die attach in power semiconductor packaging, where melting temperatures of 280°C or higher are required (Liu, Lee, & Bachorik, 2013). In addition, investigating thermal aging of solder joints is essential for evaluating strength reliability, particularly in industries requiring exposure to high operating temperatures (Sabri, Shnawah, Badruddin, & Said, 2013).

The current scope of investigating a SAC305 solder joint with a porous Cu interlayer added is therefore expanded to include thermal aging treatment. The objective is to study the effect of high temperature storage on joint reliability particularly on joint strength and microstructure. As-soldered joints with added P15 or P25 porous Cu interlayers served as samples for this study. The joint samples would undergo isothermal aging treatments at a single temperature of 150ºC for a duration of 100, 200 and 500 h.

All joint samples may be considered for isothermal aging treatment. However, it would be more meaningful to test only joint samples with favorable tensile strengths as obtained in as-soldered treatment. Thus joint samples having tensile strengths higher than 45 MPa would be desired since 45 MPa has been considered the threshold level for use in most electronic applications. Results from tensile tests showed solder joints at 300 s soldering time tend to give a relatively higher tensile strengths than that with shorter soldering time for both samples with P15 and P25 porous Cu interlayer addition. Thus all3 joint samples

from as-soldered treatments with soldering time of 300 s are subjected to isothermal aging evaluation.

4.6.1 Tensile Properties

Figure 4.23 presents the joint strength of the solder joint with P15 interlayer after isothermal aging for different soldering temperatures. It can be seen that the solder joint with P15 exhibited a significant reduction in joint strength with increasing aging time. The strength of the solder joint with P15 porous Cu at 267°C soldering temperature gradually decreased by about 10 MPa for every 100 h of aging time added from 0–200 h and continued to decrease until it reached 15 MPa at 500 h of aging. In contrast, the sample with P15 porous Cu soldered at 287°C exhibited radically decreased strength from 45 MPa to 25 MPa after undergoing isothermal aging at 150°C for the first 100 h, after which the strength gradually and slightly decreased until it reached 20 MPa at 500 h of aging. At high soldering temperature of 307°C, the strength of the solder joint with P15 porous Cu also gradually reduced from 55 MPa at 0 h to 22 MPa at 200 h and continued to drop until it reached 20 MPa at 500 h. On the other hand, the sample with P25 porous Cu at 267°C and 287°C soldering temperatures, the higher joint strength degraded sharply from about 50 MPa to 25 MPa during the first 100 h and later dropped further to 16-20 MPa after 500 h aging time as shown in Figure 4.24. At 307°C, a gradual reduction in strength was clearly observed with a decrease from 50 MPa at 0 h to 22 MPa at 500 h.

The results show that both joints with added of P15 and P25 porous Cu had strengths very much reduced to 20 MPa after 500 h aging time. After 100 h aging time, both solder joints with added of P15 and P25 porous Cu still possess strength of 45 MPa. If 45 MPa is taken as the threshold strength to ensure joint reliability, then both SAC305 with added of P15 and P25 porous Cu may be applied in microelectronic assemblies operating at relatively high temperature (e.g.150°C) and running time of 100 h or less.

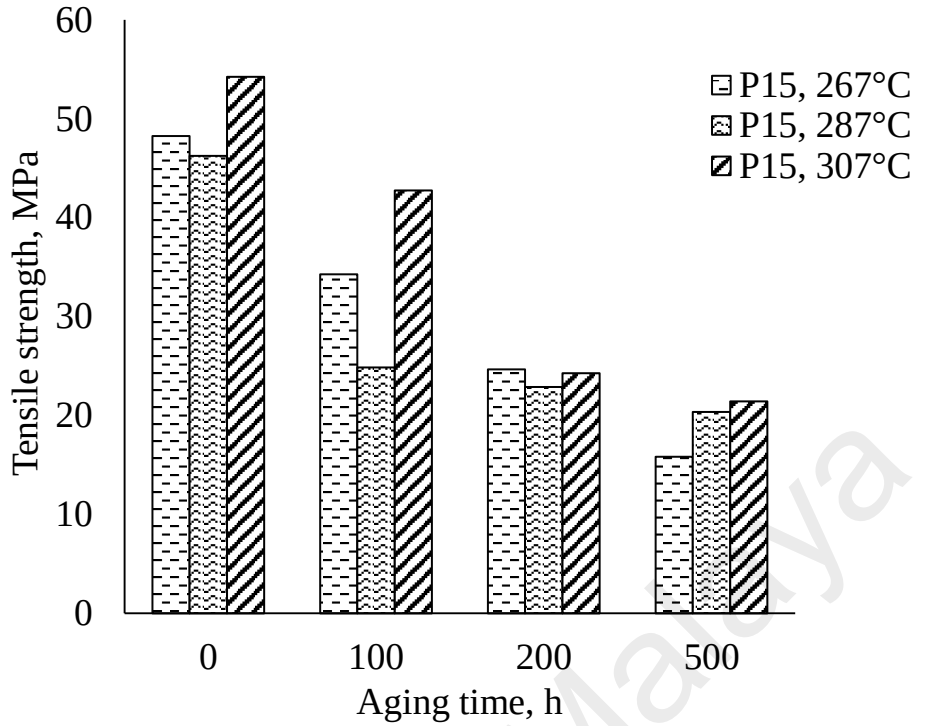

Figure 4.23 : Effect of aging time and soldering temperature on the joint strength of a solder joint with P15

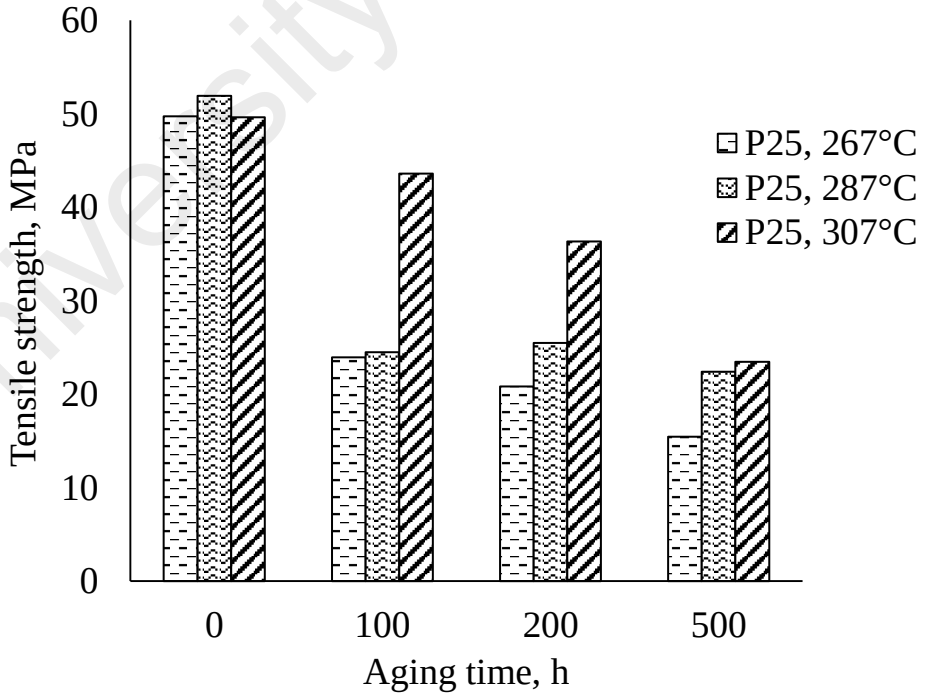

Figure 4.24 : Effect of aging time and soldering temperature on the joint strength of a solder joint with P25

4.6.2 Fractured Surface Analysis

Fracture morphology was observed in order to understand the effect of isothermal aging on failure behavior and to study the dominant factor in improving solder joint reliability. For illustrative purposes, samples of SEM photo-micrographs of fractured surfaces taken after tensile testing for sample aged at 0, 100, 200 and 500 h for joints soldered with P15 and P25 porous Cu interlayer are shown in Figure 4.25 and Figure 4.26, respectively.

Figure 4.25(a) displays a typical fracture of as-soldered samples (0 h aging time) with lots of dimples and residual solder on the surface. The fracture form of the porous Cu interlayer is obvious as shining dimples on the broken surface. With increasing aging time, the fractured surface appears to have a reduced amount of dimples and is therefore less rough than that at 0 h (Figure 4.25(b)-(d)). This suggests brittle fractures occurred in the IMC layer which can be attributed to the breaking up of Cu_6Sn_5 in the IMC layer that grows at excessive temperatures. This can be explained by the large presence of Cu_6Sn pieces in the IMC phase on the fracture surface resulting in lower joint strength, especially at 500 h aging time (~20 MPa). The reduction in joint strength is caused by the coarsening of the IMC grains that developed from the atomic reactions of the solder alloy and porous Cu during isothermal aging. Therefore, it can be concluded that the penetration of molten solder into the porous Cu in the solder joint tends to increase with increasing porosity and significantly influences the fracture morphology and strength of the joint.

Analysis of fractured surface of as-soldered sample of P25 porous Cu as shown in Figure 4.26(a), showed failure mostly occurred at the inner solder interlayer and SAC305/porous Cu interface while less occurred inside the IMC layer. After 100 h aging, the dimple-like fractured surfaces reduced significantly and the cleavage-like surfaces increased gradually with more cracks occurring at the SAC305/IMC interface as shown

in Figure 4.26(b)-(d). After 500 h aging, the flat cleavage-like surfaces almost covered the fractured surface with cracks at the IMC/IMC interface. Prolonged aging time such as 500 h resulted in excessive IMC growth which exhibited a deleterious effects on joint strength.

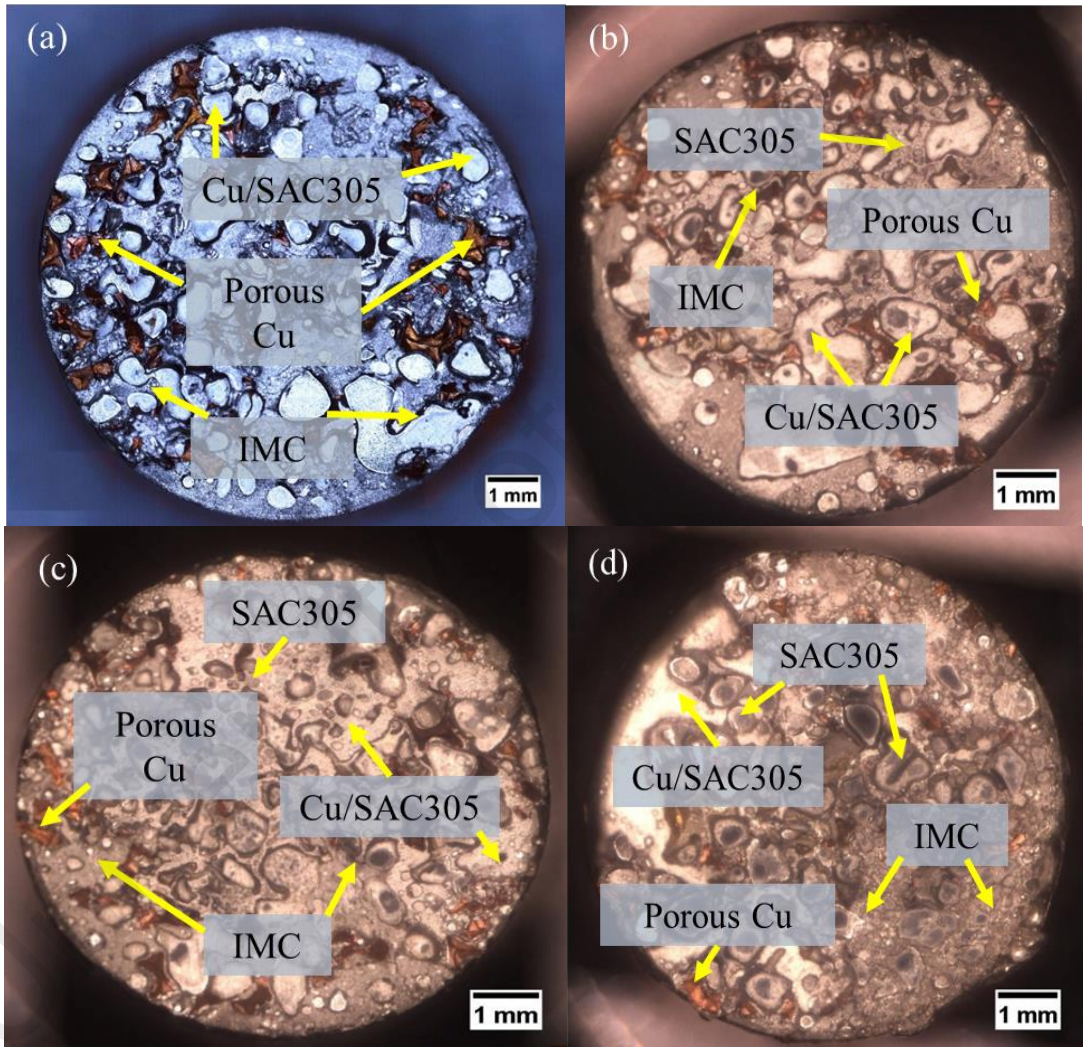

Figure 4.25 : Effect of isothermal aging at 150°C for (a) 0h, (b) 100 h, (c) 200 h and (d) 500 h on the fracture morphology of a solder joint with an added P15 porous Cu interlayer

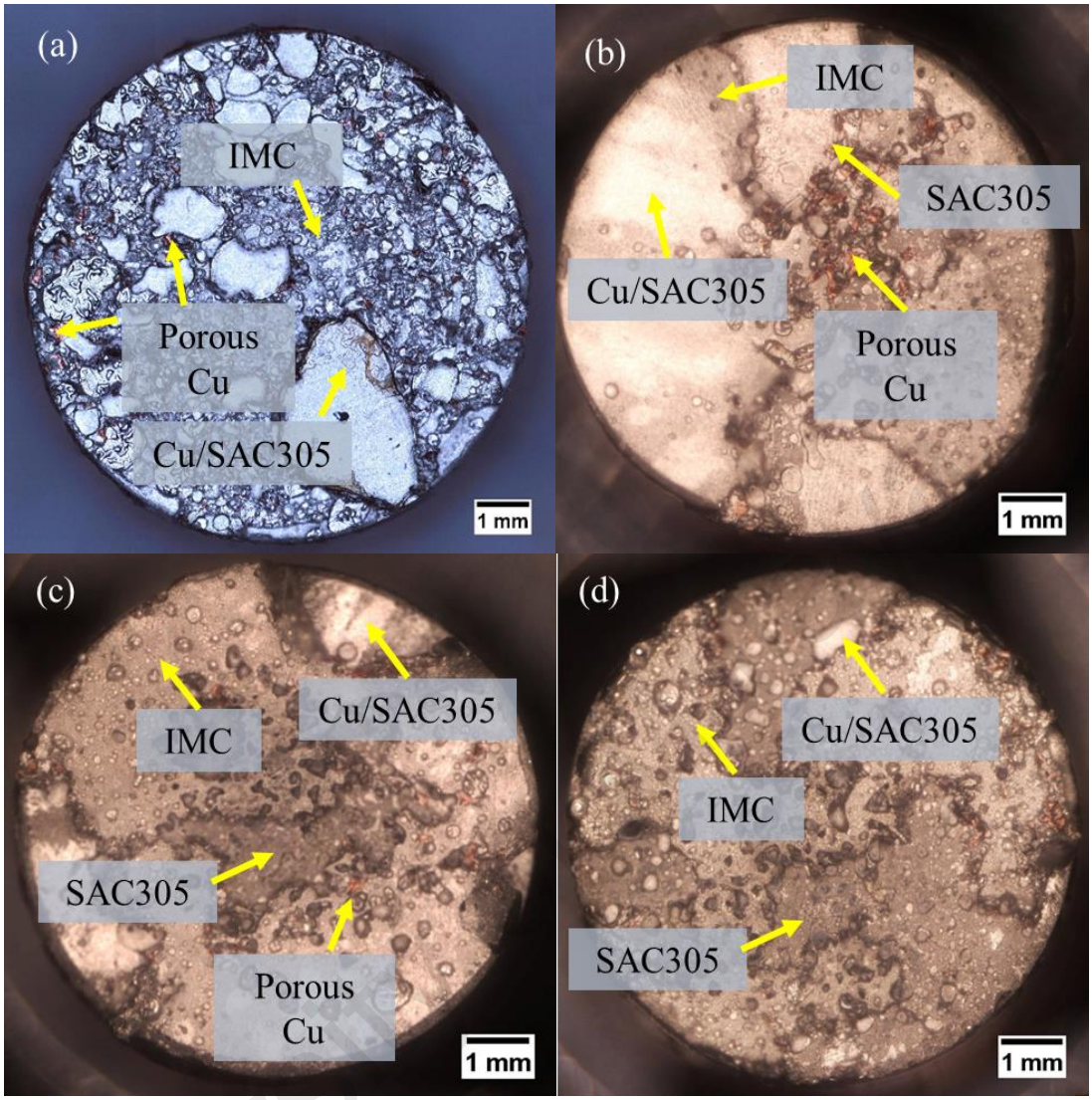

Figure 4.26 : Effect of isothermal aging at 150°C for (a) 0h, (b) 100 h, (c) 200 h and (d) 500 h on the fracture morphology of a solder joint with an added P25 porous Cu interlayer

4.6.2.1 Fracture Mode

To show the relationship between failure mode and aging time, the fracture mode percentages for solder joints with added P15 and P25 porous Cu are presented in Figure 4.27 and Figure 4.28, respectively. Fractures are visible in the following regions: i) Cu/SAC305 interface, ii) porous Cu, iii) inside solder and iv) IMC phase of the solder joint. It was found that mixed fractures failure at the SAC305/Cu interface and inside the solder were dominant in the solder joint at 0 h of aging time. With increasing aging time,

the percentage of brittle failure (fractures at IMC) increased. The IMC phase fracture possibly occurs inside Cu_6Sn_5, inside Cu_3Sn, in the Cu_6Sn_5/Cu_3Sn interface and in the Cu_6Sn_5/solder interface. IMC layer growth and the fractured surface roughness influenced the mechanical characteristic of the solder. Increased IMC thickness had increase the stress concentration at the solder/porous Cu interface, leading to deteriorating the joint strength. In addition, bright dimples of broken porous Cu disintegrate. All these factors led to diminished joint strength. The crack analysis for both solder joint with P15 and P25 have similar characteristics of fracture mode.

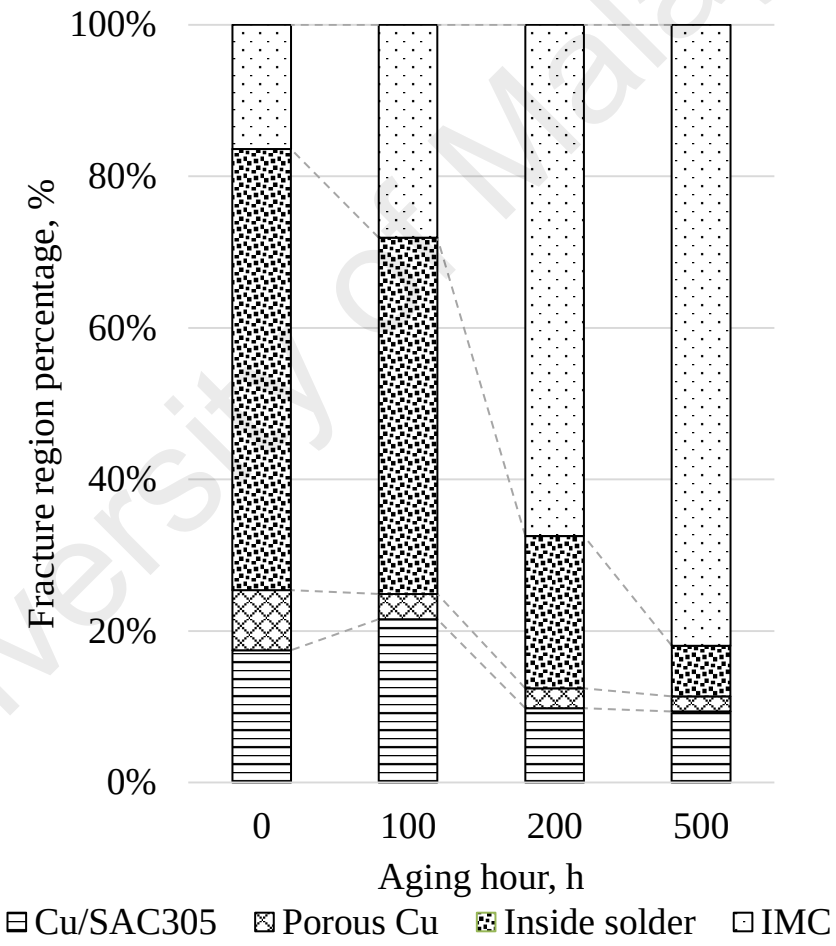

Figure 4.27 : Fracture mode percentage for a solder joint with P15 porous Cu against aging time

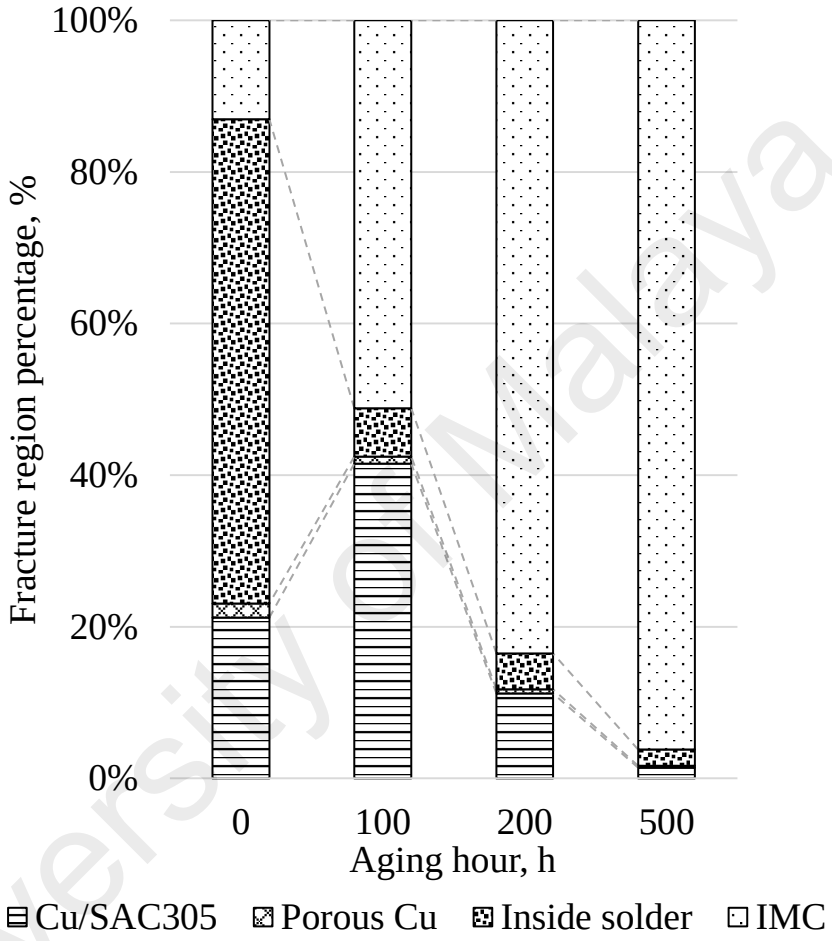

Figure 4.28 : Fracture mode percentage for a solder joint with added P25 porous Cu against aging time

4.6.2.2 XRD Analysis

X-ray diffraction (XRD) analysis was performed to examine the phase of IMC. The fracture behavior observed in section 4.6.2 is verified by the XRD patterns. Figure 4.29 and Figure 4.30 show the XRD patterns of solder joints with P15 and P25 porous Cu interlayers at various aging times (i.e. 100, 200 and 500 h), respectively.

According to Figure 4.29, Cu element is the predominant peak at all aging times. However, the Cu_6Sn_5 IMC phase later increased with increasing aging time (100 – 500 h). This may be due to the fact that more diffusion of Cu-Sn atoms occurred at the porous Cu/SAC305 interface during molten solder penetration in the soldering process. Subsequently, further IMC layer growth occurred during thermal storage.

In contrast, Figure 4.30 shows Cu_6Sn_5 and Cu_3Sn of IMC as the predominant elements. This may be attributed to the fact that more molten solder penetrated inside the P25 porous Cu and the interfacial reaction rate was higher in the solder joint with P25 porous Cu compared to P15 porous Cu. Fractures occurred more in the SAC305/IMC interface and less in the solder and Cu substrate/solder interfaces.

Therefore, based on the XRD measurements of both solder joints with P15 and P25 porous Cu interlayers, aging time had increased the predominant elements were Cu_6Sn_5 and Cu_3Sn. This was due to IMC thickness growth along the solder/solid interfaces, which was further influenced by the long exposure times to high temperatures.

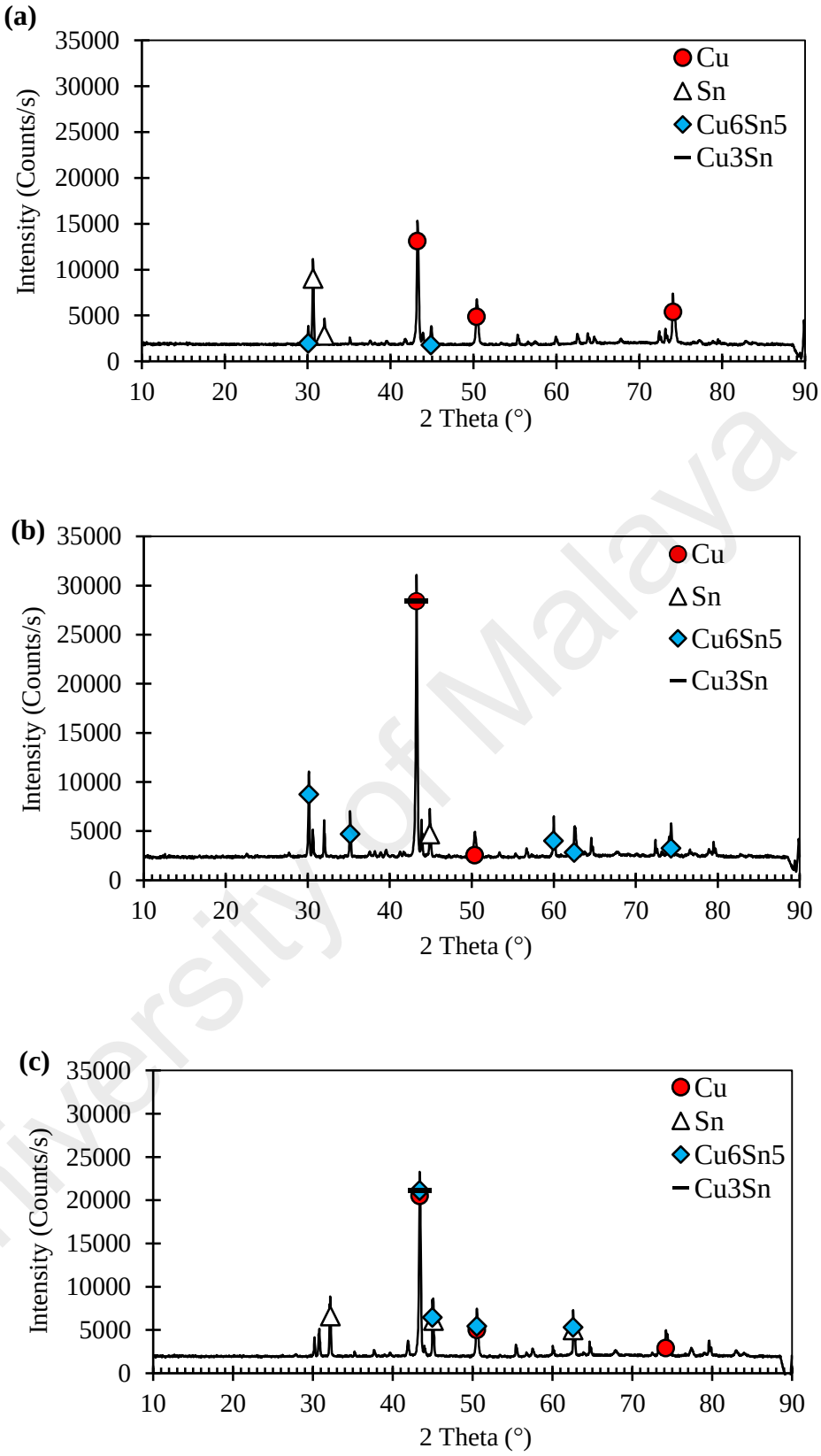

Figure 4.29 : XRD analysis of fractured surface with P15 porous Cu after (a) 100 h, (b) 200 h and (c) 500 h aging time

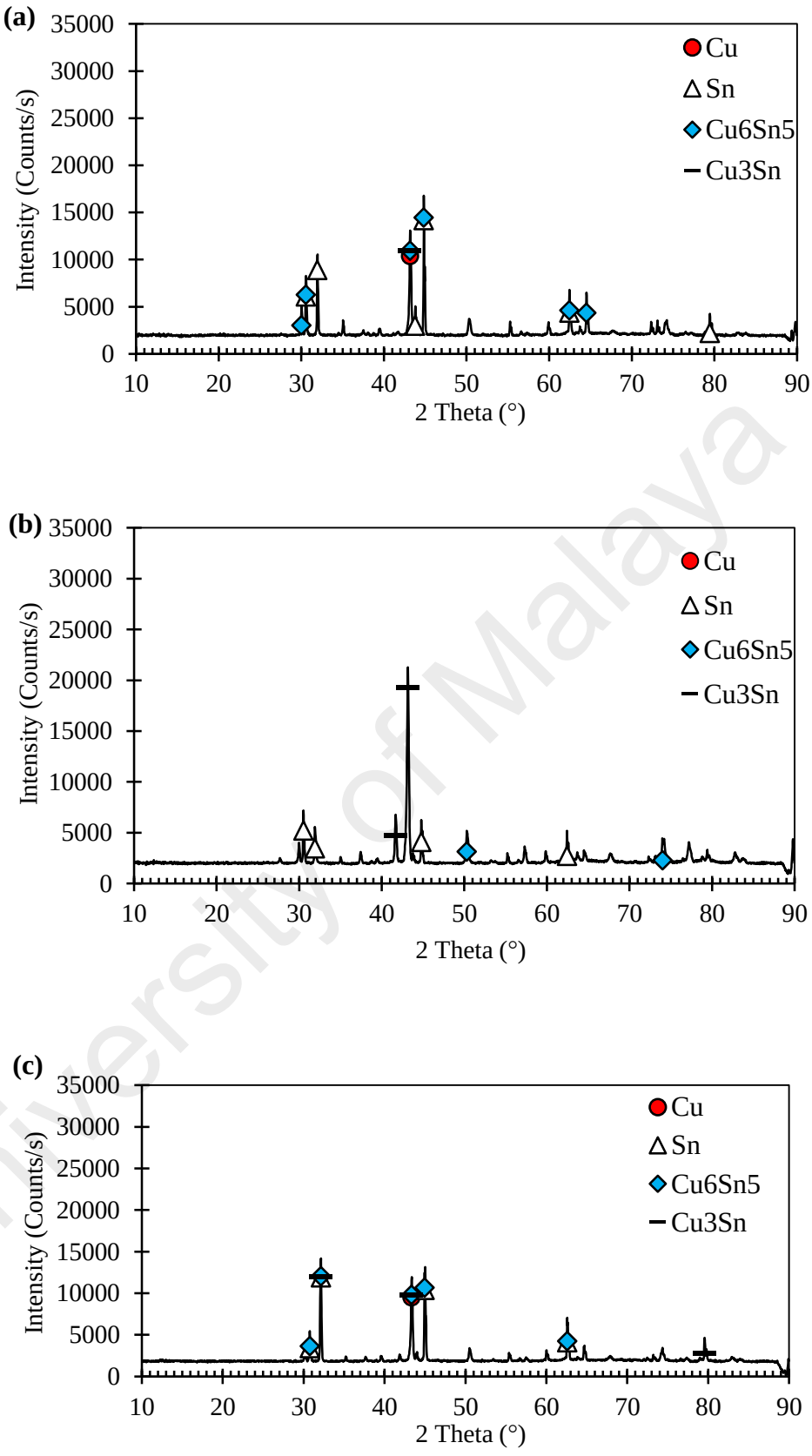

Figure 4.30 : XRD analysis of fractured surface with P25 porous Cu after (a) 100 h, (b) 200 h and (c) 500 h aging time

4.6.3 Interfacial Microstructure Analysis

The overall solder properties are dependent on the microstructure of the solder joint (Smith & Madeni, 2002). This section focuses on IMC formation at the joint interfaces namely on its thickness as aging progresses. It also includes analysis on the cross-sectional morphology.

4.6.3.1 IMC Layer Thickness

The IMC layer of an aged sample consists of Cu_6Sn_5 and Cu_3Sn phases, as confirmed by EDS analysis. Figure 4.31 illustrates the method used to measure IMC thickness at the solder joint interface. It is observed that the IMC layer is not uniform, with some areas thicker than the others. Therefore, several readings were taken at different areas using ImageJ software before the average IMC thickness was calculated.

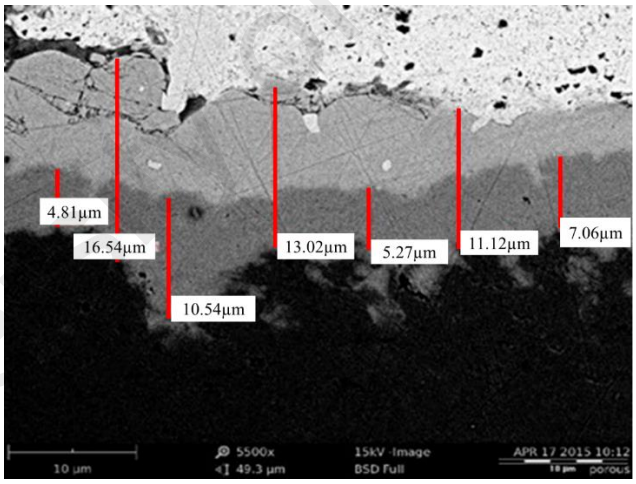

Figure 4.31 : IMC thickness measurement

The average thickness for an aged IMC sample with P15 and P25 porous Cu, (at soldering temperatures of 267°C, 287°C, 307°C for 300 s) is plotted for two conditions: 1) IMC growth at the SAC305/Cu substrate interface and 2) IMC growth at the SAC305/porous Cu (P15 and P25) interfaces. The graphs are plotted as a function of IMC thickness and aging time for both porosity at each of the soldering temperature (267°C, 287°C and 307°C).

Figure 4.32 represents the IMC thickness at the SAC305/Cu substrate interface as a function of aging time at soldering temperature of 267°C. Based on the figure, the thickness of both Cu_3Sn and Cu_6Sn_5 layers increased significantly during the first 200 h of aging, after which no increase or a marginal increase in thickness was generally observed. The thickness of total IMC layer (Cu_3Sn + Cu_6Sn_5) also increased from 4 µm to 8 µm after 500 h of aging for both solder joints (with P15 and P25 porous Cu interlayers).

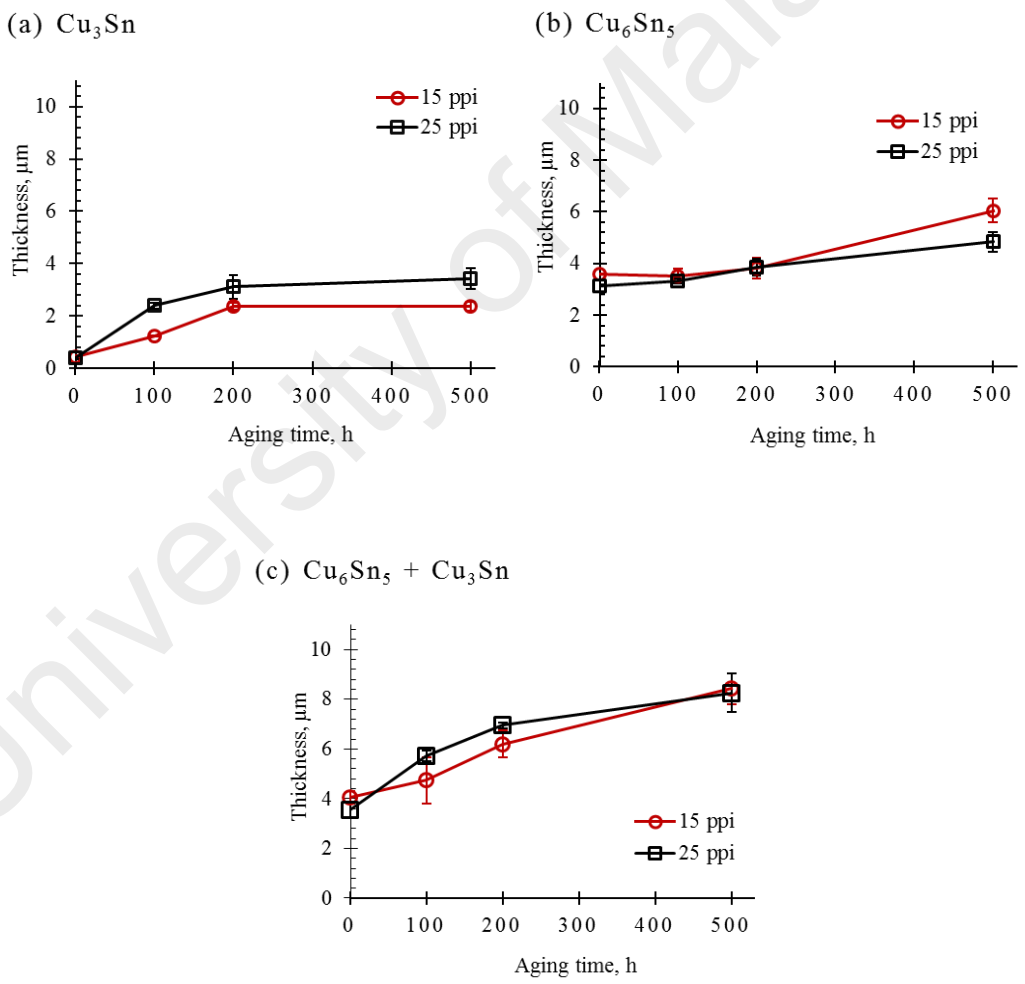

Figure 4.32 : IMC thickness versus aging time according to porosity of the solderCu substrate interface at soldering temperature of 267°C

Figure 4.33 denotes the IMC thickness at the SAC305/substrate interface as a function of aging time and soldering temperature of 287°C. According to the figure, the thickness of Cu_6Sn_5 increased by 1.0 and 1.5 µm after 500 h in the solder joints with P15 and P25 porous Cu interlayers, respectively. Cu_3Sn grew to 3.5 µm after 500 h of aging in both solder joints with porous Cu interlayers. Cu_3Sn growth was more than 3 times faster than Cu_6Sn_5 growth at soldering temperature of 287°C. The thickness of the entire IMC layer (Cu_3Sn+ Cu_6Sn_5) increased from 4.8 µm to 10.0 µm after 500 h aging time in both solder joints with P15 and P25 porous Cu interlayers. It is obvious that the increase in total IMC thickness was mainly due to the growth of Cu_3Sn rather than the Cu_6Sn_5 layer.

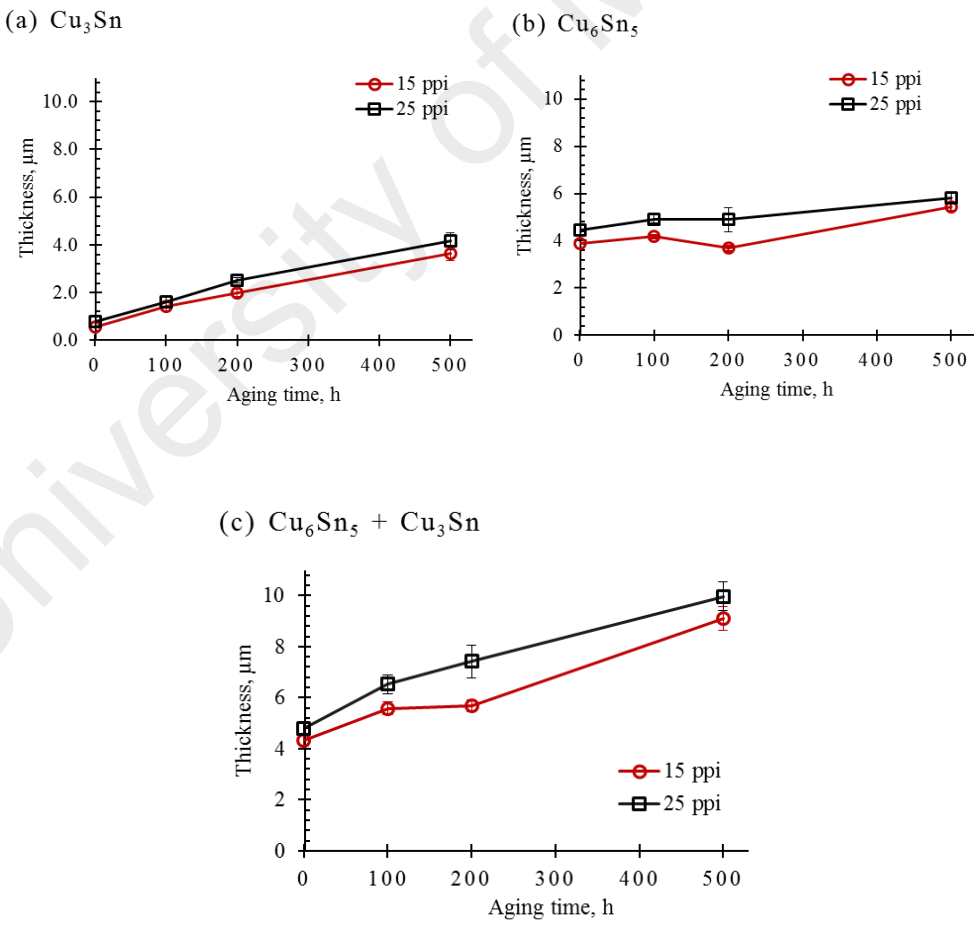

Figure 4.33 : IMC thickness versus aging time and according to porosity of solder/Cu substrate interface at soldering temperature of 287°C

Figure 4.34 illustrates the IMC thickness at the SAC305/Cu substrate interface as a function of aging time at soldering temperature of 307°C. The increase in IMC thickness was mainly due to the growth of Cu_3Sn. However, the thickness changes rate from the initial hour to 200 h of aging was much faster at 307°C compared to the other soldering temperatures (i.e. 267 and 287°C). This is due to the thickness of Cu_3Sn IMC increase rapidly during the first 200 h of aging time at the interface of Cu_3Sn/Cu_6Sn_5 IMC. The accelerated growth of this Cu_3Sn IMC was effected by consuming the thick Cu_6Sn_5 layer that had developed. Moreover, Cu_3Sn layer expanded on both sides (Cu interface and Cu_3Sn/Cu_6Sn_5 interface) during thermal aging at 150°C, resulting in thicker and faster formation of IMC layer. The thickness the entire IMC layer ($Cu_3Sn + Cu_6Sn_5$) increased from 5.3 µm to 9.0 µm after 500 h aging time for both solder joints with P15 and P25 porous Cu interlayers.

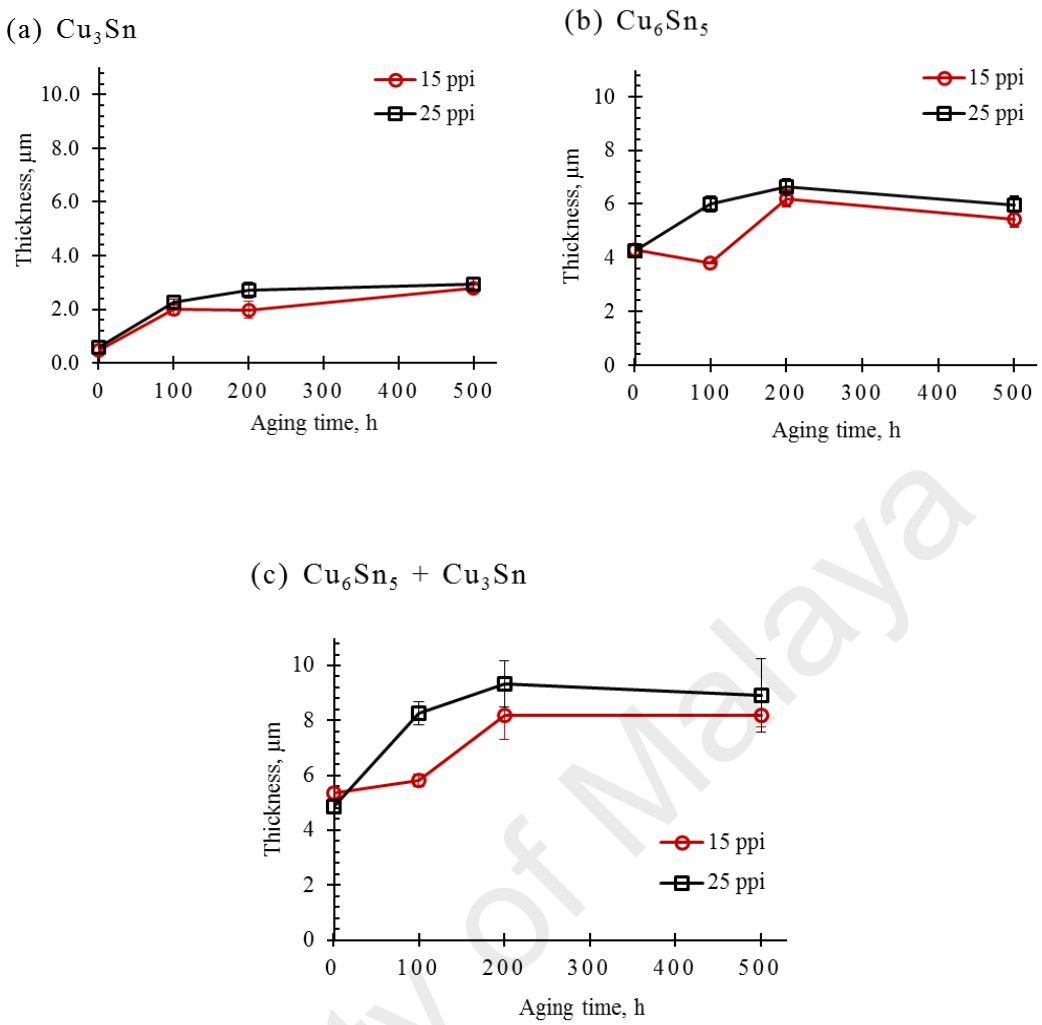

Figure 4.34 : IMC thickness versus aging time and porosity of the solder/Cu substrate interface at soldering temperature of 307°C

Figure 4.35 represent IMC thickness at the SAC305/porous Cu interface as a function of aging time at soldering temperature of 267°C. It is observed that the Cu_3Sn layer thickness increased during the first 200 h of aging for both solder joints with P15 and P25 porous Cu interlayers. Thereafter the thickness decreased very slowly from 2.0 to 1.8 µm for the P15 porous Cu interlayer and increased marginally from 2.0 to 3.0 µm for the porous Cu at 500 h aging time. However, the Cu_6Sn_5 layer did not appear to grow. This means the IMC did not increased in thickness due to the consumption rate of Cu_6Sn_5 for Cu on Cu_3Sn IMC layer was lower at SAC305/porous Cu interface for soldering

temperature of 267°C. Meanwhile, the thickness of the total IMC layer (Cu_3Sn+ Cu_6Sn_5) also increased slowly from the initial 4.3 µm to approximately 7.0 µm after 500 h of aging for both solder joints with P15 and P25 porous Cu interlayers.

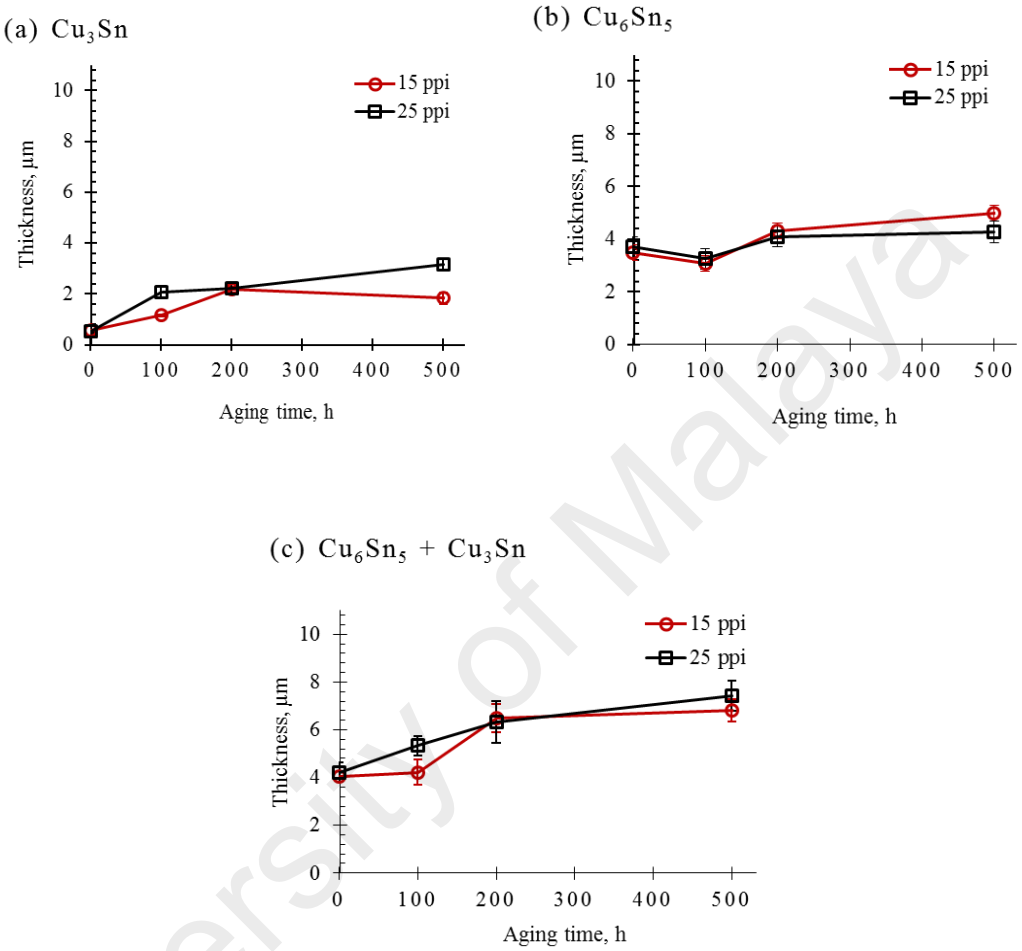

Figure 4.35 : IMC thickness versus aging time and porosity of solder/porous Cu interface at soldering temperature of 267°C

Figure 4.36 illustrates the IMC thickness at the SAC305/porous Cu interface as a function of aging time at soldering temperature of 287°C. According to the figure, both Cu_3Sn and Cu_6Sn_5 layer thickness increased significantly with aging time for the solder joints with P15 and P25 porous Cu interlayers. The thickness of the total IMC layer (Cu_3Sn + Cu_6Sn_5) increased from 4.3 µm to 9.4 µm and 10.8 µm after 500 h of aging for

the solder joints with P15 and P25 porous Cu interlayers, respectively. The growth rate was relatively faster at 287°C than 267°C.

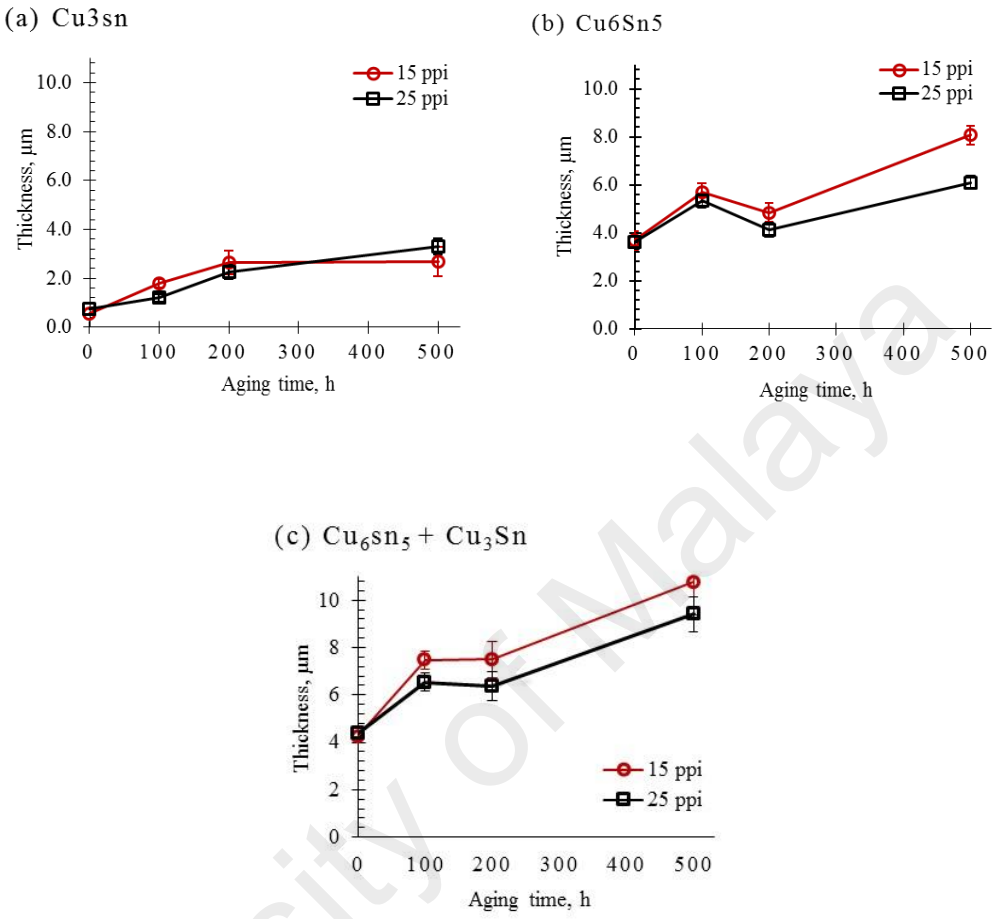

Figure 4.36 : IMC thickness versus aging time and porosity of solder/porous Cu interface at soldering temperature of 287°C

Figure 4.37 illustrates the IMC thickness at the SAC305/porous Cu interface as a function of aging time at soldering temperature of 307°C. The results are similar to those presented in Figure 4.36, where both Cu_3Sn and Cu_6Sn_5 layers thickness increased significantly during the first 200 h of aging for the solder joints with P15 and P25 porous Cu interlayers; thereafter the Cu_3Sn thickness remained constant at about 3.0 µm at 500 h of aging for both porous Cu layers. After 200 h aging time, Cu_6Sn_5 in both P15 and P25 porous Cu interlayers gradually reduced from 8.0 µm and 5.0 µm at 200 h aging time to

7.5 µm and 4.5 µm at 500 h aging time, respectively. Despite the general increase in total IMC layer thickness (Cu_3Sn + Cu_6Sn_5) during the first 200 h of aging in both solder joints with P15 and P25 porous Cu interlayers, it thereafter decreased slowly from 10.3 µm to 10.0 µm and from 8.0 µm to 7.5 µm, respectively, at 500 h aging time.

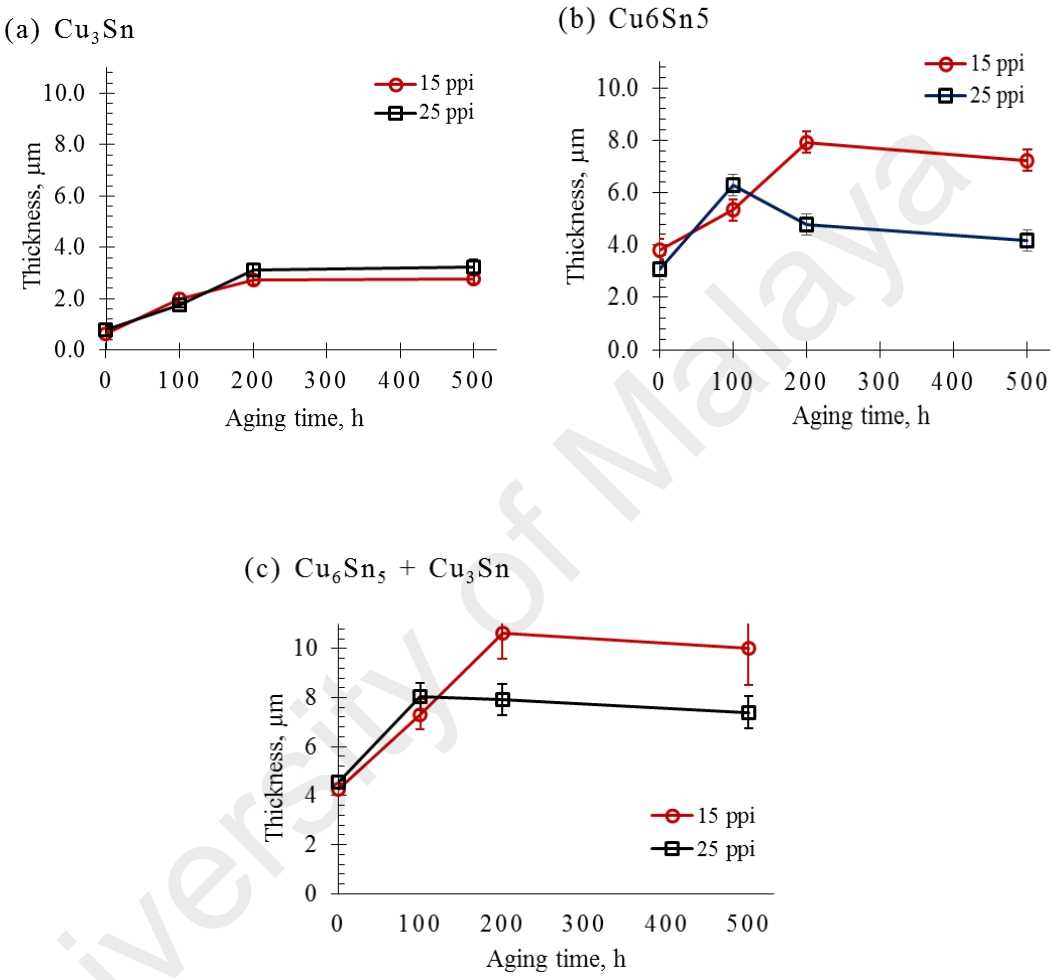

Figure 4.37 : IMC thickness versus aging time and porosity of solder/porous Cu interface at soldering temperature of 307°C

During soldering, a reaction took place between the substrate material and the solder, leading to the formation of a secondary phase, which is a combination of Sn (from the solder material) and Cu, in the form of a Cu_6Sn_5 and/or Cu_3Sn IMC phases. The observation was made at two interlayers where IMC formed: first, IMC growth at the

SAC305/Cu substrate interface and second, IMC growth at SAC305/porous Cu interface for both samples (P15 and P25).

4.6.3.2 Cross-sectional Morphology

Figure 4.38 presents the IMC morphology at the SAC305/Cu substrate interface at (a),(c) 100 h, (b),(d) 200h and (c),(e) 500 h aging time for (a)-(c) P15 porous Cu and (d)-(f) P25 porous Cu, respectively. According to the figures, the layer consists of two types of IMC phases, Cu_6Sn_5 and Cu_3Sn. The Cu_3Sn phase with a relatively darker contrast appears below the Cu_6Sn_5 phase. This new IMC layer, Cu_3Sn is observed in the solid-state reaction at the interface between Cu_6Sn_5 and the Cu substrate. In the initial stage, Cu_6Sn_5 exhibited a typical scallop shape in the SAC solder (Figure 4.38(a)). As aging time increased, the Cu_6Sn_5 layer appeared smoother and flatter. Peng et al. reported that the increase in total IMC layer at 500 hours of aging at 150°C for the SAC solder was more greatly influenced by the growth of Cu_3Sn rather than Cu_6Sn_5 (Peng, Monlevade, & Marques, 2007). It is postulated that at high temperature, Cu_6Sn_5 is likely converted to Cu_3Sn at the interface. The reaction can be derived from the following equation:

$$Cu_6Sn_5 + 9\ Cu \rightarrow 5\ Cu_3Sn \qquad (4.1)$$

Moreover, the amount of Cu atoms diffusing in the Cu_6Sn_5/solder interface was greatly reduced, while for Cu_6Sn_5 the amount increased.

The broken IMC with voids and cracks was observed at SAC305/IMC interface for P15 solder joint due the brittleness of the formed IMC. With prolonged aging time the IMC layer became rougher and rougher. At 100 h, it is observed that the IMC layer began to crack at the brittle Cu_6Sn_5 IMC layer (Figure 4.38(b)). With long-term storage, a large amount of Cu atoms near the existing IMC diffused therein, creating large voids that weakened the solder bonding near the IMC. With continuous high-temperature thermal

storage, the solder joint strength decreased rapidly, as observed in Figure 4.38(c). The IMC was growing until the diffusion of Cu atoms was blocked by the voids and cracks. Subsequently the growth rate of IMC formation was reduced at SAC305/Cu substrate interface.

On the other hand, the IMC evolution at the SAC305/Cu substrate interface for P25 shows no major destruction with increasing aging time where the IMC morphology was transformed from weaving layer to a uniform layer (Figure 4.38(d)-(f)). Only the typical scallop-type of Cu_6Sn_5 IMC formed at the interface and a thin Cu_3Sn began to grow.

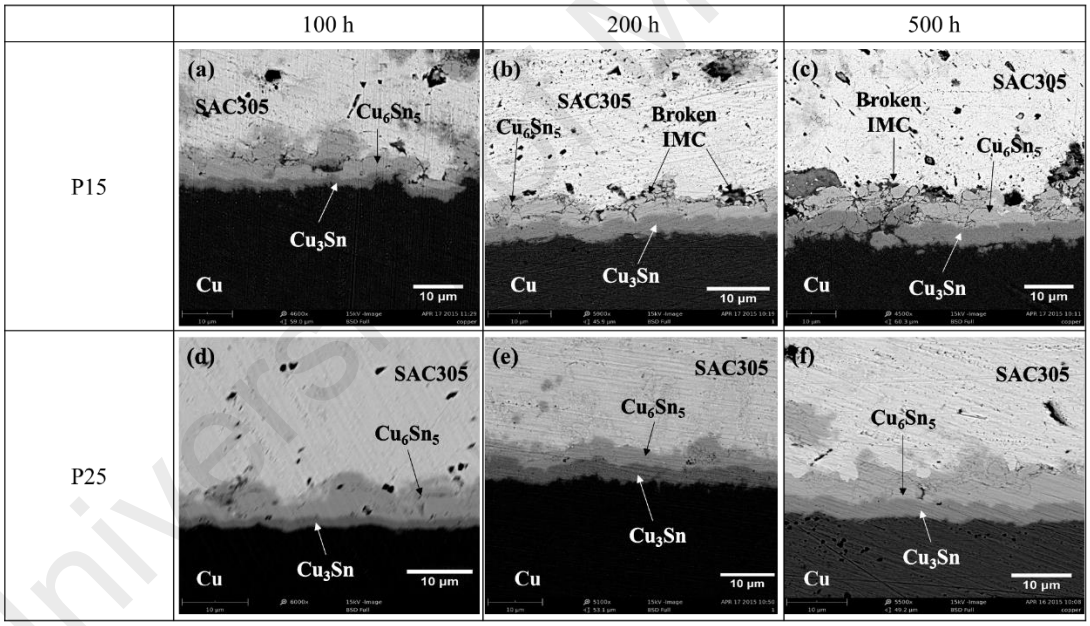

Figure 4.38 : IMC formation at SAC305/Cu substrate interface with aging time of (a),(d) 100 h, (b),(e) 200 h and (c), (f) 500 h in SAC305 with added (a)-(c)P15 and (d)-(f) P25 aged at 150°C for solder joint at 300 s, 307°C

In this research, IMC evolution at the SAC305/porous Cu interface as seen in Figure 4.39 was similar to that in the SAC305/Cu substrate interface as shown in Figure 4.38. However, no cracks or voids were detected at 100 h of aging at the porous Cu interface for P15 and P25. Voids were only detected when the aging time increased to 200 h for P15. These voids grew and spread along the SAC305/IMC interface, which induced cracks at the IMC interface and affected joint reliability negatively. The voids formed due to the different diffusion properties of Sn and Cu in porous Cu and the solder alloy during the aging process. Thus, Cu_3Sn became thicker while Cu_6Sn_5 became thinner. In contrast, for the aged sample with a P25 porous Cu interlayer, the IMC layer interface seemed strong since no voids were detected at 200 h of aging and only the thickness of Cu_3Sn increased. Voids and cracks appeared at the SAC305/Cu_6Sn_5 interface with prolonged time to 500 h. It is believed that strain concentration occurred in the joint close to the SAC305/Cu_6Sn_5 interface. Hence, cracks formed easily, as has been reported earlier (Chen, Yu, Mei, Li, & Chen, 2014).

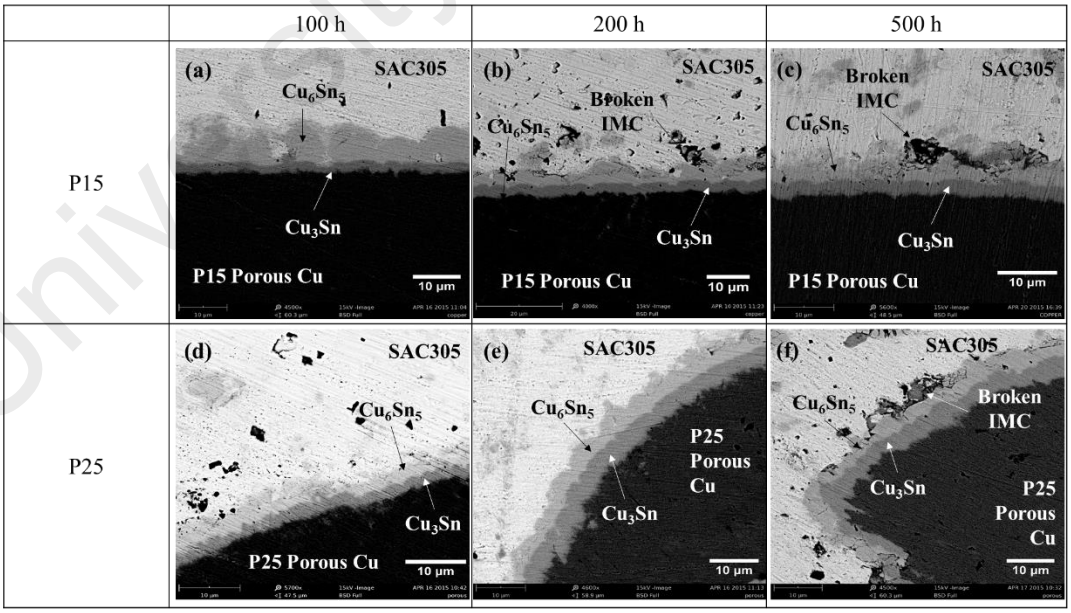

Figure 4.39 : IMC formation at SAC305/porous Cu interface at aging times of (a),(d) 100 h, (b),(e) 200h and (c), (f) 500 h in SAC305 with added (a)-(c)P15 and (d)-(f) P25 aged at 150°C for solder joint at 300 s, 307°C

4.7 Summary

Increasing the soldering temperature from 267°C to 307°C generally improved the strength of solder joints with a porous Cu interlayer added at all corresponding soldering times. The addition of P15 and P25 porous Cu has resulted in strength increment of about 10-20 MPa compared to solder joints without any porous Cu added.

A thin IMC layer was observed at the interfaces for all samples at 60 s soldering time. At higher soldering time of 180 s and 300 s, IMC thickness at the SAC305/Cu substrate interface for both control and with porous Cu samples increased 1 µm for every 20°C increase in soldering temperature. Higher IMC layer thickness as measured for joints soldered at the highest temperature of 307°C offered the highest strengths to the solder joints with P15 and P25 at 54 MPa and 51 MPa, respectively.

At aging temperature of 150°C, there is a degradation of strength of the solder joints for all samples with the porous Cu interlayer addition with increase in aging time from 100 h to 500 h. Microstructure analysis revealed at both interfaces of solder/Cu and solder/porous Cu, the IMC layer at 267°C soldering temperature was generally thinner than at higher soldering temperatures at 500 h aging time. At the SAC305/Cu interface, the growth rate of IMC during isothermal aging was higher for the solder joint with P25 porous Cu than P15. This is because during isothermal aging, Cu_3Sn grew rapidly into both sides of Cu and Cu_6Sn_5 interface. After 200 h of aging, the cracks formed earlier at Cu_6Sn_5 interface for solder joint with P15. The IMC was growing until the diffusion of Cu atoms was blocked by the voids and cracks. Subsequently the growth rate of IMC formation was reduced.

CHAPTER 5: CONCLUSIONS AND RECOMMENDATIONS

The effect of adding porous Cu interlayer to the Sn-3.0Ag-0.5Cu solder alloy (SAC305) on joint strength in Cu substrate joining was investigated. The main results obtained in this research are summarized as follows:

1) The joint tensile strength was affected by soldering temperature, soldering time and pore size of porous Cu
2) The strength at each soldering temperature of soldering time were n the following order: SAC305 with P25 porous Cu > SAC305 with P15 porous Cu > SAC305 without porous Cu. SAC305 with added P15 and P25 porous Cu produced highest joint strengths of 51 MPa and MPa, respectively when soldered at 307°C with 300 a soldering time
3) Fractures propagated along the Cu_6Sn_5/SAC305 interface and inside SAC305 in joints without porous Cu interlayer. In the case of solder joints soldered with P15 or P25 porous Cu interlayer, fractures occurred at the SAC305/IMC interface, the IMC/Cu interface, and/or in porous Cu itself.
4) An IMC layer comprising mainly Cu_6Sn_5 and traces of Cu_3Sn is formed at the interfaces of SAC305/Cu substrate and SAC305/porous Cu interlayer. The Cu_6Sn_5 IMC layer in the SAC305/Cu substrate interface was in discontinuous scalloped IMC compared to a more uniform and continuous IMC layers at SAC305/porous Cu interface (P15 & P25).
5) The tensile strength of solders with added P15 and P25 porous Cu interlayer generally decreased with increasing aging time for all soldering temperatures. The strength of both joints dropped to as low as 20 MPa after 500 h aging time. However, at 100 h aging time both solder joints possessed strength of 45 MPa.

6) In aged samples, the IMC thickness at both SAC305/Cu substrate interface and SAC305/porous Cu interfaces increased sharply during the first 200 h of aging. Overall, the total IMC layer thickness increased from the initial 4.0-4.5 μm at 0 h for IMC at the SAC305/Cu substrate and SAC305/porous Cu interfaces to 7.0-10.5 μm at 500 h aging time. When compared to as-soldered joints, the significant increase in total IMC layer thickness in the aged is attributable to the conspicuous Cu_3Sn layer.

Future Recommendations

The current study on configuring a soldering technique with the addition of a porous Cu interlayer is an innovation in this research area. Many more aspects involving the actual role and effect of porous metal during soldering need to be studied. A matter of significant importance is the search for lead-free solder alloys for use in advanced applications, where exposure to long periods of time at high temperatures often prevails. In addition, as solder joint is utilized for interconnection of electronic devices, the solder will act as medium for electrical and thermal continuity in electronics assemblies. Hence, in order to determine its suitability for use in electronic application, further investigation would focus on the electrical properties such as conductivity and electromigration of Sn-3.0Ag-0.5Cu solder alloy with addition of porous Cu interlayer. Despite the increase in cost should porous metal technology be recommended, the various benefits and advantages to industries should offset the concern raised. Furthermore, with the potentials generated from the present work, there is a need to continue investigations on the utilization of porous Cu in the soldering process.

REFERENCES

Abtew, M., & Selvaduray, G. (2000). Lead-free solders in microelectronics. *Materials Science and Engineering R: Reports*, *27*, 95–141.

Ag, O. M. G., Kg, C., & Chaussee, R. (1999). Lead Free Soft Solder Die Attach Process for Power Semiconductor Packaging, *SEMICON China 2002 Technology Symposium*, 1–6.

Amagai, M. (2008). A study of nanoparticles in Sn-Ag based lead free solders. *Microelectronics Reliability*, *48*(1), 1–16.

Anderson, I. E. (2007). Development of Sn-Ag-Cu and Sn-Ag-Cu-X alloys for Pb-free electronic solder applications. In *Lead-Free Electronic Solders: A Special Issue of the Journal of Materials Science: Materials in Electronics* (pp. 55–76). Boston, MA: Springer US.

Anderson, I. E., Cook, B. a., Harringa, J., & Terpstra, R. L. (2002). Microstructural modifications and properties of Sn-Ag-Cu solder joints induced by alloying. *Journal of Electronic Materials*, *31*(11), 1166–1174.

Anderson, I. E., Walleser, J., & Harringa, J. L. (2007). Observations of Nucleation Catalysis Effects during Solidifi cation of SnAgCuX Solder Joints, JOM 59(7), 38-43.

ASM International. (2004). *ASM Handbook, Volume 3, Alloy Phase Diagrams*. *Aging* (Vol. 7).

Bai, J. G., Calata, J. N., & Lu, G. (2007). Processing and Characterization of Nanosilver Pastes for Die-Attaching SiC Devices, *IEEE Transaction on Electronics Pacakaging Manufacturing*, *30*(4), 241–245.

Banhart, J. (2001). Manufacture, characterisation and application of cellular metals and metal foams. *Progress in Materials Science*, *46*(6), 559–632.

Bukat, F. (2010). Investigation of Sn-Zn-Bi solders – Part I : surface tension , interfacial tension and density measurements of SnZn7Bi solders.

Che, F. X., Zhu, W. H., Poh, E. S. W., Zhang, X. W., & Zhang, X. R. (2010). The study of mechanical properties of Sn–Ag–Cu lead-free solders with different Ag contents and Ni doping under different strain rates and temperatures. *Journal of Alloys and Compounds*, *507*(1), 215–224.

Chellvarajoo, S., Abdullah, M. Z., & Samsudin, Z. (2015). Effects of Fe2NiO4 nanoparticles addition into lead free Sn-3.0Ag-0.5Cu solder pastes on microstructure and mechanical properties after reflow soldering process. *Materials and Design*, *67*(February 2016), 197–208.

Chen, G., Wu, F., Liu, C., Xia, W., & Liu, H. (2015). Effects of fullerenes reinforcement on the performance of 96.5Sn-3Ag-0.5Cu lead-free solder. *Materials Science and Engineering A*, *636*, 484–492.

Chen, G., Yu, L., Mei, Y.-H., Li, X., Chen, X., & Lu, G.-Q. (2014). Reliability comparison between SAC305 joint and sintered nanosilver joint at high temperatures for power electronic packaging. *Journal of Materials Processing Technology*, *214*(9), 1900–1908.

Cheng, F., Gao, F., Nishikawa, H., & Takemoto, T. (2009). Interaction behavior between the additives and Sn in Sn–3.0Ag–0.5Cu-based solder alloys and the relevant joint solderability. *Journal of Alloys and Compounds*, *472*(1-2), 530–534.

Chidambaram, V., Hattel, J., & Hald, J. (2011). High-temperature lead-free solder alternatives. *Microelectronic Engineering*, *88*(6), 981–989.

City, S. L, (2013). (12) United States Patent (10) Patent N0.US7,766,218B2, *2*(12).

Drevin-Bazin, a., Lacroix, F., & Barbot, J.-F. (2013). SiC Die Attach for High-Temperature Applications. *Journal of Electronic Materials*, *43*(3), 695–701.

Dutta, I., Kumar, P., & Subbarayan, G. (2009). Microstructural coarsening in Sn-Ag-based solders and its effects on mechanical properties. *JOM*, *61*(6), 29–38.

El-Daly, a. a., Desoky, W. M., Elmosalami, T. a., El-Shaarawy, M. G., & Abdraboh, a. M. (2015). Microstructural modifications and properties of SiC nanoparticles-reinforced Sn-3.0Ag-0.5Cu solder alloy. *Materials and Design*, *65*, 1196–1204.

El-Daly, a. a., & Hammad, a. E. (2011). Development of high strength Sn–0.7Cu solders with the addition of small amount of Ag and In. *Journal of Alloys and Compounds*, *509*(34), 8554–8560.

Fallahi, H., Nurulakmal, M. S., Arezodar, a. F., & Abdullah, J. (2012). Effect of iron and indium on IMC formation and mechanical properties of lead-free solder. *Materials Science and Engineering: A*, *553*, 22–31.

Fang, F., Zheng, C., Lou, H., & Sui, R. (2001). Bonding of silicon nitride ceramics using Fe – Ni r Cu r Ni r Cu r Fe – Ni interlayers, (January), 178–181.

Gao, F., Takemoto, T., & Nishikawa, H. (2006). Effects of Co and Ni addition on reactive diffusion between Sn-3.5Ag solder and Cu during soldering and annealing. *Materials Science and Engineering A*, *420*(1-2), 39–46.

Gayle, F. W., Becka, G., Badgett, J., Whitten, G., Pan, T., Grusd, A., … Olson, C. (2001). High Temperature Lead-Free Solder for Microelectronics and Reliability, *JOMS 53(6)*,17–21.

George, E., Das, D., Osterman, M., & Pecht, M. (2011). Thermal Cycling Reliability of Lead-Free Solders (SAC305 and Sn3.5Ag) for High-Temperature Applications. *IEEE Transactions on Device and Materials Reliability*, *11*(2), 328–338.

Guo, F. (2006). Composite lead-free electronic solders, *Journal of Materials Science: Materials in Electronics 18*(1), 129-145.

Guo, F., Choi, S., Lucas, J. P., & Subramanian, K. N. (2001). Microstructural characterisation of reflowed and isothermally-aged Cu and Ag particulate reinforced

Sn-3 . 5Ag composite solders, *Soldering and Surface Mount Technology 13*(1), 7–18.

Guo, F., Lucas, J. P., & Subramanian, K. N. (2001). Creep behavior in Cu and Ag particle-reinforced composite and eutectic Sn-3 . 5Ag and Sn-4 . 0Ag- 0 . 5Cu non-composite solder joints, *Journal of Materials: Science Materials in Electronics 12* (1), 27–35.

Guo-kui, J., Xi-cheng, W., Peng, S., & Liu, J. (2007). Tensile Fracture Behavior of Sn-3.0Ag-0.5Cu Solder Joints on Copper, *International Symposium on High Density Packaging and Microsystem Integration*, 5–9.

Handbook of Cellular Metals. Wiley-VCH, 2003.

Harcuba, P., & Janeček, M. (2010). Microstructure changes and physical properties of the intermetallic compounds formed at the interface between Sn-Cu solders and a Cu substrate due to a minor addition of Ni. *Journal of Electronic Materials*, *39*(12), 2553–2557.

Hayashi, K., Izuta, G., Murakami, K., Uegai, Y., & Takao, H. (2002). Improvement of fatigue life of solder joints by thickness control of solder with wire bump technique [power modules]. *52nd Electronic Components and Technology Conference 2002. (Cat. No.02CH37345)*.

Hu, X., Xu, T., Keer, L. M., Li, Y., & Jiang, X. (2016). Microstructure evolution and shear fracture behavior of aged Sn3Ag0.5Cu/Cu solder joints. *Materials Science and Engineering A*, *673*, 167–177.

Huang, Y., Xiu, Z., Wu, G., Tian, Y., He, P., Gu, X., & Long, W. (2016). Improving shear strength of Sn-3.0Ag-0.5Cu/Cu joints and suppressing intermetallic compounds layer growth by adding graphene nanosheets. *Materials Letters*, *169*, 262–264.

Huangl, X., Lee, S. W. R., Li, M., & Chen, W. T. (2000). Effect of High Temperature Storage on Reliability of Sn-Ag-Cu Flip Chip Solder Bumps, *International Conference on Electronic Materials and Packaging*, 7–12.

Humpston, G., & Jacobson, D. M. (2004). *Principles of Soldering*. ASM International.

JISZ3191. Japanese Standard Association (2003).

Kanchanomai, C., Miyashita, Y., & Mutoh, Y. (2002). Low-cycle fatigue behavior of Sn-Ag, Sn-Ag-Cu, and Sn-Ag-Cu-Bi lead-free solders. *Journal of Electronic Materials*, *31*(5), 456–465.

Kang, N., Sung, H., Jun, S., & Yun, C. (2009). Alloy design of Zn – Al – Cu solder for ultra high temperatures, *467*, 246–250.

Kattner, U. R. (2002). Phase diagrams for lead-free solder alloys. *Jom*, *54*(12), 45–51.

Kim, B., Lee, C.-W., Lee, D., & Kang, N. (2014). Effect of Sb addition on Bi–2.6Ag–0.1Cu solders for high-temperature applications. *Journal of Alloys and Compounds*, *592*, 207–212.

Kim, K. S., Huh, S. H., & Suganuma, K. (2003). Effects of fourth alloying additive on microstructures and tensile properties of Sn–Ag–Cu alloy and joints with Cu. *Microelectronics Reliability*, *43*(2), 259–267.

Kim, S.-J., Kim, K.-S., Kim, S.-S., Kang, C.-Y., & Suganuma, K. (2008). Characteristics of Zn-Al-Cu Alloys for High Temperature Solder Application. *Materials Transactions*, *49*(7), 1531–1536.

Kumar, A., Fouzder, T., Chan, Y. C., Sharif, A., Wong, N. B., & Yung, W. K. C. (2010). The influence of addition of Al nano-particles on the microstructure and shear strength of eutectic Sn – Ag – Cu solder on Au / Ni metallized Cu pads. *Journal of Alloys and Compounds*, *506*(1), 216–223.

Layers, S. N. D., Cao, X., Wang, T., Ngo, K. D. T., Member, S., & Lu, G. (2011). Characterization of Lead-Free Solder and Using Thermal Impedance, *IEEE Transaction on Components, Packaging and Manufacturing Technology 1* (4), 495–501.

Lee, C. C., Wang, P. J., & Kim, J. S. (2007). Are intermetallics in solder joints really brittle? *Proceedings - Electronic Components and Technology Conference*, 648–652.

Lee, L. M., & Mohamad, A. A. (2013). Review Article Interfacial Reaction of Sn-Ag-Cu Lead-Free Solder Alloy on Cu : A Review, *Advances in Materials Science and Engineering*, *2013*.

Li, G., Shi, Y., Hao, H., Xia, Z., Lei, Y., Guo, F., & Li, X. (2009). Effect of rare earth addition on shear strength of SnAgCu lead-free solder joints. *JOURNAL OF MATERIALS SCIENCE-MATERIALS IN ELECTRONICS*, *20*, 186–192.

Li, H., Qu, L., Zhao, H., Zhao, N., & Ma, H. (2013). Mechanism of Cu 6 Sn 5 layer act as a diffusion barrier layer, *ICEPT*, 1086–1089.

Li, J. F., Agyakwa, P. a., & Johnson, C. M. (2012). Effect of trace Al on growth rates of intermetallic compound layers between Sn-based solders and Cu substrate. *Journal of Alloys and Compounds*, *545*, 70–79.

Lin, D. C., Srivatsan, T. S., Wang, G.-X., & Kovacevic, R. (2006). Microstructural development in a rapidly cooled eutectic Sn–3.5% Ag solder reinforced with copper powder. *Powder Technology*, *166*(1), 38–46.

Liu, W., Lee, N.-C., & Bachorik, P. (2013). An innovative composite solder preform for TLP bonding — Microstructure and properties of die attach joints. *2013 IEEE 15th Electronics Packaging Technology Conference (EPTC 2013)*, (c), 635–640.

LIU, W., WANG, C. qing, TIAN, Y. hong, & CHEN, Y. rong. (2008). Effect of Zn addition in Sn-rich alloys on interfacial reaction with Au foils. *Transactions of Nonferrous Metals Society of China (English Edition)*, *18*, 617–622.

Lord, R. A., & Umantsev, A. (2005). Early stages of soldering reactions. *Journal of Applied Physics*, *98*(6), 63525. http://doi.org/10.1063/1.2058186

Lu, H., Bailey, C., & Mills, L. (2015). Impact of Uneven Solder Thickness on IGBT Substrate Reliability, *ECTC IEEE 65*, 1888–1893.

Lu, H., Tilford, T., Bailey, C., & Newcombe, D. R. (2007). Lifetime prediction for power electronics module substrate mount-down solder interconnect. *Proceedings of International Symposium on High Density Packaging and Microsystem Integration 2007, HDP'07*.

Matsumoto, T., & Nogi, K. (2008). Wetting in Soldering and Microelectronics. *Annual Review of Materials Research*, 38,251-273.

Mayappan, R., Ismail, A. B., Ahmad, Z. A., Ariga, T., & Hussain, L. B. (2006). Effect of sample perimeter and temperature on Sn–Zn based lead-free solders. *Materials Letters*, *60*(19), 2383–2389.

Mei, Y., Chen, G., Guo-Quan, L., & Chen, X. (2012). Effect of joint sizes of low-temperature sintered nano-silver on thermal residual curvature of sandwiched assembly. *International Journal of Adhesion and Adhesives*, *35*, 88–93.

Monsalve, E. R. (1984). Lead Ingestion Hazard in Hand Soldering Environments, *Naval Weapon Centre*, *18*.

Moon, K.-W., Boettinger, W. J., Kattner, U. R., Biancaniello, F. S., & Handwerker, C. a. (2000). Experimental and thermodynamic assessment of Sn-Ag-Cu solder alloys. *Journal of Electronic Materials*, *29*(10), 1122–1136.

Nadia, A., & Haseeb, a. S. M. a. (2011). Effects of addition of copper particles of different size to Sn-3.5Ag solder. *Journal of Materials Science: Materials in Electronics*, *23*(1), 86–93.

Nai, S. M. L., Wei, J., & Gupta, M. (2009). Interfacial intermetallic growth and shear strength of lead-free composite solder joints. *Journal of Alloys and Compounds*, *473*(1-2), 100–106.

Nawaz, K., Bock, J., & Jacobi, A. M. (2012). Thermal-Hydraulic Performance of Metal Foam Heat Exchangers. *International Refrigeration and Air Conditioning Conference*, 1–10.

Nguyen, V. L., & Kim, H.-K. (2014). Mechanical Properties of Lead-Free Solder Joints Under High-Speed Shear Impact Loading. *Journal of Electronic Materials*, *43*(11), 4171–4178.

Nishikawa, H., Takemoto, T., Kifune, K., Uetani, T., & Sekimori, N. (2004). Effect of Iron Plating Conditions on Reaction in Molten Lead-Free Solder. *Materials Transactions*, *45*(3), 741–746.

Nogita, K., Read, J., Nishimura, T., Sweatman, K., Suenaga, S., & Dahle, A. K. (2005). Microstructure Control in Sn – 0 . 7 mass % Cu Alloys, *Materials Transactions 46*(11), 2419–2425.

Ogunseitan, O. a. (2007). Public health and environmental benefits of adopting lead-free solders. *Jom*, *59*(7), 12–17.

Öhrström, L., & Reedijk, J. (2016). Names and symbols of the elements with atomic numbers 113, 115, 117 and 118 (IUPAC Recommendations 2016). *Pure and Applied Chemistry*, *88*(12), 1225–1229.

Pang, J. H. L., Xu, L., Shi, X. Q., Zhou, W., & Ngoh, S. L. (2004). Intermetallic growth studies on Sn-Ag-Cu lead-free solder joints. *Journal of Electronic Materials*, *33*(10), 1219–1226.

Peng, W., Monlevade, E., & Marques, M. E. (2007). Effect of thermal aging on the interfacial structure of SnAgCu solder joints on Cu. *Microelectronics Reliability*, *47*(12), 2161–2168.

Pietriková, A., Bednarˇ, J., & Duriˇ, J. (2011). In situ investigation of SnAgCu solder alloy microstructure, *Journal of Alloys and Compounds 509*, 1550–1553.

Puttlitz, K. J., & Stalter, K. A. (2004). *Handbook of Lead-Free Solder Technology for Microelectronic Assemblies*. CRC Press.

Rizvi, M. J., Chan, Y. C., Bailey, C., Lu, H., & Islam, M. N. (2006). Effect of adding 1wt% Bi into the Sn–2.8Ag–0.5Cu solder alloy on the intermetallic formations with Cu-substrate during soldering and isothermal aging. *Journal of Alloys and Compounds*, *407*(1-2), 208–214.

Rzepka, S., Hofer, E., Simon, E., Meusel, E., & Reichl, H. (2002). Stress analysis and design optimization of a wafer-level CSP by FEM simulations and experiments. *IEEE Transactions on Electronics Packaging Manufacturing*.

Sabri, M. F. M., Shnawah, D. A., Badruddin, I. A., Said, S. B. M., Che, F. X., & Ariga, T. (2013). Microstructural stability of Sn–1Ag–0.5Cu–xAl (x=1, 1.5, and 2wt.%) solder alloys and the effects of high-temperature aging on their mechanical properties. *Materials Characterization*, *78*, 129–143.

Sharif, A., Lim, J. Z., Made, R. I., Lau, F. L., Phua, E. J. R., Lim, J. D., … Chen, Z. (2013). Pb-Free Glass Paste: A Metallization-Free Die-Attachment Solution for High-Temperature Application on Ceramic Substrates. *Journal of Electronic Materials*, *42*(8), 2667–2676.

Sharma, A., Jang, Y.-J., Kim, J. B., & Jung, J. P. (2017). Thermal cycling, shear and insulating characteristics of epoxy embedded Sn-3.0Ag-0.5Cu (SAC305) solder paste for automotive applications. *Journal of Alloys and Compounds*, *704*, 795–803.

Shen, J., Cao, Z., Zhai, D., Zhao, M., & He, P. (2014). Effect of isothermal aging and low density current on intermetallic compound growth rate in lead-free solder interface. *Microelectronics Reliability*, *54*(1), 252–258.

Shirzadi, A. a., Zhu, Y., & Bhadeshia, H. K. D. H. (2008). Joining ceramics to metals using metallic foam. *Materials Science and Engineering: A*, *496*(1-2), 501–506.

Shnawah, D. A., Sabri, M. F. M., Badruddin, I. A., Said, S. B. M., Ariga, T., & Che, F. X. (2013). Effect of Ag Content and the Minor Alloying Element Fe on the Mechanical Properties and Microstructural Stability of Sn-Ag-Cu Solder Alloy

Under High-Temperature Annealing. *Journal of Electronic Materials*, *42*(3), 470–484.

Shohji, I., Osawa, T., Matsuki, T., Kariya, Y., Yasuda, K., & Takemoto, T. (2008). Effect of Specimen Size and Aging on Tensile Properties of Sn-Ag-Cu Lead-Free Solders. *Materials Transactions*, *49*(5), 1175–1179.

Smith, D. R., & Madeni, J. C. (2002). Properties of Lead-Free Solders Properties of Lead-Free Solders.

Suganuma, K. (2001). Advances in lead-free electronics soldering, *Current Opinion in Solid State and Materials Science 5*, 55–64.

Suganuma, K. (2003). *Lead-Free Soldering in Electronics: Science, Technology, and Environmental Impact*. CRC Press.

Suganuma, K., Kim, S., & Kim, K. (2009). High-Temperature Lead-Free Solders : Properties and Possibilities, *JOM 61*(1), 64-71.

Suganuma, K., (2006). The current status of lead-free soldering, *ESPEC Technology Report* (13), 1–8.

Tang, Y., Li, G. Y., Chen, D. Q., & Pan, Y. C. (2014). Influence of TiO2 nanoparticles on IMC growth in Sn--3.0Ag--0.5Cu--xTiO2 solder joints during isothermal aging process. *Journal of Materials Science: Materials in Electronics*, *25*(2), 981–991.

Thewsey, D. J., & Zhao, Y. Y. (2008). Thermal conductivity of porous copper manufactured by the lost carbonate sintering process. *Physica Status Solidi (a)*, *205*(5), 1126–1131.

Tu, K. (2007). *Solder Joint Technology- Materials, Properties, and Reliability*. *Reactions* (Vol. 117).

Tu, X., Yi, D., Wu, J., & Wang, B. (2017). Influence of Ce addition on Sn-3.0Ag-0.5Cu solder joints: Thermal behavior, microstructure and mechanical properties. *Journal of Alloys and Compounds*, *698*, 317–328.

Tukker, A., Buist, H., Oers, L. Van, & Voet, E. Van Der. (2006). Risks to health and environment of the use of lead in products in the EU, *49*, 89–109.

Vann, K., Musson, S., & Townsend, T. (2006). Evaluation of a modified TCLP methodology for RCRA toxicity characterization of computer CPUs, *129*, 101–109.

Vianco, P. T., & Rejent, J. A. (1999). Properties of Ternary Sn-Ag-Bi Solder Alloys : Part I — Thermal Properties and Microstructural Analysis, 1127–1137.

Wang, F., Gao, F., Ma, X. I. N., & Qian, Y. (2006). Depressing Effect of 0 . 2wt .% Zn Addition into Sn-3 . 0Ag-0 . 5Cu Solder Alloy on the Intermetallic Growth with Cu Substrate during Isothermal Aging. *Journal of Electronic Materials*, *35*(10), 1818–1824.

Wang, H., Gao, F., Ma, X., & Qian, Y. (2006). Reactive wetting of solders on Cu and Cu6Sn5/Cu3Sn/Cu substrates using wetting balance. *Scripta Materialia*, *55*(9), 823–826.

Wang, M., Wang, J., & Ke, W. (2014). Corrosion behavior of Sn-3.0Ag-0.5Cu solder under high-temperature and high-humidity condition. *Journal of Materials Science: Materials in Electronics*, *25*(3), 1228–1236.

Wu, C. M. L., Yu, D. Q., Law, C. M. T., & Wang, L. (2004). Properties of lead-free solder alloys with rare earth element additions. *Materials Science and Engineering: R: Reports*, *44*(1), 1–44.

Wu, J., Xue, S. B., Wang, J. W., Liu, S., Han, Y. L., & Wang, L. J. (2016). Recent progress of Sn???Ag???Cu lead-free solders bearing alloy elements and nanoparticles in electronic packaging. *Journal of Materials Science: Materials in Electronics*, *27*(12), 12729–12763.

Xia, Y., Xie, X., Lu, C., & Chang, J. (2006). Coupling effects at Cu (Ni)– SnAgCu – Cu (Ni) sandwich solder joint during isothermal aging, *417*, 143–149.

Yang, K.-S., Chung, C.-H., Lee, M.-T., Chiang, S.-B., Wong, C.-C., & Wang, C.-C. (2013). An experimental study on the heat dissipation of LED lighting module using metal/carbon foam. *International Communications in Heat and Mass Transfer*, *48*, 73–79.

Yang, W., Felton, L. E., & Messler, R. W. (1995). The effect of soldering process variables on the microstructure and mechanical properties of eutectic Sn-Ag/Cu solder joints. *Journal of Electronic Materials*, *24*(10), 1465–1472.

Yang, W., Lin, T., He, P., Wei, H., Xing, L., & Jia, D. (2014). Microstructure and mechanical properties of ZrB2–SiC joints fabricated by a contact-reactive brazing technique with Ti and Ni interlayers. *Ceramics International*, *40*(5), 7253–7260.

Yao, W., & Basaran, C. (2013). Electromigration damage mechanics of lead-free solder joints under pulsed DC: A computational model. *Computational Materials Science*, *71*, 76–88.

Yoon, J., Kim, S., & Jung, S. (2005). IMC morphology , interfacial reaction and joint reliability of Pb-free Sn – Ag – Cu solder on electrolytic Ni BGA substrate, *392*, 247–252.

Yoon, J.-W., Noh, B.-I., & Jung, S.-B. (2010). Interfacial reaction between Au–Sn solder and Au/Ni-metallized Kovar. *Journal of Materials Science: Materials in Electronics*, *22*(1), 84–90.

Yu, C.-Y., Lee, J., Chen, W.-L., & Duh, J.-G. (2014). Enhancement of the impact toughness in Sn–Ag–Cu/Cu solder joints via modifying the microstructure of solder alloy. *Materials Letters*, *119*, 20–23.

Zaharinie, T., Moshwan, R., Yusof, F., Hamdi, M., & Ariga, T. (2014). Vacuum brazing of sapphire with Inconel 600 using Cu/Ni porous composite interlayer for gas pressure sensor application. *Materials & Design*, *54*, 375–381.

Zeng, K. (2009). Lead-free soldering: Materials science and solder joint reliability. *JOM*, *61*(6), 28.

Zhang, L., Xue, S. B., Zeng, G., Gao, L. L., & Ye, H. (2012). Interface reaction between SnAgCu/SnAgCuCe solders and Cu substrate subjected to thermal cycling and isothermal aging. *Journal of Alloys and Compounds*, *510*(1), 38–45.

Zhang, L., Xue, S., Gao, L., Chen, Y., Yu, S., Sheng, Z., & Zeng, G. (2009). Effects of trace amount addition of rare earth on properties and microstructure of Sn–Ag–Cu alloys. *Journal of Materials Science: Materials in Electronics*, *20*(12), 1193–1199.

Zheng, H., Ngo, K. D. T., & Lu, G.-Q. (2015). Thermal characterization system for transient thermal impedance measurement and power cycling of IGBT modules. *Microelectronics Reliability*.

LIST OF PUBLICATIONS AND PAPERS PRESENTED

1. Nashrah Hani Jamadon, Farazila Yusof, Mohd Hamdi Abdul Shukor, Tadashi Ariga (2012, November), *Effect of Adding Porous Cu on the Microstructure and Mechanical Properties of Pb-Free Solder Joint*, Electronic Manufacturing Technology Symposium (IEMT), 2012 35th IEEE/CPMT International, Ipoh, Perak (Scopus)
2. Nashrah, H.J., Miyashita, Y., Farazila, Y., Ariga, T., & Mohd, H. (2013, September), *Effect of Porous Cu Interlayer on Microstructure and Mechanical Properties of Pb-Free Solder Joint*, Preprints of the National Meeting of JWS, 2013, 350–351, 25th Japan Welding Society Conference, Okayama University of Science, Okayama, Japan (Proceeding)
3. Jamadon, N. H., Miyashita, Y., Yusof, F., Hamdi, M., Otsuka, Y., & Ariga, T., (2013, November), *Effect of adding porous Cu interlayer into Sn-Ag-Cu lead-free solder joint on microstructure and tensile strength*, Materials and Processing Conference 2013(21), 532;1-3, Tokyo Metropolitan University, Tokyo, Japan (Proceeding)
4. Jamadon, N. H., Miyashita, Y., Yusof, F., Hamdi, M., Otsuka, Y., & Ariga, T., (2013, November), *Formation behaviour of reaction layer in Sn-3.0Ag-0.5Cu solder joint with addition of porous Cu interlayer*, Materials Science and Engineering, 61, 012020, International Symposium on Interfacial Joining and Surface Technology, Nov, 27-29, 2013, Osaka University, Osaka, Japan (Scopus)
5. Jamadon, N. H., Yusof, F., Shukor, M. H. A., Ariga, T., & Miyashita, Y., (2014, November) *Addition of porous Cu interlayer to Sn-3.0Ag-0.5Cu lead-free solder joint for high temperature application,* 36th International Electronics Manufacturing Technology Conference, Johor Bahru, Johor, (Scopus - BEST PAPER AWARD)
6. Nashrah Hani JAMADON, Farazila YUSOF, Mohd Hamdi ABD. SHUKOR, Tadashi ARIGA, Yukio MIYASHITA, (2015, January) *Utilization of porous Copper interlayer in the soldering of SAC305 with Copper substrate,* International

Sustainable Technology, Energy and Civilization Conference: ISTECC 2015 (16th Kyoto University Southeast Asian Forum), Kuala Lumpur (Proceeding)

7. Jamadon, N. H., Miyashita, Y., Yusof, F., Hamdi, M., Ariga, T., *Effects of Adding Porous Cu Interlayer With Different Porosities To Sn-3.0Ag-0.5Cu Lead Free Solder Joint*, (2015, April), International Brazing & Soldering Conference, American Welding Society (IBSC 2015), California, USA (Proceeding)
8. Jamadon, N., Tan, A., Yusof, F., Ariga, T., Miyashita, Y., & Hamdi, M. (2016, September), *Utilization of porous Cu interlayer for the enhancement of Pb-free Sn-3.0Ag-0.5Cu solder joint*, *Metals* 2016, *6*(9), 220 (ISI Cited Paper)
9. J. Nashrah Hani, J. Mohd Fadzil, Y. Farazila, A. Tadashi, M. Yukio, A. S. Mohd Hamdi., (2017, January), *The effect of temperature on the formation behavior of reaction layer in SnAg3.0Cu0.5 (SAC305) solder joint with the addition of porous Cu interlayer,* Material Science and Engineering Technology, 2017 (ISI Cited Paper)
10. Nashrah Hani Jamadon, Nor Diyana Ahmad, Farazila Yusof, Tadashi Ariga, Yukio Miyashita, Mohd Hamdi Abd Shukor., *Effect of isothermal aging on mechanical properties of Sn-3.0Ag-0.5Cu solder alloy with porous Cu interlayer addition*, Lecture Notes in Mechanical Engineering, Springer 2017(Scopus)